

Annual Technical Progress Report

IMPROVING CO₂ EFFICIENCY FOR RECOVERING OIL IN HETEROGENEOUS
RESERVOIRS

DOE CONTRACT NO. DE-FG26-01BC15364

New Mexico Petroleum Recovery Research Center
New Mexico Institute of Mining and Technology
801 Leroy Place
Socorro, NM 87801
(505) 835-5142

Report Date:	December 20, 2002
Contract Date:	September 28, 2001
Completion Date:	September 27, 2004
DOE Award of 1 st year:	\$337,000
Program Manager:	Reid B. Grigg
Principal Investigator:	Reid B. Grigg
Other Major Contributors:	Robert K. Svec
Contracting Officer's Representative:	Daniel J. Ferguson
Reporting Period:	Oct. 1, 2001–Sept. 30, 2002

TABLE OF CONTENTS

LIST OF TABLES	iii
LIST OF FIGURES.....	iv
ABSTRACT	viii
EXECUTIVE SUMMARY.....	xiv
CHAPTER I. INDUSTRY INJECTIVITY SURVEY	1
Introduction	1
Procedure.....	2
Results	2
CHAPTER 2. PHYSICAL EFFECTS OF WAG FLUIDS ON CARBONATE CORE PLUGS ...	5
Introduction	5
Experimental Parameters.....	5
Results	6
Conclusions	13
Implications for Field Injectivity.....	14
CHAPTER 3. EVALUATION OF CO ₂ -BRINE-RESERVOIR ROCK INTERACTION WITH LABORATORY FLOW TESTS AND REACTIVE TRANSPORT MODELING	15
Introduction	15
Previous Research	15
Software, Hardware, and Procedures	17
Results	20
Discussion	24
Summary	24
CHAPTER 4. COST REDUCTION AND INJECTIVITY IMPROVEMENTS FOR CO ₂ FOAMS FOR MOBILITY CONTROL	26
Introduction	26
Field Tests	26
Laboratory Tests.....	28
Improving Surfactant Adsorption.....	29
Improving Injectivity.....	30
CO ₂ Foam Cost Reduction	31
Conclusions	32

CHAPTER 5. MOBILITY CONTROL AGENTS	34
Introduction	34
Interference of Cosurfactants during Concentration Determination	34
Effects of Dilution Procedures and Delay Time before Measurements	34
Multiple Run in a Single Core	35
Conclusions	35
ACKNOWLEDGMENTS	36
REFERENCES	37
APPENDIX A. LIST OF SPE ARTICLES ON EXAMINED RESERVOIRS	83

LIST OF TABLES

Table 1. CO ₂ Miscible Project Locations in the United States with Number of Total and Active Listed.....	43
Table 2. CO ₂ Flooded Fields in the Permian Basin.....	43
Table 3. Rock Types.....	45
Table 4. Injectivity Changes.....	46
Table 5. What Has or Has Not Gone Well?	46
Table 6. Mystery	46
Table 7. Research Focus.....	46
Table 8. Core Properties.....	46
Table 9- Brine Composition.....	47
Table 10. Tacer Brine Compositions.....	47
Table 11. Parameters for Segment A, Segment B, and the Entire Core.....	47
Table 12. Media Variations Used in the TRANSTOUGH Model Simulations. Porosity is 15 % for All Except for “E” with a Measured Dolomite-Anhydrite Porosity of 13%.	47
Table 13. Kinetic Reaction Rate Constants.....	48
Table 14. Experimental Brine Solution Concentrations (“**”) Indicates Concentrations That Were Varied).....	48
Table 15. Brine Alkalinity and pH Ranges (Low, Medium, High) for the Quartz-Carbonate and - Evaporite Systems	49
Table 16. Chemical Reactions Used in the Model (Secondary Species Reactions, Except HCO ₃ - and OH-, Not Presented)	49
Table 17. Parameters of the Dolomite-Anhydrite Experiment	49
Table 18. Parameters for the Sensitivity Analysis	49
Table 19. Adsorption Comparison of Four Rock Types at Two Concentrations of CD1045.....	50
Table 20. Summary of EVGSAU Foam Test Economics.....	50
Table 21. Improved Economics of Enhanced Foam	51
Table 22. Core Parameters for Adsorption and Desorption Profiles.....	51

LIST OF FIGURES

Fig. 1. High pressure coreflooding system.....	52
Fig. 2. BSE image of pre-flood Indiana limestone, 500 micron scale.	52
Fig. 3. Photo of post-flood Indiana limestone core, sliced to reveal extent of dissolution channel.	53
Fig. 4. BSE image of dissolution of grains and cement adjacent to channel, 200 micron scale.....	53
Fig. 5. BSE image of dissolution of grains and cement, 500 micron scale.....	54
Fig. 6. BSE image of remnant calcite overgrowth and large calcite crystals, 100 micron scale.....	54
Fig. 7. BSE image of remnant overgrowths, grain replacement and large calcite crystals, 200 micron scale.	55
Fig. 8. Indiana limestone core permeability.....	55
Fig. 9. BSE image of pre-flood Seminole San Andres core, 100 micron scale.	56
Fig. 10. BSE image of pre-flood Seminole San Andres core, 200 micron scale.	56
Fig. 11. BSE image of post-flood Seminole San Andres core S139B, 500 micron scale.....	57
Fig. 12. BSE image of post-flood Seminole San Andres core S139B, 100 micron scale.....	57
Fig. 13. BSE image of flooded Seminole San Andres core S139B, 100 micron scale.	58
Fig. 14. Photo of dissolution features in sliced Seminole San Andres core S141B.....	58
Fig. 15. Closeup of anhydrite dissolution channels in Seminole San Andres core S141B.....	59
Fig. 16. Photo of post-flood dissolution features in sliced Seminole San Andres core S139B. ...	59
Fig. 17. Seminole San Andres core 139B permeability.	60
Fig. 18. Injectivity profile when the small oil contamination injection was followed by CO ₂ half cycle.	60
Fig. 19. Injectivity profile when the small oil contamination injection was followed by brine half cycle.....	61
Fig. 20. Porosity trends for the system, Segment A, and Segment B.	62
Fig. 21. Pore volume for the system, Segment A, and Segment B.	62
Fig. 22. Permeability trends for the system, Segments A and B.....	63
Fig. 23. Development of the solution channel at three points during the flood.....	63
Fig. 24. Sectioned core segments after flooding.....	64
Fig. 25. Chemical and BSEI sample locations along the sectioned core.	64
Fig. 26. Ca concentration along the flooded core.	65

Fig. 27. Mg concentration along the flooded core.	65
Fig. 28. Mn concentration along the flooded core.	66
Fig. 29. Sr concentration along the flooded core.	66
Fig. 30. The model used to represent laboratory core experiments.	67
Fig. 31. Experimental vs. simulated total bulk porosity and permeability values as a function of injected fluid volume (see Fig. 17).	67
Fig. 32. Porosity volume fraction for the dolomite-anhydrite system at selected times indicated in the figure.	68
Fig. 33. Calcite volume fraction after 174 days. The results are for three different brine pHs and alkalinities.	68
Fig. 34. Effect of increasing time step in TOUGH2 at the first 0.1m of the simulated domain. Manual mass fraction calculation using the Reid et al. ⁵⁶ relation in EOSCO2.	69
Fig. 35. Volume fraction of halite versus distance into the column at selected times indicated in the figure.	69
Fig. 36. Volume fraction of gypsum versus distance into the column at selected times indicated in the figure.	70
Fig. 37. Porosity volume fraction for the quartz-evaporite system at selected times indicated in the figure.	70
Fig. 38. Volume fraction magnesite versus distance into the column at selected times indicated in the figure.	71
Fig. 39. Volume fraction calcite versus distance into the column at selected times indicated in the figure.	71
Fig. 40. Porosity volume fraction for the quartz-carbonate system at selected times indicated in the figure.	72
Fig. 41. Plot enlargement of porosity in the quartz-carbonate system near the initial porosity value.	72
Fig. 42. Volume fraction of calcite versus distance into the column at selected times indicated in the figure.	73
Fig. 43. CD1045 adsorption isotherm data for four Berea core tests using different cores and two different studies.	74
Fig. 44. Comparison of CD1045 adsorption of Indiana limestone, Baker dolomite, and San Andres dolomite.	74

Fig. 45. Lignosulfonate adsorption on Berea sandstone cores. Two different researchers and different cores.	75
Fig. 46. Adsorption isotherms versus injection methods of CD1045 with and without cosurfactant lignosulfonate in Berea sandstone.	75
Fig. 47. Comparison of the two series of tests showing adsorption reduction of CD1045 at an equilibrium concentration of 0.05 wt% CD1045 versus injection method of cosurfactant Lignosulfonate in Berea sandstone.	76
Fig. 48. Lignosulfonate adsorption isotherm in Indiana limestone.	76
Fig. 49. Adsorption isotherms versus injection methods of CD1045 with and without cosurfactant lignosulfonate in Indiana limestone.	77
Fig. 50. Comparison of adsorption reduction of CD1045 at an equilibrium concentration of 0.05 wt% versus injection method of cosurfactant lignosulfonate in Indiana limestone.	77
Fig. 51. Comparison of oil production from the low permeability region of a dual permeability core versus injected PV using different surfactant systems.	78
Fig. 52. Comparison of pressure drop across a dual permeability core during fluid injection for different surfactant systems.	78
Fig. 53. The influence of lignosulfonate on CD1045 concentration measurement results.	79
Fig. 54. The influence of CD1045 on lignosulfonate concentration measurement results.	79
Fig. 55. The influence of shaking methods on measurement error.	80
Fig. 56. The influence of delayed measurement time on errors.	80
Fig. 57. Four adsorption profiles.	81
Fig. 58. Four desorption profiles.	81
Fig. 59. The four adsorption corrected for the incomplete desorption of the previous run.	82

DISCLAIMER

“This report was prepared as an account of work sponsored by an agency of the United States Government. Neither the United States Government nor any agency thereof, nor any of their employees, makes any warranty, express or implied, or assumes any legal liability or responsibility for the accuracy, completeness, or usefulness of any information, apparatus, product, or process disclosed, or represents that its use would not infringe privately owned rights. Reference herein to any specific commercial product, process, or service by trade name, trademark, manufacturer, or otherwise does not necessarily constitute or imply its endorsement, recommendation, or favoring by the United States Government or any agency thereof. The views and opinions of authors expressed herein do not necessarily state or reflect those of the United States Government or any agency thereof.”

ABSTRACT

This document is the First Annual Report for the U.S. Department of Energy under contract No., a three-year contract entitled: "Improving CO₂ Efficiency for Recovering Oil in Heterogeneous Reservoirs." The research improved our knowledge and understanding of CO₂ flooding and includes work in the areas of injectivity and mobility control. The bulk of this work has been performed by the New Mexico Petroleum Recovery Research Center, a research division of New Mexico Institute of Mining and Technology. This report covers the reporting period of September 28, 2001 and September 27, 2002.

Injectivity continues to be a concern to the industry. During this period we have contacted most of the CO₂ operators in the Permian Basin and talked again about their problems in this area. This report has a summary of what we found.

It is a given that carbonate mineral dissolution and deposition occur in a formation in geologic time and are expected to some degree in carbon dioxide (CO₂) floods. Water-alternating-gas (WAG) core flood experiments conducted on limestone and dolomite core plugs confirm that these processes can occur over relatively short time periods (hours to days) and in close proximity to each other.

Results from laboratory CO₂-brine flow experiments performed in rock core were used to calibrate a reactive transport simulator. The calibrated model is being used to estimate in situ effects of a range of possible sequestration options in depleted oil/gas reservoirs. The code applied in this study is a combination of the well known TOUGH2 simulator, for coupled groundwater/brine and heat flow, with the chemistry code TRANS for chemically reactive transport.

Variability in response among rock types suggests that CO₂ injection will induce ranges of transient and spatially dependent changes in intrinsic rock permeability and porosity. Determining the effect of matrix changes on CO₂ mobility is crucial in evaluating the efficacy and potential environmental implications of storing CO₂ in the subsurface.

Chemical cost reductions are identified that are derived from the synergistic effects of cosurfactant systems using a good foaming agent and a less expensive poor foaming agent. The required good foaming agent is reduced by at least 75%. Also the effect on injectivity is reduced by as much as 50% using the cosurfactant system, compared to a previously used surfactant system. Mobility control of injected CO₂ for improved oil recovery can be achieved with significant reduction in the chemical cost of SAG, improved injectivity of SAG, and improved economics of CO₂ injection project when compared to reported systems.

Our past work has identified a number of mobility control agents to use for CO₂-foam flooding. In particular the combination of the good foaming agent CD 1045 and a sacrificial agent and cosurfactant lignosulfonate. This work scrutinizes the methods that we are using to determine the efficiency of the sacrificial agents and cosurfactant systems. These have required concentration determinations and reusing core samples. Here, we report some of the problems that have been found and some interesting effects that must be considered.

EXECUTIVE SUMMARY

This report is a summary of the first year findings of the three-year DOE contract No DE-FG26-01BC15364, "Improving CO₂ Efficiency for Recovering Oil in Heterogeneous Reservoirs." This study is being performed at the New Mexico Petroleum Recovery Research Center (PRRC), a research division of New Mexico Institute of Mining and Technology (NMIMT). The work strives to improve industry understanding of CO₂ flooding mechanisms with the ultimate goal of economically recovering more of the U.S. oil reserves. The principle interests are in the related fields of mobility control and injectivity.

During the first year of this project a number of people joined in this effort with Dr. Reid B. Grigg (principle investigator and a section head at the PRRC) and Research Geophysicist Robert K. Svec to accomplish this work. Dr. Brian J. McPherson, Professor of Hydrology for NMIMT, is contributing on aspects of fluid-rock interaction modeling with graduate student Tristan P. Wellman. Mr. F. David Martin has contributed as a contract advisor and industry liaison. Dr. Zheng-Wen Zeng, Research Associate, joined after completing a PhD in the Department of Petroleum and Geological Engineering at the University of Oklahoma. Dr. Baojun Bai and Ms. Liu Yi have both interrupted their careers in China's IOR Industry to join this effort while working on PhDs in Petroleum Engineering.

Through correspondence and on site interviews, concerns of project engineers for the various CO₂ projects in the Permian Basin have been identified. Injectivity continues to be a concern to the industry and in many cases is the factor that makes or breaks a project. During this period we have contacted most of the CO₂ operators in the Permian Basin. Injectivity continues as a major factor in making or breaking existing projects and is a significant concern for future projects.

Results of laboratory CO₂-brine core flow experiments were used to calibrate a reactive transport simulator. The results from this model are very encouraging in our efforts to estimate in situ effects of CO₂ and brine on the rock matrix. Response among rock types suggests that CO₂ injection will induce transient and spatially dependent changes in intrinsic rock permeability and porosity. As expected this is dependent of rock type. Determining the effect of matrix changes on CO₂ mobility is crucial in evaluating structure and potential environmental implications of long term resonance of CO₂ in the subsurface.

Chemical cost reductions are derived from the synergistic effects of cosurfactant systems using a good foaming agent and a less expensive poor foaming agent. The required good foaming agent is reduced by at least 75%. Also the effect on injectivity is reduced by as much as 50% using the cosurfactant system, compared to a previously used surfactant system. Mobility control of injected CO₂ for improved oil recovery can be achieved with significant reduction in the chemical cost improved injectivity, and improved economics of CO₂ injection project when compared to reported systems.

Our past work has identified a number of mobility control agents to use for CO₂-foam flooding. This work scrutinizes the methods that are used to determine the efficiency of the sacrificial agents and cosurfactant systems, and report on interference between the components in determining concentration, preparation methods, and of cleaning procedures. This work indicates that earlier results appear to conservatively estimate benefits of the cosurfactant systems.

We believe that this work will be of great benefit in developing new fields, improving economics of existing fields, and as ground work for future studies.

CHAPTER I. INDUSTRY INJECTIVITY SURVEY

Introduction

The petroleum industry has been injecting carbon dioxide (CO₂) into geological formations for about fifty years. Currently, about 2 billion standard cubic feet per day (BCFD) of CO₂ is being injected into geological formations to improve oil recovery (IOR). For our project, we identified over 135 reservoirs into which CO₂ is being injected or has been injected into, or has been announced outside the field operating company to be a future flood. These include:

- 70 field projects that are in operation.
- 47 terminated projects, of which at least 20 were field pilots. Most of the others are field projects that have been completed or abandoned.
- 18 projects that have not been started. Of these, about 10 are still listed as future projects and the others were advertised in the past as future projects that for one reason or another (mergers, changes in company philosophy, downturn in oil prices) were not initiated.

These projects represent a number of geographic areas in the lower 48 States of the United States (USA). The states that have or have had projects are listed in Table 1, with number of total projects and active projects indicated. Besides the miscible projects, at least 25 immiscible CO₂ projects have been initiated in the USA; most began and terminated in the 1980s. Only a few projects persisted into the 1990s. Thus, around 160 projects on record have been studied as prospects for CO₂ injection with about 140 actually having had CO₂ injected into a geological formation. The injection time varied from a few months for some pilots to about thirty years for some field projects. These numbers do not include the numerous fields seriously considered for CO₂ injection but never announced outside the company as an imminent project.

Of the miscible tests, about 65% of the total projects and 70% of the current operating projects are located in the Permian Basin. Thirty different organizations have operated CO₂ projects in the Permian Basin. Projects have been performed in sandstone, limestone, and dolomite reservoirs, with over half located in San Andres formations. The other projects are found in more than a dozen different formations. Because of the concentration of projects in the Permian Basin, this region was the focus of a study to assess the effects and long term potential of CO₂ storage in geological formations. This section summarized the results in relationship to injectivity changes.

This type of study becomes more difficult to analyze as time progresses, because of mergers and personnel changes that will result in lost or limited access to valuable information. This was seen in a number of cases. For example, fields such as South Huntley and Ford Geraldine have changed operators since termination and little information was derived from the new operator. Another example is the former Amoco and Shell properties now owned by Oxy that has chosen not to participate in questions that are subject to interpretation. Information from earlier publications and interaction with engineers before the sale were available, but nothing since the purchase.

This study was not carried out as a simple survey/questionnaire but included visits to the engineering center sites of the appropriate operating companies to gather information and obtain clarifications.

Procedure

Over 150 CO₂ projects were initially identified in 16 states of the US. Of these, at least 100 projects were identified in Texas and New Mexico. Among these we found some that had not been CO₂-flooded, nor was the operator ever intending it to be a CO₂ project, as in a number of early projects outside the Permian Basin. We also combined some pilot projects with a later field project or several pilot projects in the same field into one. Table 2 is the list of the projects that were considered in this study. Where present project operators declined to participate, results from earlier work were considered.¹ Among these, some had little available information. About two-thirds of the projects listed in Table 2 had published articles related to CO₂ injection in Society of Petroleum Engineers (SPE) publications: these are listed by field in Appendix A. General observations from this survey, some of which seem intuitive, are in the following section.

Many of the problems that have been encountered could have been avoided or or at least anticipated and minimized with better reservoir characterization. This could become more severe when injecting CO₂ into a geological formation that had not been flooded and/or studied previously. Generally, produced petroleum reservoirs are extensively studied formations with fair amount of detail developed from their production history. These reservoirs still present challenges to the project engineer when starting injection of a fluid such as CO₂, as the flow paths of the CO₂ are not always well understood. Retention of CO₂ in reservoirs was significant in reservoirs that reported this finding. CO₂ and brine injectivities are often lower than expected. In many cases CO₂ saturated water seems to be reacting with the formation to significantly modify injectivity.

Results

Rock types. Four rock types listed, with particular reference to the *Oil and Gas Journal* articles on reservoir rock types (listed in the biannual Enhanced Oil Recovery updates).²⁻¹⁴ Listed in Table 3 are the rock types with the number of reservoirs reporting the indicated one or two rock types. Out of 81 reservoir reporting rock types, 43 report only dolomite as a rock type and 17 others had a mixture of dolomite and one of the other rock types. Thus, dolomite is the principle reservoir type examined in the Permian Basin CO₂ floods. Limestone and sandstone are about equal. Of the 81 projects, 72 have significant amounts of carbonates (dolomite, limestone, tripolite), or contained carbonate as at least one rock type. Thus the general statements in this report are for carbonate reservoirs.

Injectivity. In many injection projects, injectivity is a key parameter dictating the success or failure of the process. This fact is shown in this section as well as in later sections discussing problems, concerns, mysteries, and need for focused research. In many reservoirs, injectivity has been lower than expected. The CO₂ and water injectivities during WAG is often lower than the waterflood injectivity. This decrease in injectivity is more dramatic and persistent than predicted when considering relative permeability effects of multiphase flow. As shown in Table 4, the systems that indicated the magnitude of change of brine injectivity all decreased. There were no reports of water injectivity increasing once CO₂ injection occurred. The decreases ranged from 10% to as much as 100% decrease. In one case, after CO₂ injection, no brine could be injected

during the water half-cycle. The problems seemed to be greater in the carbonates, especially dolomite. The average decrease was in the 40% to 50% range.

During the CO₂ half-cycle the change from waterflood injectivity was not as severe as during brine half-cycles. Because of the lower viscosity of CO₂ (5–10% of brine at reservoir conditions) one might expect the injectivity during the CO₂ half-cycle to reach levels much higher than the waterflood injectivity. In most cases brine saturation remains sufficient to reduce the relative permeability to nearer that of brine, but even with this, CO₂ injectivity is expected to be higher than brine injectivity. For the six systems reporting, CO₂ injectivity ranged from a decrease of 40% to an increase of 30% with an average near-zero change from waterflood injectivity. This is disappointing when an increase was expected. Again, seven others reported a decrease but did not indicate the magnitude.

One might ask, what does it mean when a respondent indicates no injectivity change was noted or had no comment? In discussions with engineers this generally meant that the desired injection rates have been maintained. In many cases, whether or not injectivity changed was not determined. Thus there could be a significant decrease in injectivity that is not noted because injectivity was still sufficient for the desired injection rate.

In one reservoir it was noted that in a part of the field there were no injection problems, another area had brine injectivity decrease below the target injection rate, and in a third area both CO₂ and brine injectivity had decreased below the target rates during both half-cycles. The difference among the three areas of the reservoir was the existence of relatively high, medium, and low permeability, respectively. This is an indication that if a reservoir is operating a waterflood near the injection limit and it is converted to a CO₂ flood, there is a good possibility that the project will be injection-limited and injectivity problems must be considered.

CO₂ reservoir retention. Retention in the reservoir is an important aspect of CO₂ storage when CO₂ is being used in improved oil recovery processes. The objective of improved oil recovery is not to maximize reservoir retention rates, but to maximize profit. The maximum retention would probably correspond to the maximum sweep efficiency and thus maximum oil production, but this is often not the most economical scenario. In several homogeneous, low-permeability reservoirs, it was noted that the sweep was too efficient and the production rate was too slow and/or the timing of a significant oil increase took too long to obtain the desired rate of return on the capital investment. It appears that sufficient heterogeneity in the reservoirs was necessary for some relatively early oil recovery to recoup investment. Then after breakthrough, some action would be taken to mitigate the heterogeneity problem to continue oil recovery while minimizing CO₂ production.

Many of the floods in the Permian Basin are not mature enough for final retention to be predicted. One explanation of decreases in brine injectivity is the increase in trapped gas, so retention in a reservoir would have direct bearing on the injection rate of CO₂. Retention rates were reported for eight reservoirs. This retention ranged from 38% to 100% with an average of 71%. The reservoir that was reported at 100% was a pilot. Respondents speculate that not enough CO₂ was injected and insufficient time was allowed to see the CO₂. After 10 years they still have not seen CO₂ above background. In a more mature reservoir, retention was listed at the low end, 38%. This is the estimated total amount of CO₂ never seen at the surface once injected, so thus not recycled. Essentially 100% of the purchased CO₂ is still in the system; thus, at the end essentially 100% of the fluid will be stored in a reservoir. The other six reservoirs reported CO₂ remaining in the reservoir in the range of 60-90%. These six together also had an average of

71% retention. These estimates were from reservoirs undergoing CO₂ injection from five to 30 years.

In a few cases, it was evident that CO₂ did not go where it was expected to go. In these cases engineers made statements such as:

- a. It was believed that the CO₂ left the intended flooding area.
- b. CO₂ went into an upper and lower zone with much of the reservoir in between untouched. In this case sweep efficiency was less than had been expected.
- c. No CO₂ detected after two years of a pilot. After several years it is believed that the area sweep was better than expected and not enough time was allowed for CO₂ to arrive at the production well.

Each of the three comments above demonstrates that, with better understanding of the reservoir, unexpected results can be minimized.

What has or has not gone well? In asking engineers what has gone well in the project, we obtained inside information on what they were looking at as critical parameters. We asked what had gone well in the project. From Table 5 (to no one's surprise) it is of interest to note that the response to "what has not gone so well" had almost twice as many responses (see the next section). It was also no surprise that the principal concern was the size and timing of the oil response, both as the good or bad aspect of the project. Most engineering studies centered on optimizing and predicting oil response. The fact that respondents mentioned they were pleased with injectivity indicates that it is a parameter. Again, when injectivity is lower than expected in a low permeability system, it can be a significant economic factor.

Other parameters intently considered are CO₂ breakthrough time and production peak and scaling/deposition. Scaling can be occurring within the reservoir; this is a subject being studied by the PRRC and will be covered later.

Mysteries of the system. Reported in this section are items that project engineers felt were not well understood. These are items that, if better understood, would improve the project. This could mean improved profits and in some cases a modification of the project area. Thirty-one of the responses (~90% of the total) desired better understanding of reservoir processing rates, reservoir characterization, and injectivity, which all concern the interconnection of understanding the reservoir, fluid flow, and fluid-reservoir interactions (Table 6).

Research focus. As shown in Table 7, improving sweep and productivity/injectivity were the two major areas of concern for future or continued study. Again, these responses are from individuals that are concerned about improving oil recovery, specifically, profit. The first two items are of major interest to our project: first, an understanding on how the injected fluid processes the reservoir is critical and how this is interconnected to the second response of injection and production rates.

CHAPTER 2. PHYSICAL EFFECTS OF WAG FLUIDS ON CARBONATE CORE PLUGS

Introduction

Injectivity abnormalities in water-alternating-gas (WAG) improved oil recovery (IOR) processes continue to mystify the petroleum industry.¹⁵ A couple of surveys conducted by the New Mexico Petroleum Recovery Research Center (PRRC) on carbon dioxide (CO₂) flooding indicated that loss of injectivity on WAG cycles has been a crucial limiting factor in many projects.¹ Based on the fluid flow properties of CO₂ and other IOR gases, one would intuitively expect that gas injectivity would be greater than the waterflood brine injectivity.¹⁶ However, in practice, this behavior is not always observed. Water injectivity has been reported to be higher than the waterflood brine injectivity (North Ward Estes,^{17,18} Mabee,¹⁹ and Cedar Creek Anticline^{20,21} projects) and lower in other projects (San Andres Levelland,²²⁻²⁴ Slaughter,^{23,24} and Wasson Fields^{23,24} and a number of gas injection tests²⁵). It is perplexing that some reservoirs lose injectivity and others increase injectivity after the first slug of gas (CO₂) is injected, and that this phenomenon may occur on a local scale. Injection wells in the same field and reservoir may have significantly different behavior.

The change of injectivity has been investigated in the laboratory by several research groups with mixed results.^{19,26} Change in rock properties due to fluid/rock interactions can account for some of the field injectivity behavior.²⁷⁻³⁰ In this study, cores of quarried Indiana (Salem) limestone and San Andres dolomite from the Seminole Field in the Permian Basin (Gaines County, Texas) were tested in order to investigate the relationship between WAG fluids and the formation rock. Pressure transient data was collected for calculation of permeability and injectivity. Core flooding was conducted in the WAG sequence at in situ conditions. Crude oil was injected into the core at the start of WAG floods to examine the nature of the multiphase pressure transient that occurs in the following WAG cycle. This is referred to as the oil contamination scenario and is meant to represent the oil flowback process that may occur at the wellbore during WAG half-cycle switchover when wellbore pressure drops and a small amount of oil may flow in from the formation.

Backscatter electron imaging (BSEI) was performed on pre- and post-flood samples to detect changes in the cores. Macroscopic and microscopic dissolution features were observed in all cores exposed to WAG fluids. Carbonate and anhydrite dissolution caused changes in core permeability and porosity. Persistent features (mineral phases) that were stable under flooding conditions were identified in both core types.

Experimental Parameters

A simplified diagram of the core flooding apparatus is illustrated in Fig. 1. Large volumes of brine and CO₂ are supplied from high-pressure floating piston accumulators that are driven by external high-pressure syringe pumps. These pumps, late models with high accuracy digital control, may be configured by the system plumbing for continuous flow or alternating flow to simulate any desired injection scheme. Oil injection was accomplished through a metering pump connected by a valve ahead of the core. System pressure was maintained by a backpressure regulator (BPR) at the core outlet. Each accumulator pressure was maintained by an individual BPR in order to precisely control fluid density and avoid any fluid surges due to multiphase flow

effects. System pressures were measured by absolute and differential pressure transducers and a computer controlled data acquisition board logged the data. “P” and “dP” denote the static and differential pressure at each point respectively. Confining pressure is applied to the outer surface of the sample to eliminate fluid flow along the sample. Injection was halted periodically to measure permeability and porosity of the sample. Once permeability and porosity are measured, the system is repressurized and the experiment continues until the next permeability-porosity measurement or experiment termination.

The properties of the core samples used in the WAG floods are given in Table 8. All floods were conducted at 100°F and 2000 psig back pressure at the core outlet. Core holder overburden pressure was maintained at 4000 psig.

BSEI and compositional analysis was performed on pre-flood samples of each core and on a number of samples from along the length of each flooded core. The electron microprobe (model SX-100) utilized three wavelength-dispersive spectrometers, and an accelerating voltage of 15 kV and 20 nA beam current.

Results

Limestone. The Indiana limestone is a bioclastic grainstone and rather uniform and homogeneous. This core was cut from a quarry rock. The trimmed end was used to represent the rock property before flooding and was examined by BSE imaging in Fig. 2. Grains are composed mainly of calcite with occasional sparse quartz replacement in the grain core. Most grains and shell fragments are one mm or less in diameter and have a significant amount of porosity in their structure. Well rounded grains of both oolitic concentric layering and homogeneous limeclast structures are dominant. Thin hanging overgrowths of very fine (<10 micron) calcite crystals are found on most of the grains. In some instances the overgrowths form the boundary with the intergrain pore space. Intergranular porosity is controlled by the degree of calcite cementation. Approximately hexagonal polygons of calcite occur as small crystals in the hanging overgrowths and as larger crystals, some approaching 100 micron, in the cement.

Since this is a quarry specimen there is no formation brine associated with it. Therefore a laboratory recipe (see Table 9) was used to create brine for the experiments based on the Teague Blinebry dolomite formation brine in southeastern New Mexico. This choice was purely arbitrary and is undersaturated with respect to calcium carbonate. However a series of prolonged (hundreds of hours) brine injections demonstrated that this core was stable, or showed no detectable change in permeability and porosity with prolonged flow of this brine.

The limestone core was exposed to more than 31.5 liters of brine and 30.6 liters of supercritical CO₂ in a series of WAG injections with slug sizes ranging from 0.2 to 18 pore volumes (PV). An apparent increase in permeability was noted at the conclusion of the experiments; however, upon removing the core from the core holder large-scale dissolution was evident and the end-point permeability value was recalculated based on the length of the unchannelled section.

Post-flooding sectioning of the core revealed dramatic dissolution features, principally a channel varying from 0.1 to 0.25 in. diameter and extending from the inlet face to 11 in. deep into the core. BSEI was used to examine samples from several locations along the length of the core. Figure 3 is an example of a pre-flood BSEI of the core, showing the structure and channel before brine or CO₂ injection. After brine and CO₂ flooding, dissolution of varying degrees was observed at all examined locations. The grains and shell fragments appear to dissolve more or

less uniformly from the outside in. Figure 4 illustrates a grain that is almost completely dissolved and a shell fragment that has been completely dissolved. Also noted are some small hexagonal calcite crystals forming inside the remnant cavity left by the shell fragment and an adjacent area of possible calcite cement recrystallization. The original hanging overgrowths appear to be a very stable feature within this rock during the WAG process. In Fig. 5 overgrowths are observed to be largely intact while the grain inside is partially dissolved or even completely missing. Intergrain porosity increases by dissolution of calcite cement.

We suspect that, in this rather long core, the WAG fluid reacts with the limestone and eventually reaches a saturated state with respect to calcium carbonate. If this is correct, as the fluid advances and pressure decreases, the saturated fluid becomes super-saturated and precipitation can result. This is supported by large calcite crystals found in pores and attached to the cement in the downstream side of the core. An image of core downstream is shown in Fig. 6; calcite crystals of larger size than any found in the original texture appear to be growing on the overgrowths. These persistent overgrowths function as nucleation sites for the accumulation of calcite from the saturated solution. Most frequently, these new crystals accumulate on the exterior of the overgrowth and coarsen and grow outward into the intergranular pore space, as in Fig. 7. In a few instances this trend was reversed and the calcite accumulation was occurring on the inside of the overgrowth and filling the space formerly occupied by a carbonate grain or shell fragment (Fig. 7). The hexagonal calcite texture is more common and the crystals reach larger sizes in the flooded core. Although BSE quantitative analysis was performed for Si, Mg, Ca, Mn, Fe, Zn, Sr, and Ba, no significant compositional variation was detected between the pre-flood and flooded samples. It is possible that the crystalline structures downstream just happened to be larger due to natural variations in the system. Subsequent tests that are discussed later included tracers to aid in clarifying this aspect.

Permeability was monitored in the core during the three stages of flooding: brine, WAG, and oil/WAG. These data are shown in Fig. 8. Initial permeability was found to be stable in the range of 36 to 38 md. Exposure to CO₂ during WAG caused a significant decrease of permeability to 19 to 22 md. Further flooding with WAG and oil resulted in an apparent increase in permeability to 44 md. However the discovery of the dissolution channel allowed a permeability recalculation based on the length of the unchannelled section of core at the outlet side (approximately 11 in. long), resulting in a value of 19.5 md.

A highly detailed set of differential pressure calibration data from a multi-tap pressure sleeve was obtained for this core prior to experimental data acquisition. Permeability was calculated for the last 10.2 in. of core. Values of 34 to 37 md were obtained. This is entirely consistent with the initial brine perms determined on the whole core and indicates that the final permeability (19.5md) in this same region is the result of physical alterations due to the WAG fluids and not a pre-existing heterogeneity.

This core was observed to be extremely sensitive to fine particles during the initial brine stability tests where brine alone was flowed through the core. A runaway increasing differential pressure trend was observed when unfiltered brine was injected into the core. Also, the core was plugging due to particles originating in the system plumbing. Subsequently all brine was filtered to 1 micron and a filter pack ranging from 7 micron down to 0.5 micron was installed upstream of the core inlet. When the core inlet face was trimmed off 0.25 in., the initial permeability was restored, indicating that the plugging was occurring at the inlet face and depth of penetration was negligible. If the core permeability reduction were due to fines migration within the core, we would expect to see a sharply decreasing permeability trend as the degree of pore throat plugging

increased. Instead we see the stable permeability reduction we attribute to competing mechanisms of dissolution and subsequent deposition. The process at work in the flooded core is far more subtle, being more or less stable over the course of many weeks of flooding. The permeability decrease in the downstream section of core is therefore thought to be the result of calcite deposition in one form or another and not due to fines migration or some other mechanism.

As further evidence of a calcium carbonate saturated condition within the core during WAG, it was noted that calcium carbonate deposits had formed in the system tubing at the outlet BPR and plugged 3 ft. of stainless steel tubing. These deposits began within the 100°F airbath at precisely the spot in the BPR where the pressure dropped from 2000 psig to ambient. We believe that the WAG fluid moves through the limestone core and dissolves calcite until saturated. Then the calcium and carbonate saturated, CO₂-rich brine is free to interact with the limestone, depositing new crystals and altering cementation in the remainder of the core. Due to the duration of our tests and the large volume of fluids flooded through this core, it appears that the rates of dissolution, crystallization, and alteration are nearly balanced in terms of their effect on core permeability.

Seminole San Andres Dolomite. The Seminole San Andres dolomite cores are vuggy anhydritic, very-fine grain-dominated packstones.¹⁸ There are no major changes in mineral composition between pre-flood and flooded samples examined with BSE imaging and quantitative analysis. Figures 9 and 10 represent the texture of the pre-flood Seminole San Andres dolomite. Figures 11-13 represent the texture of the WAG flooded core. Dolomite is shaded dark gray and anhydrite is very light gray in these BSE images. Dolomite matrix and hollow core dolomite grains are evident in both pre and post-flood samples. Anhydrite occurs as large crystals and also as pore-filling material in the dolomite. In well-filled areas the anhydrite occupies both the pores between the hollow dolomite grains and the hollow spaces within the grains. Quantitative measurements of P, F, SO₃, Si, Mg, Ca, Mn, Fe, Sr, and Ba revealed no significant compositional difference between the dolomite phases present in the pre- and post-flood samples. Nor are there any carbonate crystal features in Figs. 11-13 to suggest that any recrystallization has occurred in the Seminole S139 core.

Dissolution features are most evident in photos of the flooded cores. Figures 14 and 15 represent the texture of the S141 brine flooded core at several slices along its length. Figure 16 represents the texture of the WAG flooded core S139, which was sliced at several points along its length. Anhydrite was observed to have dissolved from within both cores. Large anhydrite nodules were dissolved along the boundary with the dolomite. Small grains of anhydrite (0.08 in. diameter) were observed to have completely been removed and formed vugs (Fig. 14). It is speculated that some anhydrite-filled areas in the granular dolomite texture were washed out by brine solution from the intergrain pores and possibly from inside the grains as well. Examination of pre-flood rock and the flooded cores is not conclusive as to the dominant mechanism for core erosion. Anhydrite is clearly dissolving, but dolomite may be dissolving to a significant degree during the WAG flood (Fig. 16).

Microscope examination of the S139 WAG flooded core shows a residual crusting of dolomite grains in the new vugs. The cementing dolomite phase appears to be less stable in the flooding fluids than the dolomite grains. This residue of grains is far more prevalent in the S139 core plug that was exposed to WAG. The S141 core plug was exposed to 9.5 liters of brine only. The S139 core plug was exposed to 87 liters of brine and 57 liters of supercritical CO₂ during

brine, WAG, and crude oil displacements. Because of the disparity in the volumes it is not possible to state whether the greatly increased cement dissolution is due to the WAG process or the greater amount of brine injected. However, the S141 behavior may be explained by dissolution of anhydrite alone. Examination of the differential pressure behavior for this core reveals that permeability equilibrium was approached; however, no significant dolomite cement dissolution is observed in the BSE images. Dissolution channels visible in Fig. 15 appear to correlate with anhydrite-rich stylolite features that are oriented roughly parallel to the axis of the core. The S139 core (Fig. 16) shows significant dolomite cement dissolution, new macroscopic porosity, and residual grain texture. Initial dissolution probably is by removal of anhydrite by the same mechanism as in S141. Then the channels serve as conduits for the WAG fluids that enlarge the channels further by dissolving dolomite. These trends suggest that the WAG process is causing dissolution of dolomite in this Seminole core.

The permeability to brine for core S139 is shown in Fig. 17. The Seminole core S139 shows a strong increase in permeability that we attribute to dissolution of anhydrite minerals in the core. The permeability data also suggest that a second dissolution process is at work, causing a more gradual increase in core permeability. Indicated on Fig. 17 is the point where CO₂ injection began. Examination of the core indicates that once high conductivity channels were established by dissolving anhydrite in nodules and anhydrite filled porous dolomite, then slow dolomite dissolution was accomplished by the CO₂-rich flooding fluids. This continuing dissolution process at work on the dolomite caused the strong increase in measured permeability.

No evidence to support carbonate deposition was seen in either the permeability data or BSE imaging. No significant deposition of carbonates was found in the system tubing either. This suggests that the WAG fluids remained undersaturated with respect to carbonate minerals in the dolomite core. An extension of this work would include the flooding of a long core (not done due to limits on recovered well core size) or a composite core of several shorter segments in a series arrangement. By increasing the residence time and core mass exposed to WAG fluids we would increase the possibility of reaching saturation and inducing deposition of carbonates in these dolomite cores. Further study of carbonate deposition in dolomites could shed light on some of the perplexing WAG behavior in San Andres reservoirs.

During the WAG tests a 1.22 in³ (20 ml) aliquot (less than one-half pore volume) of crude oil was periodically injected into the core to simulate contamination from crossflow or oily water injection. Crossflow is expected to occur during times of depressurization caused by injection disruptions due to cycle changes or maintenance. The displacement by WAG tests was conducted to detect any long-term effects that the reintroduction of oil in the core might produce. Injection effects or injectivity is shown in Figs. 18 and 19 as the injection rate per pressure drop across the core versus time. Only temporary permeability reductions or decreased injectivity due to three phase relative permeability effects were observed. The temporary permeability reduction normally lasted one WAG cycle. When oil was followed by CO₂ the permeability reduction was very short-lived (less than a half-cycle) and was usually undetectable in the following brine half-cycle (Fig. 18). During these tests each half-cycle lasted about twelve hours at an injection rate of 6.1 in³/hr (100 ml/hr). When the oil injection was followed by brine, permeability reduction was long-lived and was also observable in the beginning of the CO₂ half-cycle (Fig. 19). Injectivity was also affected by the half-cycle preceding oil injection. In both Figs. 18 and 19, injectivity was the lowest when oil was preceded by a brine half-cycle. This is particularly evident in Fig. 19 where brine follows the oil injection, and to a lesser degree when followed by CO₂, in Fig. 18.

Limestone flooded with a tracer brine. As discussed previously, carbonate cores of Indiana limestone and anhydrite-rich Seminole San Andres dolomite were flooded with a synthetic field composition brine and supercritical CO₂. A strong dissolution effect was seen in both core types. The permeability data from the limestone core suggested that the processes of carbonate dissolution and precipitation could be occurring simultaneously in different regions of the core during WAG injection. Several samples from the flooded cores were examined using backscatter electron imaging (BSEI) and quantitative measurements. Samples were also analysed by atomic absorption (AA) spectroscopy. No definite structures or chemical changes could be conclusively shown to have resulted from the carbonate precipitation that was suspected to have occurred within the core. The changes could also be considered a natural difference in heterogeneity.

A new approach using a tracer brine of simplified composition was designed. The new brine would contain elements which occur only as trace impurities in the limestone. These elements, having a valence of 2+, would be available to incorporate into the new precipitated carbonate mineral and produce an enrichment which would contrast with the original rock mineral composition. The Indiana limestone, a bioclastic grainstone composed primarily (>99%) of calcite (CaCO₃), was used in the new core flood experiment. This system has sufficient permeability and porosity for our laboratory measurements and is a compositionally simple carbonate rock.

The brine formula used in the experiment, listed in Table 10, is composed of 5 salts, all chlorides. The elements Mn, Mg, and Sr are known to occur in calcite as impurities. Our Indiana limestone contains only trace amounts of these elements. If new carbonate mineral is precipitated during the flood then it may incorporate some or all of these elements from the brine. By BSEI and quantitative measurements, the sites in the core sample that are enriched with respect to these elements may be identified. This would allow us to identify the mode of precipitation. For instance, it should be possible to see if precipitation is growing on the existing grain structure or forming new grains. Also, it should allow us to locate where the precipitation occurs with respect to the pore structure, ie intergrain vs intragrain porosity.

Experiment. The apparatus used for the core flooding experiment is similar to the one used in previous work (Fig. 1). The basic equipment has been augmented by an array of differential pressure transducers and an expanded data acquisition system run by a PC. The differential pressure transducer array could not be fully utilized when the multiport sleeves failed. However, the hardware was retained in anticipation of future work.

The flooded core was composed of two pieces of Indiana limestone, referred to as Segment A and Segment B. Physical parameters of the core segments are listed in Table 11. The initial configuration for this experiment utilized a multiport viton rubber sleeve which was connected to several pressure tap connections on the core holder body. These pressure taps were connected to an array of differential pressure transducers. In theory, this should have enabled us to measure not just the pressure drop across the core, but actually to resolve the pressure drop across several regions, which would give complete coverage of permeability changes along the core.

Unfortunately this approach failed due to blockage of the pressure tap connections. This problem was very difficult to diagnose; however, we eventually discovered that the source of the blockage was in the core sleeve itself. The rubber material was able to deform enough under

pressure to block off the pressure tap connection at the sleeve/rock interface. This problem was not observed in earlier work but a dissection of the core sleeve revealed that the new sleeves had a simplified pressure tap hardware design that was not suitable to our requirements. After several failed attempts to mitigate these problems the multiport sleeve approach was abandoned. Non-tapped sleeves were substituted and the experiment continued.

These hardware problems caused several difficulties in the acquisition and analysis of the permeability data. Instead of complete resolution of the core permeability at all times during the experiment, we are left with only periodic evaluations of the core segments A and B permeabilities at irregular intervals.

The injection scheme was a constant ratio (1:1) brine and CO₂ coinjection. The initial combined flow rate was 80cc/hr (18.28ft/day), but was later reduced to 40cc/hr (9.14ft/day). The cores were periodically cleaned and dried, then removed from the core holder for inspection. Both of the core segments were measured for porosity and, after the failure of the multiport sleeve approach, each was tested for brine permeability. Then the core was reassembled into the same orientation and tested for whole core brine permeability. After this, the coinjection of brine and CO₂ continued.

Preliminary results: Over the course of the experiment 15.1 liters of each phase (brine and CO₂) were coinjected, so the total volume of coinjection was 30.2 liters. An additional 5 liters of brine were used in single-phase injection during CO₂ desaturation and the brine permeability and porosity measurements. Since the original pore volume of the core totaled 195cc, a total of 155 pore volumes (PV) of fluid was coinjected.

Strong changes to both permeability and porosity occurred in both core segments. Figures 20 and 21 show the trends in core porosity and pore volume, respectively. Note in Fig. 21 that both core segments show an initial decrease in porosity until about 55 PV injected when the porosity begins to increase. This interval corresponds to the injection of a combined rate of 80 cc/hr. This effect is stronger in segment-A, which is the upstream side of the core. The segment-A pore volume is observed to decrease from 57.64 cc to 53.61 cc (-7.0%) during the first 55 PV of injection. During the same period the segment-B porosity decreases from 137.2 cc to 129.72 cc (-5.5%). During the next 100 PV of coinjection (55 PV to 155 PV), at a combined injection rate of 40 cc/hr, porosity is observed to increase in both core segments. The segment-A pore volume increases substantially from 53.61 cc to 66.9cc (+24.8%) and the segment-B pore volume increases modestly from 129.72 cc to 135.54 cc (+4.5%). The reason for this behavior with injection rate has not yet been identified; however, it may be possible to correlate solubility and reaction rates to the chemical analysis performed for several samples along the core.

Core permeability to brine is shown in Fig. 22. Core segments A and B permeabilities are unavailable until midway through the experiment because of the instrumental failures involving the multiport sleeves mentioned earlier. However, the whole core permeability is observed to decrease monotonically during the first half of the experiment. Segment-A was originally a much higher permeability core than segment-B, so the segment-A permeability is plotted against its own axis on the right. It is very interesting to note that, during the early part of the flood, while the whole core permeability was decreasing, the formation of a solution channel was observed during periodic visual inspection of the core (Fig. 23). At 10 PV coinjected, the core inlet surface on segment-A was slightly roughened by solution of the coinjected fluids. When the core was inspected after 56 PV of coinjection a small solution channel had begun to form, apparently extending only several millimeters into the core. By 84PV of coinjection a solution channel was

clearly established, extending tortuously into the core and out of view. Termination of the experiment was triggered by the very high permeability of 1978 md measured on Segment-A after 155 PV of coinjection.

Upon sectioning, the flooded core the channel was found to extend nearly to the end of Segment-A (Fig. 24). Flow direction is indicated on the figure by the arrows. The tortuous path of the solution channel is clearly visible in segment-A. Near the end of the channel, it appears to broaden and terminate into a region of solution enhanced porosity. On the adjacent face of segment-B there also appears to be a region (highlighted by the oval) of solution-enhanced porosity. These two regions were in contact when the core segments were installed in the core holder during flooding. There are no visible solution or deposition features in the remainder of Segment-B.

By reference to the permeability plot in Fig. 22 we see that the whole core permeability was decreasing while this solution channel (an intrinsically very high-perm feature) was making progress through core segment A. Therefore another process, which was capable of reducing the core permeability, must have taken place simultaneously and to a degree that overrode the solution channel permeability enhancement effect. The only factors which might affect core permeability in this way are fines migration with subsequent pore plugging or occlusion of pores by the deposition of new mineral material. The introduction of any foreign external particles is prevented by filters (0.5 micron) at the core inlet. Also it must be noted that the porosity of segment A decreases during the initial stage of solution channel formation, so some deposition must be occurring which temporarily overrides the channel's effect on porosity.

A chemical and BSEI analysis was performed at the conclusion of coinjection to examine the core at several points along its length. Preliminary results have been received for the chemical analysis, but the BSEI work is only half completed with no quantitative results or images yet available. Observations of the samples to date reveal an increase of heavy elements (primarily Mn), which were present in the brine but not present in the fresh rock. These elements were added to the brine as chlorides. A scan of the samples revealed no chlorine present, so residual brine salt may be ruled out as the source. The precise mode of deposition or the abundance along the core can not yet be determined because only half the samples have been examined thus far.

The results of the chemical analysis are clear and tend to support the theory that new material was deposited that incorporated some brine elements. The sectioned core segments were sampled by removing 0.5 in.-diameter core plugs at regular intervals, indicated in centimeters on Fig. 25. Flow direction is indicated by the arrows. Each core plug was cut in half, with one piece used for the chemical analysis and the other used for BSEI. Chemical samples were pulverized to powder and dissolved in acid, then analyzed by the ICP-MS method for Ca, Mg, Mn, Sr, Fe, Zn, Pb, Ba, Na, and K. Fresh rock samples trimmed from the core segments before flooding were used to establish baseline rock properties. Elements present in the original core material as detritus (Na, K, Fe) show a scatter of concentrations throughout the core and are not diagnostic of any process related to flooding. Elements such as Ba, Zn, Pb, which may be present in the CaCO₃ grains, cement, and overgrowths are present along the core in only trace amounts and show no significant variation along the core. These elements were not intentionally added to the brine and so are believed to reflect only the original rock composition occurring as trace impurities within the calcite structures.

The elements Ca, Mg, Mn, and Sr are expected to be present in the coinjected fluid because they were included in the brine as chlorides, and also, in the case of Ca, because of

dissolution of the CaCO_3 at the core inlet. The Ca plot in Fig. 26 shows a significant increase over the baseline at the 30 to 35 cm points. However this data is somewhat ambiguous due to the analytical method (ICP-MS), which is designed for trace studies and thus may have resulted in increased analytical error. The identical samples will be retested using an EDTA titration method, which will give tighter controls and higher resolution in this highly concentrated range (>310000 ppm). The Mg data in Fig. 27 reveal a similar enrichment peak compared to Ca. The Mg concentration is generally significantly elevated above the baseline level. The Mn data are very strongly elevated (up to 1000 times) above the baseline level (Fig. 28). The trend is a peak at 15 cm and trails off toward the end of the core. This trend is also seen in the Sr data (Fig. 29). The Sr peak is found also at 15 cm and trails off toward the end of the core. The Sr peak is over twice the baseline level and all the data are significantly elevated with respect to the baseline.

The trends in the elements Ca, Mg, Mn, and Sr, added to the brine to serve as “tracers”, reveal distance correlatable trends. In the case of Mn and Sr the peaks correspond, within spatial resolution, to the position of the solution channel that had reached approximately 17 cm into the core. For Ca and Mg the spatial trend is shifted more towards the middle of the core and may reflect the region where Ca saturation was maximized by the interaction of the coinjected fluids and the CaCO_3 core matrix.

Due to the simplified brine composition used, there are no anions present in the brine beyond trace contaminants, except chloride. Preliminary results of the BSEI reveal no chlorine present in the samples. Therefore any of the “tracer” elements that were added to the brine and appeared in the flooded core must be present as carbonates, most likely as components of a calcite-based mineral or perhaps as distinct carbonate phases. This question will be resolved by the BSEI tests currently underway. The carbonate anions needed to form these new minerals must be contributed either by the solution of the original core calcite near the inlet or by the abundant bicarbonate present in the solution due to the supercritical CO_2 in the coinjection stream. Unfortunately, no practical method has yet been devised to investigate if and to what extent the CO_2 contributes to this process.

Conclusions

1. Dissolution features were observed in both the dolomite and limestone cores. In the dolomite core, anhydrite dissolution occurred during brine flood and dolomite dissolution occurred during the WAG cycles. In the limestone core the calcite dissolved during the WAG process.
2. In the shorter dolomite core no carbonate deposition was detected, while in the longer limestone core significant carbonate was deposited downstream. But in neither case was significant impurity compositional difference detected with respect either to pre- and post- flooding samples or position along the core.
3. In the limestone core both permeability increases and decreases were noted. The permeability increases were caused by dissolution of calcite grains and cement and channel formation. The permeability decreases appear to be caused by precipitation of calcite in the downstream area of the core once calcium carbonate saturation is reached in the WAG fluid.
4. Oil contamination tests performed in both core types showed no evidence that oil contamination would cause permanent permeability reduction. In each case, the system

returned to pre-oil conditions after CO₂ was injected into the system. However, an injectivity reduction effect was noted if the oil slug was followed by a brine half-cycle.

Implications for Field Injectivity

What implications do these laboratory tests have for CO₂ flooding field projects? Since the cores were only 5 to 20 in. long, they most closely simulate near-wellbore conditions. Dissolution of carbonate or other soluble minerals occurring near wellbore would increase porosity, permeability, and injectivity. Both dissolution and deposition of carbonate could occur as fluid advances a short distance into the reservoir. As fluid flows away from the wellbore, the carbonate solubility decreases with the rapid pressure drop. If the fluid is at or near saturation then solid mineral phases will precipitate, changing formation porosity, permeability, and/or injectivity. Thus, injectivity can be both increasing and decreasing locally; whichever process dominates will be measured at the surface. Though these tests indicate that oil contamination effects should only be temporary near-wellbore, they might have implications deeper into the reservoir.

CHAPTER 3. EVALUATION OF CO₂-BRINE-RESERVOIR ROCK INTERACTION WITH LABORATORY FLOW TESTS AND REACTIVE TRANSPORT MODELING

Introduction

The long-term goals of the work in this area of study is to understand the effect on injectivity and flow in improved oil recovery from CO₂-brine-reservoir rock interactions and to assess the viability and environmental implications of CO₂ injection into the subsurface. Following injection, some mineral or aqueous trapping may occur,¹ transforming CO₂ into less mobile forms, effectively providing permanent sequestration. However, as in-situ pH decreases, dissolution of the rock matrix may occur, increasing fluid mobility. If CO₂ is in a supercritical state, buoyancy may induce CO₂ flow towards the surface. If buoyancy forces dominate and CO₂ returns to the surface, potential environmental and safety hazards could result. However, if CO₂ is injected into low permeability units at sufficient depths, the likelihood of permanent sequestration increases. Wawersik et al.³² provide a comprehensive review of science and engineering issues associated with geologic CO₂ sequestration.

As presented earlier, we have conducted several coreflooding experiments at reservoir conditions to quantify fluid-mineral interactions and the resulting permeability-porosity relationships of various rock types. A current pilot injection project³³ by Los Alamos National Laboratory, New Mexico Petroleum Recovery Research Center, Sandia National Laboratories, and Strata Oil will provide data to test a new reactive transport simulator on a reservoir scale.

In this section, we focus on comparing simulator predictions to laboratory coreflooding experiments as a means to evaluate model efficacy. Specifically, we detail comparisons of the reactive transport simulations to laboratory results that were presented in a previous chapter and paper.³⁴ Further, we discuss, using numerical predictions and laboratory results, the potential impact of injecting CO₂ in various geologic media.

Previous Research

Numerical simulation of CO₂ geologic sequestration remains in the developmental stage, with only a few studies, which are summarized in this section of the Report. Even fewer studies have employed reactive transport simulators, and much of this research is proprietary or in developmental stages. A brief overview of published previous work in CO₂ sequestration modeling is provided in this section.

Non-reactive transport modeling began in the early 90s when Van der Meer³⁵ simulated CO₂ sequestration in a circular anticlinal stratigraphic trap. In his simulations Van der Meer injected 2750 ton day⁻¹ of CO₂ into six injection wells within a 164-ft-thick sandstone unit dipping one degree. Lateral CO₂ migration was caused by upwardly decreasing pressure gradients, and vertical migration occurred from buoyancy forces resulting from density contrasts between CO₂ and brine. Van der Meer concluded that two to three percent of the porous media could be used to store CO₂ before it escaped past the edges of the anticlinal limbs of a stratigraphic trap. A subsequent study by Holt et al.³⁶ modified the black oil simulator ECLIPSE 100 to include the solubility of CO₂ in H₂O and incorporated empirical relative permeability relations between liquid and gas phases, previously neglected by Van der Meer.³⁵ However, reactive chemistry between the fluid and media was not considered in either. Their findings showed that injection rate and absolute permeability were the dominant factors of migration of injected CO₂. In

addition, they found that under high injection rates viscous forces dominated fluid flow, with CO₂ preferentially flowing through higher conductivity pathways, whereas under low injection rates gravity segregation dominated and a stability front resulted.

Another study by Van der Meer⁶ addressed CO₂ injection into a two-dimensional, quasi-infinite aquifer and concluded that it was possible to sequester significant amounts of CO₂ in the subsurface but added that capturing the combined effects of viscous fingering and gravity segregation would require three-dimensional modeling. A study by Lindeberg³⁸ described simulations of CO₂ injection at 26,000 ft depth in a horizontally finite aquifer. CO₂ was injected at a rate of 1.65×10^5 ton day⁻¹ for 25 years into a 525-meter thick unit. He concluded that CO₂ storage was feasible beneath horizontal seals provided that injection locations are sufficiently deep.

Law and Bachu³⁹ conducted a study incorporating the STARS model to simulate multidimensional, multicomponent flow and transport of CO₂ injected into a sedimentary basin for 30 years. The STARS model allows phase partitioning between separate and dissolved phase CO₂. They limited their injection rates so that pressure was below 90% lithostatic, to avoid hydrofracturing and varied porosity and permeability and other parameters to assess the effects of CO₂ injection rate, amount, and distribution. As did previous studies, they neglected chemical reactions between the media and fluid. They concluded that the most important factors affecting CO₂ storage potential include intrinsic permeability and injection pressure, while the unit thickness is moderately important. Variable porosity produced minimal effects on the results.

Weir et al.⁴⁰ used the multiphase, multicomponent TOUGH2 model to simulate CO₂ injection in geologic media. In their model, they injected CO₂ at an average rate of 9500 ton day⁻¹ to a depth of 9700 ft in a 9840-ft-deep fresh water aquifer. They neglected reactive chemical reactions between the fluid and media. Their results showed that using a 20:1 ratio of horizontal to vertical permeability, 12% of the injected CO₂ would escape to the atmosphere in 12 years. They also concluded that the most significant factor affecting volumetric CO₂ storage potential is intrinsic permeability.

Patterned after the work of Weir et al.,⁴⁰ Cole⁴¹ developed a CO₂ equation of state for use with the TOUGH simulator that incorporated the effect of capillary pressure phenomena. In addition he changed the previously employed variable switching technique used in TOUGH2 to a persistent set of primary variables applicable in both saturated and unsaturated conditions. Cole performed a sensitivity analysis to assess which physical parameters controlled the long-term storage of CO₂. His analyses indicated that, in agreement with previous studies, absolute permeability was the dominant mechanism controlling CO₂ migration. However the injection rate and injection depth were also of significant importance. Again, he did not consider chemical reactions among media, formation fluid, and injected CO₂.

Johnson et al.⁴² used the simulator package NUFT⁴³ to model CO₂ sequestration in geologic media. The NUFT simulator models the reactive transport of CO₂ injected into geologic media. Simulations were patterned after field-scale CO₂ injections that are taking place at Statoils North-Sea Sleipner facility. The near field geologic system at the facility consists of 650 ft thick porous sandstone saturated with saline formation water and an 82-ft-thick shale capping layer. CO₂ injection was simulated at a rate of 30 ton day⁻¹ for 10 years (prograde) followed by a period of 10 years of zero injection (retrograde). Their findings indicated that intra-aquifer structures have the most control of separate phase CO₂ migration paths and solubility within the aquifer unit, but that a capping layer at least 25 meters thick is required to prevent CO₂ from eventually escaping into the atmosphere. Results from the simulations showed that intra-aquifer structures

attenuated the supercritical CO₂ plume, causing more fluid to interact with a larger body of formation fluid and resulting in more dissolved CO₂ and smaller vertical migration velocities. However, regardless of whether intra-shale units were present, the immiscible CO₂ plume migrated toward the surface. In each simulation, the low permeability capping layer effectively confined all injected CO₂. These simulations indicated negligible mineral precipitation. The significance of the minimal precipitation (0.05 to 0.2% volume fraction) is questionable in light of the uncertainties present in estimating reactive transport modeling parameters such as mineral kinetic reaction rates. The simulations showed magnesite to be the dominant mineral to precipitate in the capping layer, with the maximum precipitation less than 1 percent of the total volume after 30 years. The magnesite precipitation is hypothesized to seal the microfractures present in the shale unit and therefore acts to increase its sealing ability with continued CO₂ flushing. The overall results revealed that precipitation may be an influencing factor in cases where minute changes in porosity result in extreme permeability changes.

In summary, previous work indicates it is possible to sequester CO₂ in the subsurface for long periods under ideal conditions. Previous studies also suggest that absolute permeability of both the aquifer and capping layer are the dominant geologic controls on CO₂ migration.

Software, Hardware, and Procedures

TRANSTOUGH Simulator. The TRANSTOUGH simulator is a combination of three individual modules: TOUGH2,⁴⁴ EOSCO2,⁴¹ and TRANS.⁴⁵ TOUGH-EOSCO2⁴¹ can simulate the flow of mass and energy, including multiphase CO₂. At the convergence of each time step, execution control is passed from TOUGH-EOSCO2 to TRANS, which then repeats the TOUGH-EOSCO2 time step, simulating the coupled chemical processes at the thermodynamic conditions simulated by TOUGH-EOSCO2. In the present form the modules are sequentially coupled. To minimize potential numerical errors an independent driver program was created to facilitate execution control and variable updates, rather than modify each module directly.¹⁵ Coupled variables are therefore updated and passed at the convergence of each time step through the driver program. Together, the coupled TRANSTOUGH model simulates multidimensional, multiphase, multicomponent, nonisothermal, reactive transport in porous media.

Some of the limitations of this version of the TRANSTOUGH simulator are intrinsic to each coupled module, while others are a direct result of the sequence compiling approach we adopted. The main limitation of EOSCO2 is that it models a pure H₂O-CO₂ system. In other words, the CO₂ equation of state does not incorporate the influence of other chemical species on fugacity or solubility, for example. Therefore simulations are limited to low total-dissolved-solids brines. In addition, our model simulations tended to be unstable unless upstream weighting was employed, which promotes excessive front smearing. We reduced front smearing by decreasing time step size with the tradeoff of increasing computational expense in the simulation. The main limitation of the version of TRANS used in this work is the extended Debye-Huckel equation to calculate activity coefficients, which is usually accurate for brine solutions below 1 molal (M). Therefore, brine concentrations are limited to 1 M.

Details of the version of TRANSTOUGH model used in this study were presented by Wellman,⁴⁶ who presents a summary of model structure, module design, mathematical relations, and evaluation of both global mass balance and sequentially coupling chemical transport and flow. Mass balance error was tested for both one- and two-dimensional systems and found to be

both a function of injection rate and time step size. In all cases global mass balance errors were less than 1.6% but could be constrained to less than one percent by decreasing time step size.

Model domain. All CO₂-brine injection experiments involve the same basic mechanical configuration discussed earlier (Fig. 1). The laboratory core experiments were simulated using a one-dimensional 100-cell horizontal column with each cell measuring 0.018 in. by 0.018 in. by 0.2 in. (Fig. 30). Non-boundary cell volumes were preserved to match the experimental dimensions, but the Dirichlet effluent cell was assigned a larger volume of $3.5 \times 10^7 \text{ ft}^3$ to maintain constant boundary conditions for temperature and pressure. In comparison to Cole,⁴¹ the experimental injection rate to cell volume ratio was four to five orders of magnitude greater. This required injection of fluids to be partitioned across the first four grid cells, inducing fluid flow from the injection area towards the effluent cell. We assigned the Dirichlet effluent cell a constant pressure of 2000 psi to represent the BPR in the core flooding system. Pressure in the remaining model cells was allowed to fluctuate.

Rock characteristics. Two models were developed explicitly to simulate actual core flow experiments. One was a dolomite-anhydrite system representing San Andres core from the Seminole field in west Texas. The second was calcite representing quarried limestone. Three other rock types were evaluated in sensitivity analyses to complement the two coreflow experiments. The mineralogical volumetric percentages for each media are presented in Table 12. Quartz was chosen for its low reactivity with formation fluids. Evaporite and carbonate mineral fractions within quartz sandstone were chosen to characterize chemical reactivity of lithologically heterogeneous media.

The anhydrite mineral fraction in the experimental dolomite-anhydrite rock was estimated to be about 20% by visual inspection of several trimmings from the core stock. The resulting amount of dolomite was calculated as the residual fraction, accounting for the measured porosity.

Mineral reaction kinetics. In order to determine the influences of varying lithology, fluid-mineral reaction rates must be quantified for simulator input. Mineral kinetics in TRANS are calculated as a function of the prescribed kinetic rate and the degree to which the fluid is in equilibrium with the geologic media. The rate of reaction in TRANS decreases as the system approaches equilibrium and conversely increases as the system diverges from equilibrium.

The reaction kinetics for calcite in a chemically unsaturated solution were estimated using a relation from Sjoberg and Rickard,⁴⁷ given by

$$R = K[H]^{0.90} \tag{1}$$

where the hydrogen activity ([H]) and temperature (T), control the reaction rate (R). In this relation the kinetic term (K) is a function of temperature. The rate was determined as the product of the rate constant, and hydrogen activity. Based on a temperature of 100°F and a brine solution of pH 4.0, the calcite reaction rate was estimated as $\sim 5.0 \times 10^{-7} \text{ lbmol lb}^{-1} \text{ sec}^{-1}$. However, to be compatible with the TRANS simulator, the mineral reaction rate must be specified in terms of surface area rather than per unit mass.

An idealized relation was employed to estimate the surface area to volume ratio where

$$S = (6 / D)\lambda , \tag{2}$$

in which it is assumed that the effective surface area to volume ratio (S) could be approximated by spherical grain particles of diameter (D), corrected for a roughness coefficient (λ). The roughness coefficient depends on the degree of weathering, physical mineral properties, and in some cases laboratory preparation.⁴⁸ We assumed a roughness coefficient of 1. We estimated a mean grain size diameter of 0.004×10^{-3} in.⁴⁹ Using a roughness coefficient of 1 and mean grain diameter of 0.004 in. in the above relation (Eq 2), the surface area to volume ratio of the calcite media was estimated at 60,000 to 1. Applying our surface area to volume estimation and multiplying by mineral density (165 lbs ft³), the reaction rate of calcite was calculated to be $\sim 1 \times 10^{-7}$ lbmol in⁻²sec⁻¹, within an order of magnitude of laboratory values measured at 77°F.⁵⁰ Since the solubility of calcite decreases as a function of temperature, we expected a lower solubility.

In addition to calcite reaction rates, Stumm also measured reaction rates of dolomite and quartz.⁵⁰ The dolomite reaction rate was measured to be roughly an order of magnitude slower than calcite. The quartz reaction rate was reported to be roughly eight orders of magnitude slower than calcite. These relative mineral rate differences were used to estimate the reaction rates of dolomite and quartz, relative to the calculated kinetic reaction rate of calcite at 100°F. In addition, since the dolomite-anhydrite sample in the completed experiment exhibited porous cavities, the effective surface area of fluid-mineral contact decreased.⁴⁸ To account for the decrease in effective surface area, the dolomite reaction kinetics were decreased by an order of magnitude. Therefore, model reaction rates for dolomite and quartz were calculated to be 1×10^{-9} lbmol in⁻² sec⁻¹ and 1.0×10^{-15} lbmol in⁻² sec⁻¹ respectively. However, due to the widely reported difficulties of precipitating dolomite under laboratory conditions,^{51,52} dolomite reaction kinetics were turned off in simulations without an initial dolomite mineral fraction. Dolomite precipitation requires microbial intervention.⁵³ The TRANSTOUGH simulator predicts dolomite precipitation in a microbe-rich environment, and in laboratory environments (microbe-poor environments) reaction kinetics must be manually turned off.

Reaction rates of magnesite and dolomite were assumed to be equal. Initial evaporite reaction rates were estimated as an order of magnitude faster than calcite at 1×10^{-6} lbmol in⁻² sec⁻¹. As with dolomite (in the dolomite-anhydrite sample) the reaction rate of anhydrite was adjusted for preferential flow due to cavities present in the experiment sample. In addition, the anhydrite was observed to be concentrated in nodules rather than being dispersed through the sample. We decreased the reaction rate by an additional order of magnitude to account for the lower effective reactive surface area of the nodules in relation to a disperse media. Table 13 summarizes the mineral kinetics used in this study. These reaction rate estimations were used for all simulations.

Brine composition. The base brine composition used in all TRANSTOUGH simulations, summarized in Table 14, is based on samples of Seminole brine from west Texas. All species, except pH and CO₂(aq), are identical in all simulations. The CO₂(aq) concentration and pH concentrations tabulated in Table 14 are those used in the completed dolomite-anhydrite experiment.

A sensitivity analysis was conducted to evaluate the effect of changing brine pH and alkalinity, and media type; i.e., by varying the values tabulated in Table 14. The range of alkalinity in siliclastic aquifers typically ranges from 50-200 ppm, while alkalinity in carbonate aquifers is much greater, usually ranging from 200-400 ppm.⁵⁴ The dolomite-anhydrite experiment employed an alkalinity value of 305 ppm. These reported minimum, maximum, and experimental values (input as HCO₃⁻) were simulated for each media type to characterize the impact of alkalinity. Simulations representing pure quartz and pure calcite media used

appropriate published ranges for siliclastic and carbonate aquifers. Quartz alkalinity values were assigned to the quartz-*evaporite* media, while the carbonate alkalinity values were assigned to the quartz-*carbonate* media. The experimental alkalinity in the suite of siliclastic simulations is greater than the typical maximum for siliclastic aquifers. However, such high alkalinity could be used to represent a scenario of fluid flushing from a carbonate into a siliclastic aquifer. The solution pH was varied in a similar manner as alkalinity.

A pH range of deep basin reservoirs of 6.5 and 8.5 was used. Since the solution pH in the laboratory flow experiment was calculated as 8.4, we set the upper pH limit to 8.4 instead of 8.5. As a result, pH was varied among 6.5, 7.5, and 8.4. Table 15 summarizes the parameters used in the sensitivity analysis. Values labeled “*” designate the brine fluid composition of the dolomite-anhydrite experiment.

Chemical reactions. The chemical reactions (Table 16) used by the TRANS simulator are prescribed through a modified version of a thermodynamic chemical database from Wolery.⁵⁵ Homogeneous reactions involving aqueous species were treated as local equilibrium reactions. Therefore CO₂(aq) and H₂O instantaneously partition into their associated secondary species at each time step. The described mineral reactions are kinetically driven. This suite of highly simplified aqueous reactions was employed for both the sensitivity analysis and the completed dolomite-anhydrite experiment-model comparison.

Results

Dolomite-anhydrite experiments. In this section we compare TRANSTOUGH simulator predictions to the dolomite-anhydrite experiment results. Input parameters are described below.

Temperature: The core flooding system was held at 100°F, which was represented in the TRANSTOUGH simulator as an isothermal system at the same temperature.

Pressure: The coreflooding system uses a BPR valve to maintain fluid exit pressure above 2000 psi. Maintaining a constant exit pressure in the TRANSTOUGH simulation was achieved by assigning a Dirichlet boundary condition at the effluent cell at the same pressure.

Porosity: the initial measured dolomite-anhydrite bulk porosity of 13% was implemented as a homogeneous porosity in the model simulation.

Permeability: the initial measured bulk permeability of 30.6 mD was implemented as a homogeneous permeability in the model simulation.

Injection Rate: CO₂ and brine injection were alternated several times over the course of the experiment. Less than 1% oil (by volume) in one time interval was also injected through the column. Oil is not modeled by EOSCO₂, is not extremely reactive with geologic media on short time scales, and is a minor component of the total volume injected. Therefore, it was deemed necessary to mention but reasonable to neglect its presence in model simulations. Also since alternating injection is currently not an option in the TRANSTOUGH simulator, fluid was injected at the average volumetric rate of 21.52 cm³ hr⁻¹ and 33.09 cm³ hr⁻¹ for the CO₂ and brine respectively. Therefore in the simulations constant brine-CO₂ flushing were simulated, contrary to the actual oscillating injections where pure fluid flow (either CO₂ or brine) will occur for portions of the experiment. Therefore, the saturation history was different. However, the same equivalent number of PV pass through the test core, at an average rate.

The input data are summarized in Table 17.

Model predictions were consistent with experimental results, suggesting that the TRANSTOUGH model may be used to simulate subsurface CO₂ injection and its effect on geologic media, at least at the bench-scale and for short time scales. Over the course of the four month experiment, approximately 145 L of supercritical CO₂ and brine were injected into the dolomite-anhydrite core. Periodically the core assembly was depressurized and drained in order to measure the porosity of the core sample. Since the core did not need to be depressurized to measure the absolute permeability, measurements were taken when the porosity was measured, and also at several times between porosity measurements. For our analysis, we compared the TRANSTOUGH simulator predictions to experimental results where both the porosity and permeability were measured (Fig. 31).

The solid lines in Fig. 31 represent the measured porosity and permeability, and the dashed lines indicate the values calculated in the TRANSTOUGH model. Model porosity ϕ and permeability k , were determined from simulation observations. For example, k is calculated from porosity where:

$$k = k_0(\phi / \phi_0)^x, \quad 3$$

k_0 and ϕ_0 are the initial permeability and porosity, respectively, and x is a fitting exponent. An exponent value of 3.4 was used to calculate the calculated permeabilities plotted in Fig. 31. From the simulated results, bulk permeability was calculated to be a harmonic average of the permeability values from all grid cells. Comparisons are shown as a function of total injected fluid volume. Although there was some attenuation in the simulated response, our comparison revealed strong agreement between TRANSTOUGH simulator predictions and experimental results. The maximum porosity difference between measured and simulated values was always less than 1.5% of the bulk volume, and the permeability differences averaged around 30% of the measured value. Because of the uncertainty in the experimental anhydrite-dolomite volume fraction estimation, the sensitivity to the anhydrite volume fraction amount was examined. The sensitivity of our estimation was tested by simulating a dolomite-anhydrite media comprising 10 and 30% anhydrite volume fractions in addition to our original 20% estimation. The analysis indicated only minor differences in the predicted bulk porosity over time.

The porosity change versus distance along the core plotted in Fig. 31 corresponded with dissolution of minerals predicted in TRANSTOUGH. Figure 32 shows the simulated porosity change at five time intervals, each across the length of the column. About 97 percent of the volume change was due to anhydrite dissolution over the time frame considered. The slight dolomite dissolution was within a few percent of being constant across the column. Figure 16 is a photo of three cross-sections of the core (injection end, middle and production end) taken after the test was terminated. As expected and predicted, the dissolution was most severe at near the injection point and decreased as the fluid traveled into the core.

Sensitivity analysis. A sensitivity analysis was performed to determine the influence of varying brine pH and alkalinity for four rock types. The sensitivity analysis was similar to a pure calcite injection experiment, which was stopped due to rock integrity failure. The parameters in these tests are summarized in Table 18.

The results of varying pH, shown in Fig. 33, suggest that only minor effects are induced by varying pH and alkalinity under constant 50 cm³ hr⁻¹ injection rates of supercritical CO₂ and brine through calcite. Even though the example medium (Fig. 33) was calcite, similar results occurred for each simulated rock type, at all pH and alkalinity values. The simulations indicated that there is a small but measurable difference in calcite dissolution under varying fluid pH and

alkalinity. As expected, the most dissolution occurred in the presence of the lowest alkalinity and lowest pH brine. The least dissolution occurred in the most resistant, highest pH, highest alkalinity brine. The intermediate brine fell between the two end cases. Although the volumetric mineral difference is measurable (0 to 5%), it is minor in relation to the overall magnitude of dissolution within the column.

Numerical dispersion in simulations. TRANSTOUGH simulation results indicated numerical smearing (dispersion) near the injection area. We hypothesized the smearing was an artifact of our model configuration. The evidence indicates that numerical smearing was sensitive to time step size. Running TOUGH2 in standalone mode using the input file from the sensitivity study, three simulations were performed varying the maximum time step size by three orders of magnitude (Fig. 34). The black dashed line indicates the manually calculated dissolved CO₂ from EOSCO2.⁵⁶ The test simulations revealed an increase (nonlinear) in the smearing response as the maximum time step was increased. Figure 34 shows that there is little difference in the profiles using 25 and 250 sec time step. However, the 2500 sec time step shows evidence of significant numerical smearing. Note units are in percent CO₂. In addition, the CO₂ solubility relation employed in EOSCO2 is positively correlated with pressure. Therefore, dissolved CO₂ concentration should be greatest near injection, where the pressure is the greatest, but this is not the case. TOUGH2 predicts lower dissolved CO₂ concentrations near the injection area. In general, the laboratory experiments were very difficult to simulate. In comparison to Cole,¹⁰ the experimental injection rate to cell volume ratio was four to five orders greater in magnitude, which required injection of fluids to be partitioned across the first four grid cells. The extreme injection rates may be the cause of the numerical dispersion. Also, perhaps an alternative experimental representation (input model) in the TRANSTOUGH simulator would improve results. However, integration of the aqueous CO₂ concentration with distance along the core would show that numerical dispersion occurs over a relatively small area. As further support, TRANSTOUGH predictions of the completed dolomite-anhydrite experiment were in strong agreement with measured results. In short, we chose a time step that allowed for moderate numerical smearing but large enough to allow for reasonable simulation run times.

Results of four rock types. In light of the minor differences found in physical changes to the media and for the purpose of brevity, graphical output was restricted to simulations using the brine solution with pH 8.4 and 305 ppm alkalinity. The results are similar for all pH values and alkalinity of each simulated lithology. For the analysis, the response was compared for each media type listed in Table 12, under constant injection of CO₂ and brine.

Simulation time was limited to 1.5×10^7 seconds (~174 days or almost six months), the duration of a prolonged laboratory experiment.

Our simulation results suggest that the pure quartz sandstone was the least reactive media, as is to be expected. Quartz reaction kinetic rates are orders of magnitude slower than most carbonates minerals.⁵⁰ As a result, negligible matrix changes were observed over the six month simulated time scale. CO₂ dissolution in the brine dropped pH from 8.4 to 3.3. All other species concentrations were unaffected by the CO₂ or quartz media and remained constant. Results of the quartz simulations indicate that chemical processes associated with CO₂ and brine injection in pure quartz sandstone are minor.

Contrary to the pure quartz media, the simulated quartz-evaporite sandstone showed significant matrix changes due to CO₂ and brine injection. As with the pure quartz media, the

maximum dissolved CO₂ reaches ~1 M and pH decreases to 3.3. At 1.2 days, Na⁺ and Cl⁻ concentrations increase from ~0.4 M to approximately 2 M across the column. At the same time, SO₄²⁻ and Ca²⁺ concentrations double across the column. The increase in concentration along the column is likely an indication that fluid flow is fast relative to the mineral reaction rates and brine concentrations. In other words, with smaller Damköhler numbers we expect these concentration increases of chemical species across the column to attenuate. The reason for the disparity in the species concentration is preferential mineral dissolution.

At early time in the simulation the majority of the dissolution is from halite. Figure 35 shows that all the halite was dissolved by 3.5 days. By about 88 days all of the evaporite minerals including gypsum had dissolved (Fig. 36). This test demonstrates that significant matrix changes may result on short time scales when both CO₂ and brine fluids are flushed through evaporite rock assemblages. The dissolution of halite was almost even across the column versus an advancing front for the gypsum. This is an indication of the fast rate of gypsum dissolution approaching local equilibrium, whereas halite had a slower rate of dissolution compared to its achieving local equilibrium as used in the model simulations. These result in a uniform increase in porosity along the length of the column until halite completely dissolves, followed by a sharp front at which porosity increases associated with gypsum. These are shown in Fig. 37.

The quartz-carbonate system had significant but less pronounced dissolution than that of the quartz-evaporite media. In agreement with previous results, the aqueous CO₂ concentration remained constant at ~1 M throughout the simulation. In the initial stages of injection the brine pH is 5. The cause of the elevated pH is carbonate dissolution, buffering the brine from the effects of CO₂ acidification. Mg²⁺ concentration linearly increased from 1×10^{-2} to 3×10^{-2} M along the column, caused by dissolution of magnesite. In Fig. 38 the volume fraction of magnesite is shown as a function of distance along the column for different times. Only about 5 percent of the magnesite remains when the simulation was terminated. Calcite dissolved near the injection point where it is undersaturated due to the acidic conditions, and reprecipitated further along the column as the pH increased. At 174 days the carbonates were nearly dissolved, which reduced the buffering of the brine solution. As a result, pH was held at ~3.8 from 0.0 to 0.4 m along the column.

At 0.4 m into the column, significant calcite remained (Fig. 39) at the end of the simulation and the solution pH had increased back up to ~5. However, contrary to models of other media, this model predicts calcite mineralization of approximately 0.1 volume fraction from 0.4 m to 0.5 m along the column. This mineralization could be seen throughout the simulation, increasing with time at the end of the column. If such a phenomenon does indeed occur, it may benefit CO₂ sequestration in two ways. First, dissolution near the injection site may increase storage capacity within the medium, increasing localized CO₂ storage. Second, mineralization may act to reduce the matrix permeability and subsequently CO₂ mobility near the outer boundaries of the main plume. In tandem, dissolving the matrix should increase local storage, whereupon carbonate species within the flushed brine solution precipitate at some downstream location. In this manner, CO₂ injection may act as a self-sealing mechanism. However, in this simulation only 5% of the dissolved carbonates re-precipitated at the tail end of the column.

In an improved oil recovery scenario, this deposit could reduce permeability and injectivity, as well as mobility. If our bench scale simulation were representative of a basin scale response, the amount of CO₂ flushing required to seal the media would preclude it as a viable mechanism to reduce permeability. However, if dissolution and subsequent precipitation create concentric sealing layers around the injection location, significant sealing potential may result. In summary,

the results suggest that carbonate minerals within quartz sandstone show significant dissolution in CO₂ acidified brine, and that near injection dissolution may induce downstream carbonate precipitation. Figure 40 shows the combined porosity changes from the dissolution and precipitation of the carbonate system. The combined effect is a slight reduction in the porosity ahead of the dissolution, and then a significant increase in the porosity (see Fig. 41 for an enlargement of the plot near the initial porosity value).

The calcite simulations revealed the same magnitude of dissolution as the quartz-carbonate system (Fig. 42). This simulates a test done in the laboratory on quarried Indiana limestone.³ The fluid injection rates were identical in each simulation, but the reactive volume fraction (considering quartz as essentially nonreactive) was 2.22 times greater in the pure calcite media. Therefore, if the dissolution was purely a function of the reactive media we should have observed greater matrix changes due to the larger reactive surface of the pure calcite media. However, this was not the case. Increasing the reactive surface area (pure calcite) had little effect on the bulk dissolution, demonstrating that there must be a minimum mineral volume below which decreasing mineral fractions will alter chemical processes. The same effect was observed in the dolomite-anhydrite experiment, where simulations of varying mineral fractions produced similar magnitudes of mineral dissolution. The porosity change is the inverse of the calcite change.

As in the quartz-carbonate system, calcite shows evidence of mineralization preceding the dissolution, but it is not as pronounced as that in the previous test. Results of the laboratory test on limestone included worm holes that caused the test to fail at 174 days; these are evident in the photo shown in Fig. 3. This was discussed previously in more details that included evidence of mineralization downstream, in advance of the worm hole shown in Fig 3.³⁴

Discussion

The TRANSTOUGH model was shown to quantitatively replicate the outcome of the dolomite-anhydrite and the limestone, CO₂, and brine injection experiments. Prompted by the strong agreement with experimental results, a sensitivity analysis was performed to determine which parameters control the interaction of CO₂, brine, and geologic media under deep basin pressure-temperature conditions. Simulation results, using the experimental brine composition, indicate that varying brine pH and alkalinity caused 0 to 5 percent differences on the resultant volumetric mineral fractions. The major controlling influence was found to be lithology type, while in the case of the quartz-evaporite media, dissolution may be time-dependent. A secondary influence was the magnitude of fluid flushed through the media in relation to the reactive surface area.

Summary

Although the TRANSTOUGH model remains in the developmental stages, simulated results compared favorably to experimental results, suggesting that the model accurately simulates CO₂ sequestration under deep reservoir conditions, at least for small spatial scales.

Additional TRANSTOUGH simulations were performed employing a range of geologic media, solution pH, and brine alkalinities. The results indicate that under equivalent volumetric fluid injection of CO₂ and brine little difference in the magnitude of dissolution occurs with variation in brine pH and alkalinity. The results of the laboratory experiments and the corresponding bench scale numerical simulations suggest that chemical reactivity with the

geologic media can be extreme, depending on mineral kinetic reaction rates and the volume of brine fluid present.

Bench scale simulations and laboratory experiments are a necessary first step to better characterization of CO₂-brine-media interactions. Reservoir scale simulations are critical in gaining an understanding of the more applicable large scale effects of heterogeneities that may be incurred from CO₂ injection.

CHAPTER 4. COST REDUCTION AND INJECTIVITY IMPROVEMENTS FOR CO₂ FOAMS FOR MOBILITY CONTROL

Introduction

Viscous fingering, gravity override, reservoir heterogeneity, and reduced injectivity are potential problems in gas injection processes.^{14,15,56-59} In a CO₂ flood, the large viscosity contrast between the reservoir crude oil and injected CO₂ (often >1 cp versus <0.1 cp) induces an unfavorable mobility ratio that can result in early gas breakthrough (increased processing and compression cost) and poor reservoir sweep (lower oil production). Processes such as the injection of water alternating with gas (WAG),⁶⁰ direct CO₂ thickeners,^{61,62} and surfactant solution alternating with gas (SAG)^{63,64} are being used or have been proposed to mitigate these problems. Each has its potential and limitations.

Our recent work has concentrated on understanding and improving the SAG process.⁶⁴⁻⁷⁰ It has been shown both in the laboratory and, more importantly, in field demonstration projects that CO₂ foam can improve CO₂ floods in heterogeneous reservoirs. Extensive laboratory evaluations on the effectiveness of CO₂ foam have been reported, but only a limited number of field tests have been performed, with mixed results.⁷¹⁻⁸⁰ Better economics through improved sweep, decreased cost of additives, improved injectivity, and/or decreased gas production will improve the probability of increasing oil production by using foam. With these factors in mind, this section of the report will look at means to improve economics by reducing the cost of adding foaming agents and improving injectivity.

Field Tests

This section summarizes several CO₂ foam field trials. In most cases gas production decreased, saving on gas processing and recycle cost, and oil production increased, but injectivity decreased, which can be detrimental when the project is injection volume-limited or close to it. The economics on several of the tests appeared to be favorable. We feel that the results of this paper will increase the prospects of economical CO₂ foam floods. At the end of this section, using the results from a completed field tests, we will demonstrate how the information from this study would improve the economics of future tests.

Pennzoil's Rock Creek Trial (1984-85). The US Department of Energy (DOE), the New Mexico Petroleum Recovery Research Center (PRRC), and Pennzoil⁷¹ conducted a joint CO₂ foam field trial at Rock Creek, Roane County, West Virginia. This was a trial on two ten-acre five-spots that were on an average WAG ratio of 1:1, using the surfactant Alipal CD128 both in the SAG and preflush slug. No indication of an oil bank was found. Injectivity reduction was noted both during the preflush slug and the foam test.

Chevron's Rangely Weber Sand Unit Trials (1988-1990). A foam field trial⁷² was conducted in the Rangely Weber Sand Unit, in northwestern Colorado. The CO₂ flood was started at a 1:1 WAG ratio in October 1986. The major concern was early CO₂ breakthrough caused by thief zones between injectors and producers. The foam project began in April 1989. The treatment included a 12,000 bbl surfactant slug followed by 55,000 bbl of 79% quality foam. This was not a SAG test, but coinjection of surfactant solution and gas. Chaser™ CD1040 was used, with an

average surfactant concentration in the injected brine of about 0.46 wt%. Foam was placed in the reservoir in spite of a large hydraulic fracture in the injector. Performance improved in at least one offset producer and foam lowered CO₂ injectivity for two months during the CO₂ chase period. The test was an apparent success in that the foam treatment paid out in about two months.

Chevron's North Ward-Estes trial (1990-91). The second Chevron CO₂ foam field trial⁷³ was in the North Ward-Estes field in Ward and Winkler Counties in west Texas. The original CO₂ flood was initiated in 1989 with a project area of 3,840 acres and WAG ratio of 1:1. Over about two years, foam was injected into an injector using a four-cycle SAG process, followed by continuous CO₂ injection after each. Chaser™ CD1040 was used as the surfactant. During the SAG cycles, CO₂ injectivity reduction by 40% to 85% was an indication of foam formation. Foam apparently diverted CO₂ from the thief zone regions, as indicated by a sharp decline in CO₂ production from the problem producer and increased production at other offset producers. The most significant economic incentive was the reduction in CO₂ production and improved CO₂ utilization.

Phillips' East Vacuum Grayburg San Andres Unit (EVGSAU) trial (1991-93). The EVGSAU operators with the PRRC and DOE performed a CO₂ foam field trial in Lea County, New Mexico. While the CO₂ flooding was favorable, some wells showed excessive CO₂ breakthrough, thus increasing CO₂ recycling and compression costs. Laboratory results showed that Chaser™ CD1045 was an effective foaming agent at reservoir conditions for EVGSAU cores.⁷⁴ The field trial at EVGSAU⁷⁵⁻⁷⁸ confirmed these findings. The surfactant showed great effectiveness as a CO₂ mobility reduction agent. For most of the trial a concentration of 0.25 wt% surfactant was used. A short test at 0.10 wt % was showing favorable results before mechanical problems ended the trial prematurely. Gas production was decreased and oil production increased in several wells. The economics of this trial⁷⁷ will be discussed later in this paper.

Mobil's Slaughter and Greater Aneth Field trials (1991-94). Mobil performed four pattern-scale CO₂-foam field trials.⁷⁹ Two trials were carried out at Slaughter Field in a San Andres reservoir (west Texas), and the other two at Greater Aneth Field in a platform carbonate reservoir (southern Utah). Two different surfactants, Rhodapex (formerly Alipal) CD128 and Chaser™ CD1045, and two injection methods, SAG and coinjection of CO₂ and surfactant solution, were tested. Altogether, 160,000 lb. of active surfactant was injected, with one well undergoing 18 months of foam treatment. The treatments resulted in a significant reduction in gas production with indications of increased oil production. Other research also found that foam significantly reduced CO₂ injectivity in all cases. Coinjection was operationally more difficult and reduced injectivity significantly more than SAG.

Unocal/Long Beach Oil Development Co. Wilmington Immiscible Trial (1984). Unocal and Long Beach Oil Development Co. reported an immiscible CO₂ foam trial in the Wilmington field in southern California⁸⁰ in which Alipal CD128 was used as the surfactant. The purpose of the foam emplacement field test was to divert the CO₂-N₂ gas, injected in the immiscible flooding project, from the highly water-saturated S zone to lower oil-containing zones. A total of about 21,000 bbl of 1 wt% Alipal CD128 solution was used with a volume of gas sufficient to provide foam quality of about 90%. About 70 vertical ft of formation in the test well accepted fluid. A

radial penetration of about 40 ft for the foaming solution was calculated, with a potential foam bank extending out to 110 ft around the wellbore. The project was successful in reducing in-depth permeability of the S zone sand and diverting part of the injected gas to the lower T zone. Skin damage in the well was greatly decreased, and gas injectivity was notably reduced.

Laboratory Tests

Surfactant-based mobility control in CO₂ flooding can effectively mitigate problems normally associated with the miscible gas recovery process. Previous laboratory results⁸¹⁻⁸³ indicate that the change of flow and displacement behavior of CO₂-foam reduces the mobility of CO₂ and increases the displacement efficiency. Laboratory tests have shown improved mobility control with and without oil present.^{81,84} Several surfactants have been identified as relatively good mobility control agents in heterogeneous rocks.^{64,85,86} Previous work has shown the effect of foam on delaying CO₂ breakthrough time and the resulting favorable impact on oil recovery.^{67,70,87} The decrease or elimination of foam formation in the presence of oil has been reported by several authors.^{81,87-90}

Mixed surfactant systems. In the search to improve foam performance a number of mixed surfactant systems have been tested.⁶⁹ Substantial mobility reduction is observed when mixed surfactants are coinjected with CO₂. The stability of mixed surfactant systems correlates well with their performance in mobility reduction and mobility dependence on rock permeability. A few mixtures generated more stable foam than did either of their individual components and yielded improved mobility reduction as well.

Sacrificial agents. Surfactant-based mobility control in CO₂ flooding is an effective way to mitigate problems normally associated with the miscible gas recovery processes. For CO₂-foam to propagate through a reservoir at a satisfactory rate, mitigation of the loss of foaming agent by adsorption is a critical factor. As a common practice, most foam applications involve preinjecting a sufficient amount of foaming agent into the reservoir to precondition the reservoir, which usually increases the surfactant expense substantially. Therefore, use of a lower-cost sacrificial agent is economically necessary to minimize the loss of costly foaming agent and ensure a satisfactory foam displacement.

Lignosite[®] 100, a calcium lignosulfonate, is an inexpensive byproduct of the paper industry that has been used as a sacrificial agent in surfactant flooding processes. Because of its preferential adsorption onto reservoir rock, significant reduction of surfactant loss was reported in several surfactant flooding applications⁹¹⁻⁹³ where the lignosulfonate minimized the loss of primary surfactants due to adsorption. The use of lignosulfonate as a sacrificial agent in CO₂-foam application has been reported in a patent.⁹⁴ This study examined lignosulfonate both a sacrificial agent and cosurfactant. The appeal of lignosulfonate is its relatively low cost compared to that of the good foaming agents and its ready availability as a byproduct from the pulp and paper industry. The addition of chemicals to an oil recovery process adds value to the process, but also carries with it the concern of cost effectiveness. There are two areas of concern that affect the required amount of chemical for the SAG process: the amount of chemical that is required to create the desired phenomena, in this case CO₂ foam, and the amount of chemical required to satisfy reservoir adsorption of injected chemicals.

Improving Surfactant Adsorption

The experimental setup for the adsorption and flow tests are well documented in earlier work; they will not be covered here.^{68,70,85} Calculations show that the adsorption requirements of the rock are often greater than those required to generate a foam. A reservoir having 20% porosity will require 1552 bbls of fluid for 100% saturation of an acre-ft. Surfactant concentrations required for a foam range from 0.05 to 0.5 wt%, or 0.18 to 1.8 lbs/bbl of brine. A typical chemical adsorption of 1 mg/cc on a reservoir core equates to 2714 lbs/acre-ft or 1 kg/M³ in a reservoir. This would require all the surfactant available from 1508 bbls of a 0.5 wt% surfactant solution, which is about 1 acre-ft pore volume (PV). At the lower concentration, the same level of saturation would require over 15,000 bbls or about 10 PV of solution. It is apparent that most of the injected surfactant is required to satisfy the adsorption requirement of the reservoir.

Figure 42 is a plot for adsorption of CD1045 in Berea sandstone. This figure contains four series of adsorption curves produced in two different studies, using different core samples.⁶⁶⁻⁶⁸ This figure is very instructive because it shows the trend of increasing adsorption with increasing surfactant concentration and possible scatter due to method and rock samples. Figure 43 contains adsorption isotherms for three different carbonate cores. Again the trend is similar, but with a lower magnitude.

In each case shown in Figures 42 and 43 there is a significant concentration effect. Table 19 summarizes the adsorption decrease in Berea sandstone, Indiana limestone, Baker dolomite, and San Andres dolomite when lowering the CD1045 concentration from 0.25 wt% to 0.05 wt%. In each case the decrease was at least 50%. This demonstrates the obvious importance of running the system at the lowest practical concentration of surfactant in order to decrease the required reservoir adsorption. When evaluating the economic effects, the effect of the fluid volume that will need to be injected must be considered. As an example the concentration of 0.25 wt% of Chaser CD1045 would require about 4 mg/cc of adsorbed surfactant or 12,000 bbls of solution per acre-ft for Berea sandstone. At 0.05 wt% surfactant the adsorption is 2 mg/cc; that will require 30,000 bbls of solution. The savings in required surfactant would be 5428 lb/acre-ft, but the operation would require 250% more injected fluid volume. For San Andres dolomite the volumes, assuming the same 20% porosity, would be 3,000 bbls/acre-ft versus 4,500 bbls/acre-ft to satisfy adsorption requirements that are 1 mg/cc versus 0.3 mg/cc for 0.25 wt% and 0.05 wt% surfactant concentrations, respectively.

In earlier work, we selected lignosulfonates as a test sacrificial agent to be used as an inexpensive chemical to satisfy some of the adsorption requirement of reservoir rock.⁶⁸ This agent replaces some of the required adsorption of a more expensive foaming agent. Even though it has been shown that in and of itself lignosulfonate is not a good foaming agent,^{66,67} when used with a cosurfactant such as CD1045, lignosulfonates can replace some of the good foaming agent in solution and the synergistic effect results in excellent foam. The earlier test results had similar displacements when the surfactant concentration of CD1045 was reduced from 0.25 wt% to 0.05 wt% with 0.5 wt% lignosulfonate in the reduced CD1045 system. This would have a compound effect with both a decrease in the amount of CD1045 required for a stable, effective foam and a decrease in the amount required to satisfy the adsorption requirement. As indicated earlier, this would provide more than a 50% reduction in the foaming solution and from 50% to 75% reduction in CD1045 adsorbed. Thus, significant reduction in CD1045 use could be achieved even without the consideration of lignosulfonate as a sacrificial agent, which was the original purpose of the study.

Tests have shown that lignosulfonate can also work as an effective sacrificial agent. Figure 44 shows the adsorption isotherm for lignosulfonate on Berea sandstone cores. Shown are two curves of adsorption isotherms obtained from two studies using two different cores.^{66,68,70} Figure 45 compares several methods of adding lignosulfonates for reduction of surfactant adsorption in Berea sandstone cores. These tests were all performed at low surfactant concentrations. The tests were run using a circulation method, and each point was run until the system equilibrated.⁷⁰ Four sets of injection modes compare the adsorption of CD1045 versus surfactant concentration in solution at equilibrium with Berea sandstone core when:

1. CD1045 is the only surfactant injected,
2. CD1045 is injected with cosurfactant lignosulfonate,
3. CD1045 is injected alone after a preflush with lignosulfonate, and
4. CD1045 is injected with cosurfactant lignosulfonate after a lignosulfonate preflush.

In each case the concentration of lignosulfonate in the injected solution was 0.5 wt%.

Figure 46 is a bar graph comparing the results from two different studies using different Berea cores. For both sets the CD1045 equilibrium concentration was 0.05 wt%. Even though the absolute values deviate, adsorption decreases; going from CD1045 only, to coinjection, to preflush, and finally a preflush with coinjection (one case only). In order for the lower CD1045 concentrations to be effective, the method recommended would be to use a cosurfactant system for the preflush and injection (in the field the SAG process would probably be used). Using Berea, the expected reduction would be at least another 50% lower than that obtained using CD1045 only. Thus the required CD1045 for adsorption could be reduced from 4 mg/cc using 0.25 wt% CD1045 to less than 1 mg/cc using 0.05 wt% CD1045/0.5 wt% lignosulfonate solutions.

Reviewing similar work done using Indiana limestone, which is closer in composition to the dolomite reservoirs in west Texas and southeast New Mexico, a similar effect to that seen using Berea is shown with CD1045 and lignosulfonate. Figure 47 shows that lignosulfonate adsorption is greater with Indiana limestone than Berea sandstone, which is the opposite of what we saw in comparing CD1045 adsorption of Berea and limestone (compare Figures 42 and 43), respectively. The adsorption reduction is well over 50%, when decreasing from 0.25 wt% to 0.05 wt%. Figure 48 shows the effect of the injection method. Only the first three methods described above were performed and they had similar results. Figure 49 demonstrates the results on a bar graph, with reduction of only about 25%. Again, the most effective procedure would be the coinjection (SAG in field tests) of CD1045 and lignosulfonate, as a preflush and again during the foaming period. The adsorption reduction from using CD1045 alone at a concentration of 0.25 wt% to coinjection at 0.05 wt% CD1045/0.5 wt% lignosulfonate can be as much as 80% required in the solution and 75% from adsorption.

Improving Injectivity

A concern in the field has been significant injectivity changes during the course of the CO₂ flood, especially associated with the WAG process. In a project that is near its injection limit, a decrease in injectivity can cause a flood to become uneconomical. By nature it is expected that foam will cause injectivity decreases. The intent is to use foam to divert CO₂ from high permeability, well-swept regions of the reservoir to lower permeability regions where the oil saturation is higher. Thus it becomes important when and where foam is used. Another concern is how well the tested surfactant systems perform in displacing fluid in a core flood and in the

presence of oil. A series of tests have been performed in dual permeability core to examine both these concerns.

Figures 50 and 51 show oil recovery and differential pressure in a low permeability region of a dual permeability core using four different surfactant mixtures:

1. 0.05 wt% CD1045,
2. 0.25 wt% CD1045,
3. 0.025 wt% CD1045/0.5 wt% lignosulfonate, and
4. 0.05 wt% CD1045/0.5 wt% lignosulfonate.¹⁴

Before foam was formed, oil was produced out of the high permeability region with a high injectivity. As foam is formed in the swept region the differential pressure increases, which also indicates an injectivity reduction. This is accompanied with fluid/oil production from the low permeability region. In a core that is a few inches long, a pressure drop of a few psi can translate to a pressure gradient in the field that would not be practical. After the injection of 5 PV, there was no oil production from the low permeability region when using 0.05 wt% CD1045. This, with no change in pressure across the core, indicates insufficient foam to divert injection fluid from the high to the low permeability region. Each of the other three systems had fluid diversion and oil production from the low permeability region. The timing and magnitude of the oil and pressure responses are interesting. The 0.25 wt% CD1045 system had no production from the low permeability region until the production from the high permeability region was near completion and the resulting oil saturation was very low. This was followed by a sharp increase in system pressure and by displacement of fluids in the low permeability region.

In the two CD1045/lignosulfonate systems, oil production and pressure increases started much earlier and co-production occurred from the high and low permeability regions. The ultimate production in the 0.05 wt%-CD1045/lignosulfonate system from the low permeability region was at least as great as the 0.25 wt%-CD1045 system, but occurred in about half the fluid volume injected. Also the pressure drop across the core was much less, especially during the time of the bulk of the production. Though the final production for the 0.025 wt%-CD1045/lignosulfonate system was not as high as that for the other two systems, it was significant. The pressure drop was similar to no foam during the early production and never increased more than a few psi even by the end of the test.

CO₂ Foam Cost Reduction

After examining the results of laboratory tests, we thought it advantageous to take these findings and, using conservative numbers, look at the possible savings in surfactant cost in a field project. In this section, we use the EVGSAU trial because we had the most detailed information available to us for analysis.⁷⁷

Summary of foam field tests at EVGSAU.⁷⁷ A total of 105,000 lbs of Chaser™ CD1045 was used at the EVGSAU in two SAG tests. Based on laboratory tests with reservoir cores, 85% of the total surfactant was required for adsorption (90,000 lbs), and only 15% of the total surfactant was needed for foam generation (15,000 lbs). The first test consisted of five rapid SAG cycles of three days of surfactant solution followed by 12 days of CO₂ and the second test consisted of two rapid cycles.

Because a large amount of surfactant was injected during the EVGSAU pilot tests, the objective was not to determine if foam treatments were economic. However, sufficient data were

available to enable the evaluation of the effectiveness of the two tests. Revenue from the foam tests resulted from the incremental oil produced in the pattern and savings in compression costs for reinjected gas. The operator calculated the first foam test resulted in 14,700 bbls incremental oil and the second test resulted in 4,460 bbls incremental oil. The operational parameters in effect at the time of the two foam tests are given in Table 20. Additional oil revenue from the two tests was \$180,008 and compression savings were \$44,250. After subtracting the surfactant costs of \$176,000 the net revenue of \$48,258, while encouraging, was not sufficient to provide an attractive rate of return.

Estimate of cost reduction with enhanced foam. The economic analysis of the EVGSAU tests suggested foam treatments could prove economical if smaller or lower-cost adsorption slugs or lower surfactant concentrations were used that would provide the same incremental oil. To estimate the cost reduction that might be possible, we used the parameters from the EVGSAU field tests and assumed that enhanced foam with inexpensive lignosulfonate could reduce the adsorption of the expensive foaming agent (CD1045) as well as lower the CD1045 concentration required to provide effective foam. In the absence of laboratory tests with dolomite reservoir cores, we assume the lignosulfonate can reduce adsorption of CD1045 by 15%. This is conservative estimate because, as shown earlier in this paper, the adsorption isotherms in Indiana limestone indicate that adsorption of 0.5 wt% lignosulfonate could be 50% less than the adsorption of 0.25 wt% CD1045 as used at EVGSAU.

Based on tests described earlier in this paper, coinjection of 0.5 wt% lignosulfonate with 0.05 wt% CD1045 provides similar foaming results as obtained with higher concentrations (0.25 wt%) CD1045 alone. If the effectiveness of the lower cost foam treatment would provide similar incremental production and compression savings as was observed earlier in the EVGSAU field foam test, we can estimate the cost reduction with the enhanced foam treatment.

We considered two possible options with the lower-cost enhanced foam treatment. Option 1 is 0.05 wt% CD1045/0.5 wt% lignosulfonate both in the preflush and in the following rapid SAG injection. Thus the concentration of CD1045 will be one-fifth of that used at EVGSAU, and the concentration of lignosulfonate will be twice the concentration of CD1045 used at EVGSAU. Option 2 is to preflush with 0.5 wt% lignosulfonate and use 0.05 wt% CD1045/0.5 wt% lignosulfonate in the rapid SAG. We used a cost of lignosulfonate of \$0.25/lb active. Estimates of the cost reduction and net revenue projections with the enhanced foam are shown in Table 21. These estimates suggest that the lower-cost enhanced foam approach could significantly increase the net revenue (almost a threefold improvement) from foam field projects.

Conclusions

There are several concepts inferred from the laboratory tests that should be considered for field tests:

1. The concentration of CD1045 with lignosulfonate can be lowered well below the concentration required without lignosulfonate and still have significant foaming/diversion capability, thus oil production.
2. The cosurfactant system had significant oil production with much less effect on injectivity (lower pressure drop).
3. The cosurfactant system foaming properties seemed to be less sensitive to oil saturation. Fluid diversion caused by foam started before oil saturation in the high permeability region

was reduced to miscible residual saturation.

4. The cosurfactant system appears to have the possibility of varying concentrations of the two surfactants in such a way as to tailor a system to optimize the competing effects of sweep and injectivity.
5. The cost analysis of the EVGSAU results using the results of the cosurfactant system suggests that the new technology can be profitable.

CHAPTER 5. MOBILITY CONTROL AGENTS

Introduction

Our past work has identified a number of mobility control agents to use for CO₂-foam flooding.^{67,68} In particular the combination of the good foaming agent Chaser™ CD1045 (CD1045) that has shown extremely good properties for foaming and the enhanced property of reducing mobility more at high permeabilities than at low permeabilities that we have referred to in the past as selective mobility reduction (SMR).⁹⁷ In assessing the potential cost of mobility control over 80 percent of the surfactant will be used to satisfy the adsorption requirement of the reservoir rock.⁷⁷ We have been examining sacrificial agents and cosurfactants that will reduce the cost of chemical requirements. We are in the process of scrutinizing the methods that we are using to determine the efficiency of the sacrificial agents and cosurfactant systems. These have required concentration determinations and reusing core samples. This chapter reports some of the problems that we have found and some interesting effects that must be considered.

Interference of Cosurfactants during Concentration Determination

The two surfactants that have had the most attention over the past couple of years are **Lignosite® 100** (lignosulfonate) and CD1045. Figures 53 and 54 show the influence of the second surfactant on concentration determination of the first surfactant. Figure 53 shows the results of tests of three concentrations of CD1045 that have been prepared and then mixed with different concentrations of lignosulfonate. CD1045 measurement error increases as lignosulfonate concentration increases. At the same time, the percent error of the CD1045 measurements decrease as CD1045 concentration increase if lignosulfonate concentration remain constant.

Figure 54 shows the results of tests of three concentrations of lignosulfonate that have been prepared and then mixed with different concentrations of CD1045. Lignosulfonate measurement error increases as CD1045 concentration increases. At the same time, the percent error of the lignosulfonate measurements increase as lignosulfonate concentration decrease if CD1045 concentration remain constant.

From these results we are looking at either changing the method of concentration determination in a mixed surfactant system or calibration our system to correct for interference of the second component. It is interesting to note that if the observations that we have noted to date are correct that the numbers used in Chapter 4 to estimate the cost savings of the cosurfactant system are conservative. The amount of CD1045 in the effluent is actually greater than that measured, thus the amount adsorbed on the core was less than we had previously determined. This work is continuing.

Effects of Dilution Procedures and Delay Time before Measurements

From past work we have found that CD1045 concentration should not be above 600 ppm to obtain accurate measurements in the spectrophotometer. During core flooding experiments, the concentration of CD1045 will often be above 600 ppm, thus the solution must be diluted before measurement are preformed. The dilution procedure often produces foam if shaken during dilution. Thus we looked at the results of difference preparation procedures.

Figure 55 indicate that significant error results if the measurements are made immediately after the solution is diluted whereas if allowed to set for four hours the accuracy improves no matter how vigorous the solution has been mixed. The smallest area was in the system gently mixed. The errors seem to result from the foaming action. If there is no foam after several hours the results are best. It makes sense that surfactant is taken up in the foam, decreasing the amount in solution. Figure 56 is another way to plot this. Again in each case when given time to allow for better mixing and coalescing of the foam results improve. Since CD1045 is a durable foam it required considerable time to coalesce the foam when developed.

Multiple Run in a Single Core

Since each core is unique with structure and compositional heterogeneities changes from core to core for comparison of tests it is advantage to run a series of test in the same core. This does have the problem of determining if and how much of a change has occurred in a core from test to test. We ran a series of adsorption and desorption tests in the core with the parameters shown in Table 22. Figure 57 shows the four adsorption isotherms using lignosulfonate as the surfactant. The trend indicates adsorption is less in subsequent tests. Figure 58 show the desorption isotherms. In the desorption isotherms even after enumerable pore volumes of surfactant free brine has flown through the core the adsorbed surfactant did not returned to zero. In Figure 59 the results are shown when we started the subsequent floods assuming the amount of lignosulfonate remained on the core that was indicated by the previous desorption. The results as plotted in Fig. 59 are consistent and each isotherm is within experimental scatter. This demonstrates the importance of desorption and cleaning procedures as well as the durability of the adsorbed surfactant.

Conclusions

When studying surfactant adsorption and desorption the follow are some of the parameters that must be considered:

1. Other species that are present in the solution when determining concentration,
2. Method of mixing and time allowed to equilibrate when determining concentration, and
3. Core history during any flooding experiments.

ACKNOWLEDGMENTS

The authors acknowledge the support of the US Department of Energy (contract no. DE-FC26-01BC-15364) and the State of New Mexico. The authors acknowledge the assistance of the New Mexico Tech Electron Microprobe Lab in obtaining BSEI and compositional analysis of the core materials. The Seminole San Andres dolomite cores used in this work were donated by Amerada Hess Corp. We would like to thank Elizabeth Bustamante for aiding in the preparation of this manuscript.

The correspondence and exchange of information and ideas and support of the following companies is appreciated:

Amerada Hess
Chevron Texaco
Pure
ExxonMobil
Oxy Permian
ConocoPhillips
Devon
Kinder Morgan
Transpetco
Quay Valley
Anadarko

List of Contributors

Reid B. Grigg
Robert K. Svec
David Martin
Baojun Bai
Tristan P. Wellman
Brian McPherson
Mary Harper

REFERENCES

1. Grigg, R.B. and Schechter, D.S.: "State of the Industry in CO₂ Floods," paper SPE 38849 presented at the 1997 SPE Annual Technical Conference and Exhibition, San Antonio, Oct. 6-9.
2. Morita, G.: "2002 Worldwide EOR Survey," *Oil & Gas Journal* (Apr. 15, 2002).
3. Morita, G.: "2000 Worldwide EOR Survey," *Oil & Gas Journal* (Mar. 20, 2000).
4. Morita, G.: "1998 Worldwide EOR Survey," *Oil & Gas Journal* (Apr. 20, 1998).
5. Morita, G.: "1996 Worldwide EOR Survey," *Oil & Gas Journal* (Apr. 15, 1996).
6. Morita, G.: "1994 Worldwide EOR Survey," *Oil & Gas Journal* (Sept. 26, 1994).
7. Morita, G.: "1992 Worldwide EOR Survey," *Oil & Gas Journal* (Apr. 20, 1992).
8. Morita, G.: "1990 Worldwide EOR Survey," *Oil & Gas Journal* (Apr. 23, 1990).
9. Aalund, L.R.: "1988 Worldwide EOR Survey," *Oil & Gas Journal* (Apr. 18, 1988).
10. Leonard, J.: "1986 Worldwide EOR Survey," *Oil & Gas Journal* (Apr. 14, 1986).
11. Leonard, J.: "1984 Worldwide EOR Survey," *Oil & Gas Journal* (Apr. 2, 1984).
12. "1982 Worldwide EOR Survey," *Oil & Gas Journal* (Apr. 5, 1982).
13. Matheny, S.L., Jr.: "1980 Worldwide EOR Survey," *Oil & Gas Journal* (Mar. 31, 1980).
14. Noran, D.: "1978 Worldwide EOR Survey," *Oil & Gas Journal* (Mar. 27, 1978).
15. Rogers, J. D. and Grigg, R.B.: "A Literature Analysis of the WAG Injectivity Abnormalities in the CO₂ Process," paper 59329 presented at the 2000 SPE/DOE Improved Oil Recovery Symposium, Tulsa, April 2-5.
16. Hadlow, R.E.: "Update of Industry Experience with CO₂ Injection," paper SPE 24928 presented at the 1992 SPE Annual Technical Conference and Exhibition, Washington D.C., Oct. 4-7.
17. Winzinger, R., *et al.*: "Design of a Major CO₂ Flood, North Ward Estes Field, Ward County, Texas," *SPE* (February 1991) 11.
18. Ring, J.N. and Smith, D.J.: "An Overview of the North Ward Estes CO₂ Flood," paper SPE 30729 presented at the 1995 SPE Annual Technical Conference and Exhibition, Dallas, Oct. 22-25.
19. Prieditis, J., *et al.*: "A Laboratory and Field Injectivity Study: CO₂ WAG in the San Andres Formation of West Texas," paper 22653 presented at the 1991 SPE Annual Technical Conference and Exhibition, Dallas, Oct. 6-9.
20. Christman, P.G., and Gorell, S. B.: "A Comparison of Laboratory and Field-Observed CO₂ Tertiary Injectivity," paper SPE 17335 presented at the 1988 SPE/DOE Enhanced Oil Recovery Symposium, Tulsa, April 17-20.
21. Good, P.A. and Downer, D.G.: "Cedar Creek Anticline Carbon Dioxide Injectivity Test: Design, Implementation, and Analysis," paper SPE 17326 presented at the 1988 SPE/DOE Enhanced Oil Recovery Symposium, Tulsa, April 17-20.
22. Henry, R.L., *et al.*: "Utilization of Composition Observation Wells in a West Texas CO₂ Pilot Flood," paper SPE 9786 presented at the 1981 SPE/DOE Enhanced Oil Recovery Symposium, Tulsa, April 5-8.

23. Patel, P.D., et al.: "An Investigation of Unexpectedly Low Field-Observed Fluid Mobilities During Some CO₂ Tertiary Floods," paper SPE 14308 presented at the 1985 SPE Annual Technical Conference and Exhibition, Las Vegas, Sept. 22-25.
24. Potter, G.F.: "The Effects of CO₂ Flooding on Wettability of West Texas Dolomitic Formations," paper SPE 16716 presented at the 1987 SPE Annual Technical Conference and Exhibition, Dallas, Sept. 27-30.
25. Schneider, F.N., and Owens, W. W.: "Relative Permeability Studies of Gas-Water Flow Following Solvent Injection in Carbonate Rocks," *SPEJ* (Feb. 1976) 23.
26. Kamath J., Nakagawa, F.M., Boyer, R.E., and Edwards, K.A.: "Laboratory Investigation of Injectivity Losses during WAG in west Texas Dolomites," paper SPE 39791 presented at the 1998 SPE Permian Basin Oil and Gas Recovery Conference, Midland, March 25-27.
27. Ross, G.D., et al.: "The Dissolution Effects of CO₂-Brine Systems on the Permeability of U.K. and North Sea Calcareous Sandstones," paper SPE/DOE 10685 presented at the 1982 SPE/DOE Symposium on Enhanced Oil Recovery, Tulsa, April 4-7.
28. Mathis, R.L. and Sears, S.O.: "Effect of CO₂ Flooding on Dolomite Reservoir Rock, Denver Unit Wasson (San Andres) Field," paper SPE 13132 presented at the 1984 SPE Annual Technical Conference and Exhibition, Houston, Sept. 16-19.
29. Sayegh, S.G., et al.: "Rock/Fluid Interactions of Carbonated Brines in a Sandstone Reservoir: Pembina Cardium, Alberta, Canada," *SPEFE* (December 1990) 399.
30. Bowker, K.A. and Shuler, P.J.: "Carbon Dioxide Injection and Resultant Alteration of the Weber Sandstone, Rangely Field, Colorado," *The American Association of Petroleum Geologists Bulletin*, V. 75, No. 9 (September 1991) 1489.
31. Wang, F.P, Lucia, F.J., and Kerans, C.: "Integrated Reservoir Characterization Study of a Carbonate Ramp Reservoir: Seminole San Andres Unit, Gaines county, Texas," paper 36515 presented 1996 SPE Annual Technical Conference and Exhibition, Denver, October 6-9.
32. Wawersik, R., W., et al.: "Terrestrial Sequestration of CO₂: An Assessment of Research Needs," *Advances in Geophysics* **43**, (2001).
33. Pawar, R.J., et al.: "Geological Sequestration of Carbon Dioxide in a Depleted Oil Reservoir," paper SPE 75256 presented at the 2002 SPE/DOE Symposium on Improved Oil Recovery, Tulsa, April 13-27.
34. Svec, R.K. and Grigg, R.B.: "Physical Effects of WAG Fluids on Carbonate Core Plugs," paper SPE 71496 presented at the 2001 SPE Annual Technical Conference and Exhibition, New Orleans, Sept. 30-October 3.
35. Van Der Meer, L. G. H.: "The Conditions Limiting CO₂ Storage in Aquifers," *Ener. Convers. Mgmt.*, (1993) **34** (9-11), 959-966.
36. Holt, T., I., et al.: "Underground Storage of CO₂ in Aquifers and Oil Reservoirs." *Ener. Convers. Mgmt.* (1995), **36**, 535-538,.
37. Van Der Meer, L. G. H.: "The CO₂ Storage Efficiency of Aquifers," *Ener. Convers. Mgmt.* (1995), **36** (6-9), 513-518.
38. Lindeburg, E.: "Escape of CO₂ from Large Horizontal Aquifers Confined Only by a Cap Seal," Conference: Greenhouse Gases: Mitigation Options (1995).

39. Law, H. S. and Bachu, S.: "Hydrological and Numerical Analysis of CO₂ disposal in deep aquifer systems in the Alberta sedimentary basin." *Ener. Convers. Mgmt* (1966), **37**(6-8), 1167-1174.
40. Weir, G. J., et al.: "Reservoir Storage and Contaminant of Greenhouse Gases," *Transport in porous media* (1996) **23**, 37-60.
41. Cole, B. S.: "An Equation of State for Multiphase CO₂ and Water," Independent Study (M.Sc), New Mexico Institute of Mining and Technology, (1999).
42. Johnson, J. W., et al.: "Reactive Transport Modeling of Subsurface CO₂ Sequestration: Identification of Optimal Target Reservoirs and Evaluation of Performance Based on Geochemical, Hydrologic, and Structural Constraints," *Energex*, (2000).
43. Nitao, J.J.: *Reference Manual for the NUFT Flow and Transport Code, version 2.0*, (1998), Lawrence Livermore National Laboratory, UCRL-MA-130651, 55.
44. Pruess, K.: "TOUGH2- a General-Purpose Numerical Simulator for Multiphase Fluid and Heat Flow," Lawrence-Berkeley Laboratory, (1999).
45. Lichtner, P.C. (2001) FLOTTRAN: User's Manual, Los Alamos National Laboratory report, LA-UR-02-2349.
46. Wellman, T.P.: *Concatenation of Reactive Transport Model to Simulate CO₂ Sequestration in Geologic Media*, Thesis, New Mexico Institute of Mining and Technology, (2002).
47. Sjoberg, E. L. and Rickard, D.T.: "Temperature Dependence of Calcite Dissolution Kinetics between 1 and 62°C at pH 2.7 to 8.4 in Aqueous Solutions." *Geochim. Cosmochim. Acta*, (1987), **48**, 485-493.
48. Lichtner, P. C., et al.: "Reactive Transport in Porous Media," in: *Reviews in Mineralogy*. Lichtner, P.S. and Oelkers, E.H, eds., (1996).
49. Folk, R. L.: "Spectral Subdivision of Limestone." *Amer. Assoc. Petrol. Geol. Mem.*, (1962), **1**, 62-84.
50. Stumm, W.: *Chemistry of Solid Water-Interface*, (1992), New York, Wiley.
51. Arvidson, R. S. and Luttge, A.: "Vertical Scanning Interferometry; the Holy Grail of Low Temperature Dolomite Precipitation Kinetics," *Geological Society of America, 2000 Annual Meeting Abstracts with Programs - Geological Society of America*, (2000) **32**, 7, 79.
52. Land, L. S.: "Failure to Precipitate Dolomite at 25 Degrees C from Dilute Solution Despite 1000-Fold Oversaturation after 32 Years. Geochemistry of Low Temperature Processes," *Aquatic Geochemistry*, (1998), **4**, 3-4, 361-368.
53. Lith, Y.V and Warthmann, R.: "Role of Sulfate Reducing Bacteria during Microbial Dolomite Precipitation as Deduced from Culture Experiments," *Journal of Conference, Cambridge Publications*, (2000), Sept. 3-8, **5**(2), 1038.
54. Langmuir, D.: *Aqueous Environmental Geochemistry*, Upper Saddle River, New Jersey, Prentice-Hall, (1997).
55. Wolery, T.J.: "EQ3NR, A Computer Program for Geochemical Aqueous Speciation-Solubility Calculations: User's Guide and Documentation" UCRL-53414, Lawrence Livermore National Laboratory, (1983).

56. Reid, R. C.: et al.: *The Properties Of Fluids And Gases*. New York, McGraw-Hill, (1987).
57. Holm, L. W., and Josendal, V. A.: "Mechanisms of Oil Displacement by Carbon Dioxide," *JPT* (Dec. 1974) 1427-38.
58. Benham, A. L., et al.: "Miscible Fluid Displacement-Prediction of Miscibility," *Trans.*, AIME (1960) 219, 229-37.
59. Bernard, G.G., and Holm, L. W.: "Effect of Foam on Permeability of Porous Media to Gas," *SPEJ* (Sep. 1968) 267-274.
60. Stalkup, F. I. Jr.: "Miscible Displacement," Monograph Series of SPE, Richardson, TX, (1983) 8, 26-29.
61. Grigg, R.B. and Schechter, D.S.: "State of the Industry in CO₂ Floods," paper SPE 38849 presented at the 1997 SPE Annual Technical conference and Exhibition held in San Antonio, Oct. 5-8.
62. Rogers, J.D. and Grigg, R.B.: "A Literature Analysis of the WAG Injectivity Abnormalities in the CO₂ Process," *SPEREE*, Vol. 5, No. 5, (October 2001).
63. Caudle, B. H., and Dyes, A. B.: "Improving Miscible Displacement by Gas-Water Injection," *Trans.*, AIME (1958) 213, 281-284.
64. Heller, J. P., et al.: "Direct Thickeners for Mobility Control in CO₂ Floods," paper SPE 11789 presented at the 1983 SPE International Symposium on Oilfield and Geothermal Chemistry, Denver, June 1-3.
65. Enick, R.M., Beckman, E.J., Shi, C., Huang, Z., Xu, J., and Kilic, S.: "Direct Thickeners for Carbon Dioxide," paper SPE 59325 presented at the 2000 SPE/DOE Twelfth Symposium on Improved Oil Recovery, Tulsa, April 3-5.
66. Bernard, G. G., and Holm, L. W.: "Effect of Foam on Permeability of Porous Media to Gas," *SPEJ* (Sept. 1964) 267-274.
67. Tsau, J. S. and Heller J. P.: "Evaluation of Surfactants for CO₂-Foam Mobility Control," paper SPE 24013 presented at the 1992 SPE Permian Basin Oil and Gas Recovery Conference, Midland, March 18-20.
68. Tsau, J.S. and Grigg, R.B.: "Assessment of Foam Properties and Effectiveness in Mobility Reduction for CO₂-Foam Floods," paper SPE 37221 presented at the 1997 SPE International Symposium on Oilfield Chemistry, Feb. 18-21.
69. Syahputra, A.E.: "Experimental Evaluation of Lignosulfonate as a Sacrificial Agent in CO₂-Foam Flooding," Thesis, Department of Petroleum Engineering, New Mexico Institute of Mining and Technology, August 1999.
70. Syahputra, A.E., Tsau, J.-S., and Grigg, R.B.: "Laboratory Evaluation of Using Lignosulfonate and Surfactant Mixture in CO₂ Flooding," paper SPE 59368 presented at the 2000 SPE/DOE Improved Oil Recovery Symposium, Tulsa, April 3-5.
71. Tsau, J.S., Syahputra, A.E., Yaghoobi, H., and Grigg, R.B.: "Use of Sacrificial Agents in CO₂ Foam Flooding Application," paper SPE 56609 presented at the 1999 SPE Annual Technical Conference and Exhibition, Houston, October 3-6.
72. Tsau, J.-S., Yaghoobi, H., and Grigg, R.B.: "Use of Mixed Surfactants to Improve Mobility Control in CO₂ Flooding," paper SPE 39792 presented at the 1998 SPE Permian Basin Oil and Gas Recovery Conference, Midland, March 23-27.

73. Tsau, J.-S., Syahputra, A.E., and Grigg, R.B.: "Economic Evaluation of Surfactant Adsorption in CO₂ Foam Application," paper SPE 59365 presented at the 2000 SPE/DOE Improved Oil Recovery Symposium, Tulsa, April 3-5.
74. Heller, J.P., Boone, D.A., and Watts, R.J.: "Field Test of CO₂ Mobility Control at Rock Creek," paper SPE 14395 presented at the 1985 SPE Annual Technical Conference and Exhibition, Las Vegas, September 22-25.
75. Jonas, T. M., Vasicek, S. L., and Chou, S. I.: "Evaluation of a CO₂ Foam Field Trial: Rangely Weber Sand Unit," paper SPE 20468 presented at the 1990 Annual Technical Conference, New Orleans, Sept. 23-26.
76. Chou, S. I., et al.: "CO₂ Foam Field Trial at North Ward-Estes," paper SPE 24643 presented at the 1992 Annual Technical Conference, Washington, DC, Oct. 4-7.
77. Tsau, J.S. et al.: "CO₂ Foam Field Verification Pilot Test at EVGSAU: Phase IIIA—Surfactant Performance Characterization and Quality Assurance," paper SPE 27785 presented at the 1994 SPE/DOE Symposium on Improved Oil Recovery, Tulsa, April 17-20.
78. Harpole, K.J., Semers, W.T., and Gerard, M.G.: "CO₂ Foam Field Verification Pilot Test at EVGSAU: Phase IIIC—Reservoir Characterization and Response to Foam Injection," paper SPE 27798 presented at the 1994 SPE/DOE Symposium on Improved Oil Recovery, Tulsa, April 17-20.
79. Martin, F.D. et al.: "CO₂-Foam Field Verification Pilot Test at EVGSAU Injection Project Phase I: Project Planning and Initial Results," paper SPE 24176 presented at the 1992 SPE/DOE Symposium on Enhanced Oil Recovery, Tulsa, April 22-24.
80. Martin, F.D., Stevens, J.E., and Harpole, K.J.: "CO₂-Foam Field Test at the East Vacuum Grayburg/San Andres Unit," *SPE* (November 1995), 266-272.
81. Stevens, J. E., and Martin, F. D.: "CO₂ Foam Field Verification Pilot Test at EVGSAU: Phase IIIB: Project Operations and Performance Review," paper SPE/DOE 27786 presented at the 1994 Symposium on Improved Oil Recovery, Tulsa, April 17-20.
82. Hoefner, M. L., Evans, E. M., Buckles, J. J., and Jones, T. A.: "CO₂ Foam: Results From Four Developmental Field Trials," paper SPE/DOE 27787 presented at the 1994 Symposium on Improved Oil Recovery, Tulsa, April 17-20.
83. Holm, L.W. and Garrison, W.H.: "CO₂ Diversion with Foam in an Immiscible CO₂ Field Project," *SPE* (February 1988), Vol. 3, No. 1, 112-118.
84. Kuhlman, M. I., Falls, A. H., and Wellington, S. L.: "Gas/Oil Lamellae and Surfactant Propagation in the Oil in Carbon Dioxide Foam," paper SPE/DOE 27788 presented at the 1994 SPE/DOE Symposium on Improved Oil Recovery, Tulsa, April 17-20.
85. Bernard, G.G., Holm, L.W., and Harvey, C.P.: "Use of Surfactant to Reduce CO₂ Mobility in Oil Displacement," *SPEJ* (August 1980) 281-292.
86. Wellington, S.L. and Vinegar, H. L.: "CT Studies of Surfactant to Reduce CO₂ Mobility Control," paper SPE 14393 presented at the 1985 SPE Annual Technical Conference, Las Vegas, Sept. 22-25.
87. Lee, H.O., Heller, J.P., and Hoefner, A.M.W.: "Change in Apparent Viscosity of CO₂ Foam with Rock Permeability," *SPE* (November 1991) 421-428.

88. Yaghoobi, H. and Heller, P. J.: "Laboratory Investigation of Parameters Affecting CO₂-foam Mobility in Sandstone at Reservoir Conditions" paper SPE 29168 presented at the 1994 SPE Eastern Regional Conference and Exhibition, Charleston, Nov. 8-10.
89. Heller, J. P., Lien, C. L., and Kuntamukkula, M. S.: "Foamlike Dispersions for Mobility Control in CO₂ Floods," *SPEJ* (August 1985) 603-613. Yaghoobi, H. and Heller, J.P.: "Effect of Capillary Contact on CO₂-Foam Mobility in Heterogeneous Cores," paper SPE 35169 presented at the 1996 SPE Permian Basin Oil and Gas Recovery Conference, Midland, March 27-29;
90. Hanssen, J. E., and Dalland, M.: "Foams for Effective Gas Blockage in the Presence of Crude Oil," paper SPE/DOE 20193 presented at the 1990 SPE/DOE EOR Symposium, Tulsa, April 22-25.
91. Aarra, M. G., and Skauge, A.: "A Foam Pilot in a North Sea Oil Reservoir: Preparation for a Production Well Treatment," paper SPE 18599 presented at the 1994 SPE Annual Technical Conference and Exhibition, New Orleans, LA, Sept. 25-28.
92. Kuhlman, M. I.: "Visualizing the Effect of Light Oil on CO₂ Foams," *JPT* (July 1990) 902-908.
93. Hornof, V.: "Applications of Lignosulfonates in Enhanced Oil Recovery," *Cellulose Chemistry and Technology*, (1990) **24**, 407-415.
94. Hong, S. A., Bae, J. H., and Lewis, G. R.: "An Evaluation of Lignosulfonate as a Sacrificial Adsorbate in Surfactant Flooding," *SPE* (February 1987) 17-27.
95. Hong, S. A., and Bae, J. H.: "Field Experiment of Lignosulfonate Preflushing for Surfactant Adsorption Reduction," *SPE* (November 1990) 467-474.
96. Kalfoglou, G., Prieditis, J., and Paulette, G. S.: "Lignosulfonate-Acrylic Acid Graft Copolymers as Sacrificial Agents for Carbon Dioxide Foaming Agents," Canadian Patent 2,185,499.
97. Tsau, J.S., Yaghoobi, H., and Grigg, R.B.: "Smart Foam to Improve Oil Recovery in Heterogeneous Porous Media," paper SPE 39677 presented at the SPE/DOE Eleventh Symposium on Improved Oil Recovery, Tulsa, 19-22 April 1998.

Table 1. CO₂ Miscible Project Locations in the United States with Number of Total and Active Listed

State	Total Projects	Active Projects
Alabama	1	0
California	2	0
Colorado	2	1
Kansas	1	1
Louisiana	10	0
Michigan	2	2
Mississippi	4	3
Montana	1	0
New Mexico	8	3
North Dakota	1	0
Oklahoma	6	5
Pennsylvania	2	0
Texas	80	47
Utah	3	3
West Virginia	2	0
Wyoming	11	6

Table 2. CO₂ Flooded Fields in the Permian Basin.

Total #	State Total	State	Unit	Current Operator	Current Status
1	1	Texas	Adair San Andres	Amerada Hess	Operating
2	2	Texas	Anton Irish	Oxy	Operating
3	3	Texas	Bennett Ranch	Oxy	Operating
4	4	Texas	Brahaney	Apache	Future
5	5	Texas	Brahaney Plains	Apache	Future
6	6	Texas	Cedar Lake	Oxy	Operating
7	1	New Mexico	Central Vacuum	ChevronTexaco	Operating
8	7	Texas	Cogdell	Oxy.	Operating
9	8	Texas	Cordona Lake	ExxonMobil	Operating
10	9	Texas	Dollarhide (Devonian)	Pure	Operating
11	10	Texas	Dollarhide (Clearfork "AB")	Pure	Future
12	11	Texas	East Ford	Orla Petco	Operating
13	12	Texas	East Huntley	Southwest Royalty	Terminated
14	13	Texas	East Penwell (SA)	First Permian	Operating
15	2	New Mexico	East Vacuum	Phillips	Operating
16	14	Texas	El Mar	Oxy	Operating
17	15	Texas	Ford Geraldine	Primrose Operating	Terminated
18	16	Texas	Garza	George R. Brown	Terminated
19	17	Texas	GMK South	ExxonMobil	Operating
20	18	Texas	Goldsmith	ChevronTexaco	Field Demo

Total #	State Total	State	Unit	Current Operator	Current Status
21	19	Texas	Hanford	Fasken	Operating
22	20	Texas	Hanford East	Fasken	Operating
23	21	Texas	Hanford Marmaton	Stanberry Oil	Terminated
24	22	Texas	Jess Burnes	Phillips	Never started
25	23	Texas	Kingdom Abo	ChevronTexaco	Terminated
26	3	New Mexico	Leamex	Phillips	Pilot Term.
27	24	Texas	Levelland	Oxy	Pilots Term.
28	25	Texas	Levelland	ExxonMobil	Never started
29	4	New Mexico	Loco Hills	Yates	Pilot Term.
30	26	Texas	Mabee	ChevronTexaco	Operating
31	5	New Mexico	Maljamar Pilot & Field	Conoco	Terminated
32	27	Texas	McElroy	Southland Royalty	Terminated
33	28	Texas	McElroy	ChevronTexaco	Field Demo
34	29	Texas	Means (San Andres)	ExxonMobil	Operating
35	30	Texas	Mid Cross-Devonian	Oxy	Operating
36	31	Texas	North Cowden	Oxy (four pilots)	Pilots Term.
37	32	Texas	North Cross (Crossett)	Oxy	Operating
38	33	Texas	North Dollarhide	Oxy	Operating
39	6	New Mexico	North El Mar	Quay Valley	Never started
40	34	Texas	North Farnsworth	Stanberry Oil	Terminated
41	35	Texas	North Hansford Cherokee	Dorchester	P & A
42	7	New Mexico	North Hobbs	Oxy	Future
43	36	Texas	North Van Rueder	Apache	Never started
44	37	Texas	North Ward Estes	ChevronTexaco	Terminated
45	8	New Mexico	Philmex	Phillips	Pilot Term.
46	9	New Mexico	Ranger Lake	Phillips	Never started
47	38	Texas	Rankin	Petromac Inc.	Pilot Term.
48	39	Texas	Reeves	Devon	Never started
49	40	Texas	Reinecke	Pure	Operating
50	41	Texas	Robertson (Central and N.)	Oxy	Future
51	42	Texas	Russell	ExxonMobil	Never started
52	43	Texas	Sable	Whiting	Terminated
53	44	Texas	SACROC	Kinder Morgan	Operating
54	45	Texas	Salt Creek	ExxonMobil	Operating
55	46	Texas	Seminole -Main Pay	Amerada Hess	Operating
56	47	Texas	Seminole -ROZ Phase 1	Amerada Hess	Operating
57	48	Texas	Sharon Ridge	ExxonMobil	Operating
58	49	Texas	Slaughter Alex Estate	Oxy	Operating
59	50	Texas	Slaughter Central Mallet	Oxy	Operating
60	51	Texas	Slaughter Estate & Pilot	Oxy	Operating
61	52	Texas	Slaughter Frazier	Oxy	Operating
62	53	Texas	Slaughter HT Boyd Lease	Anadarko	Operating
63	54	Texas	Slaughter (started June-89)	ExxonMobil	Operating

Total #	State Total	State	Unit	Current Operator	Current Status
64	55	Texas	Slaughter (started May-85)	ExxonMobil	Operating
65	56	Texas	Slaughter Sundown	ChevronTexaco	Operating
66	57	Texas	South Cowden	Phillips	Operating
67	58	Texas	South Cowden (Emmons)	Phillips	Future
68	59	Texas	South Cross (Crossett)	Oxy	Operating
69	60	Texas	South Huntley	Southwest Royalty	Terminated
70	61	Texas	South Welch & Pilots	Oxy	Operating
71	62	Texas	Sprayberry Trend	Pioneer	Pilot
72	10	New Mexico	State 35 Unit (Hale Mable)	Phillips	Operating
73	63	Texas	T-Star	Oxy	Operating
74	64	Texas	Twofreds-East & West	EOG	Operating
75	65	Texas	University Waddell	ChevronTexaco	Terminated
76	11	New Mexico	VGSAU	ChevronTexaco	Future
77	66	Texas	Wasson	ExxonMobil	Operating
78	67	Texas	Wasson Cornell	ExxonMobil	Operating
79	68	Texas	Wasson Denver	Oxy	Operating
80	69	Texas	Wasson ODC & Pilot	Oxy	Operating
81	70	Texas	Wasson South	Oxy	Operating
82	71	Texas	Wasson Willard & Pilot	BP	Operating
83	72	Texas	Wellman	The Wiser Oil Co.	Terminated
84	73	Texas	West Brahaney	Walsh Petroleum	Terminated
85	74	Texas	West Welch	Oxy	Operating
86	75	Texas	Yates	Marathon Oil	Operating
Operating = CO ₂ injection project in progress					
Future = Future project					
Never started = Listed as future in the past, but not expected to start up in the foreseeable future.					
Terminated = Field is under production, but CO ₂ purchase has stopped.					
Field Demo = First phase developed to evaluate field potential both technical and economical.					
Pilot = Small project intended to demonstrate technical feasibility.					
Pilot terminated = A pilot that has been terminated					
P & A = The field has been plugged and abandoned or otherwise truly terminated.					

Table 3. Rock Types

Rock Type	Dolomite	Sandstone	Limestone	Tripolite
Dolomite	43			
Sandstone	6	9		
Limestone	10	1	7	
Tripolite	1	1	0	3

Table 4. Injectivity Changes

Injectivity Changes	Brine	CO₂
None noted	4	5
No comment	7	9
Decreased (Magnitude not indicated)	5	7
Changed (Magnitude indicated)	11	6

Table 5. What Has or Has Not Gone Well?

Response	Has	Has not
Oil response at or above that predicted	25	19
Injectivity is sufficient	2	12
Gas Production within designed limits	4	13
No scaling	0	7
Other: minimum asphaltene deposit, cost inline with predictions, lower corrosion than expected, acceptable well failure rate	4	6

Table 6. Mystery

Responses	Number
Processing rate	12
Reservoir characterization	12
Injectivity	7
Scaling, asphaltenes, conformance, equipment	4

Table 7. Research Focus

Responses	Number
Sweep/profile/conformance	10
Productivity/injectivity	8
Monitoring	3
Predictions, mechanism, improve economics of known technology	8

Table 8. Core Properties

Core	Diam(in)	Length(in)	Perm(md)	Por(%)
India	1.98	20.3	35.7	12.3
S139	1.98	6.5	30.6	12.7
S141	1.98	5.8	9.7	11.3

Table 9- Brine Composition

	<u>Teague Blinebry</u>	<u>Seminole San Andres</u>
	<u>ppm</u>	<u>ppm</u>
NaCl	64700	13531
CaCl ₂	11000	4330
MgCl ₂	3810	1914
NaHCO ₃	1850	5645
Na ₂ SO ₄	5590	4831
TDS	86950 ppm	30251 ppm

Table 10. Tacer Brine Compositions

<u>Salt</u>	<u>Conc(ppm)</u>	<u>Molar strength(M)</u>
NaCl	10000	0.171
CaCl ₂	5000	0.045
MnCl ₂	5000	0.0397
MgCl ₂	5000	0.0525
SrCl ₂	5000	0.0315

Table 11. Parameters for Segment A, Segment B, and the Entire Core

	<u>Diameter [in]</u>	<u>Length [in]</u>	<u>Porosity [%]</u>
Segment A	1.98	6.75	16.91
Segment B	1.98	15.5	17.54
Entire Core	1.98	22.25	17.35

Table 12. Media Variations Used in the TRANSTOUGH Model Simulations. Porosity is 15 % for All Except for “E” with a Measured Dolomite-Anhydrite Porosity of 13%.

A. Pure Calcite	B. Pure Quartz	C. Quartz w/ Carbonates	D. Quartz w/ Evaporites	E. Dolomite w/ Anhydrite
85% calcite	85% quartz	45% quartz	40% quartz	
		20% gypsum	30% calcite	67% dolomite
		20% halite	15% magnesite	20% anhydrite

Table 13. Kinetic Reaction Rate Constants

Mineral	Reaction Rate Constants (mol cm ⁻² sec ⁻¹)
Calcite	1.0 × 10 ⁻⁵
Dolomite	1.0 × 10 ⁻⁷
Magnesite	1.0 × 10 ⁻⁷
Quartz	1.0 × 10 ⁻¹³
Anhydrite	1.0 × 10 ⁻⁶
Halite	1.0 × 10 ⁻⁴
Gypsum	1.0 × 10 ⁻⁴

Table 14. Experimental Brine Solution Concentrations (“**”) Indicates Concentrations That Were Varied)

Brine Component	Concentration [M]
Na ⁺	7.21 x 10 ⁻¹
SO ₄ ²⁻	6.55 x 10 ⁻³
Mg ²⁺	2.60 x 10 ⁻²
Cl ⁻	8.46 x 10 ⁻¹
Ca ²⁺	4.56 x 10 ⁻²
pH	8.4 **
CO ₂ (aq)	2.54 x 10 ⁻⁵ **

Table 15. Brine Alkalinity and pH Ranges (Low, Medium, High) for the Quartz-Carbonate and - Evaporite Systems

pH	Media Type	Value, ppm		
		Low	Med.	High
6.5	Quartz-Carbonate	200	305 *	400
6.5	Quartz-Evaporite	50	200	305 *
7.5	Quartz-Carbonate	200	305 *	400
7.5	Quartz-Evaporite	50	200	305 *
8.4*	Quartz-Carbonate	200	305 *	400
8.4*	Quartz-Evaporite	20	200	305 *

Table 16. Chemical Reactions Used in the Model (Secondary Species Reactions, Except HCO₃⁻ and OH⁻, Not Presented)

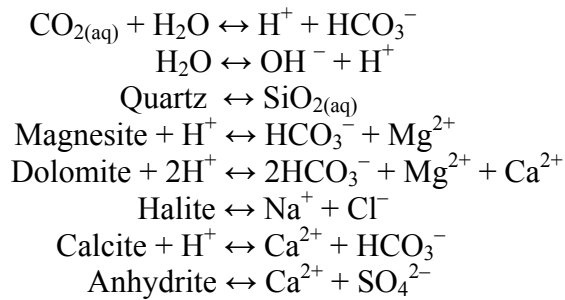


Table 17. Parameters of the Dolomite-Anhydrite Experiment

Parameter	Experiment Conditions
Temperature	100°F
Back pressure	2000 psi
Initial saturation	100% Brine
Geologic media	rock type E, Table 1
Porosity	13%
Permeability	30.6 mD
CO ₂ injection rate	21.53 cm ³ hr ⁻¹
Brine injection rate	33.09 cm ³ hr ⁻¹
Simulated Time	110.9 days

Table 18. Parameters for the Sensitivity Analysis

Parameters	Sensitivity Analysis
Temperature	100°F
Back pressure	2000 psi
Initial saturation	100% Brine
Geologic media	Rock types A – D, Table 1
Porosity	15%
Permeability	38.4 mD
CO ₂ injection rate	50 cm ³ hr ⁻¹
Brine injection rate	50 cm ³ hr ⁻¹
Brine pH	6.5, 7.5, and 8.4
Brine Alkalinity	Carbonate: 200, 305, and 400 ppm Silica: 50, 200, and 305 ppm
Total simulation time	173.6 days

Table 19. Adsorption Comparison of Four Rock Types at Two Concentrations of CD1045

	Adsorption of CD1045, mg/cc	
	0.25 wt% CD1045	0.05 wt% CD1045
Berea sandstone	4.0	2.0
Indiana limestone	1.6	0.6
Baker dolomite	1.2	0.6
E. Vacuum dolomite	1.0	0.3

Table 20. Summary of EVGSAU Foam Test Economics

EVGSAU Foam Tests	Test 1	Test2
Incremental Oil, bbl	14,700	4,460
Less Royalty (1/8), bbl	12,862	3,902
Oil Price, \$/bbl	17.50	15.45
Gross Revenue, \$	225,094	60,294
Lifting Costs, \$(5.50/bbl)	-80,850	-24,530
Oil Revenue	\$144,244	\$35,764

EVGSAU Foam Economics	
Oil Revenue	\$180,008
Compression Savings	\$ 44,250
Surfactant Costs:	
Material	\$166,000
Facilities	<u>\$ 10,000</u>
Net from Project	\$ 48,258

Table 21. Improved Economics of Enhanced Foam

Option 1:	
CD1045: 0.2 x 105,000 lbs x 0.85 x \$1.57	\$28,025
Lignosulfonate: 2 x 105,000 lbs x 0.85 x \$0.25	<u>\$44,625</u>
Materials	\$72,650
Facilities (\$1,000 more than EVGSAU)	<u>\$11,000</u>
Total Surfactant Costs	\$83,650
 Option 2:	
Lignosulfonate in Preflush:	
2 x 90,000 lbs x 0.85 x \$0.25	\$38,250
Lignosulfonate in SAG: 2 x 15,000 lbs x \$0.25	\$ 7,500
CD1045 in SAG: 0.2 x 15,000 lbs x \$1.57	<u>\$ 4,710</u>
Materials	\$50,460
Facilities (\$1,000 more than EVGSAU)	<u>\$11,000</u>
Total Surfactant Costs	\$61,460

	Enhanced Foam Economics	
	Option 1	Option 2
Oil Revenue	\$180,008	\$180,008
Compression Savings	\$ 44,250	\$ 44,250
Surfactant Costs:		
Material	\$ 72,650	\$ 50,460
Facilities	<u>\$ 11,000</u>	<u>\$ 11,000</u>
Net from Project	\$ 140,608	\$162,798

Table 22. Core Parameters for Adsorption and Desorption Profiles

Parameter	Value
Length, cm	6.10
Diameter, cm	3.79
Cross sectional area, cm ²	11.27
Core volume, cm ³	68.75
Pore volume, cm ³	15.9
Porosity, percent	19.2
Original permeability, md	320.28

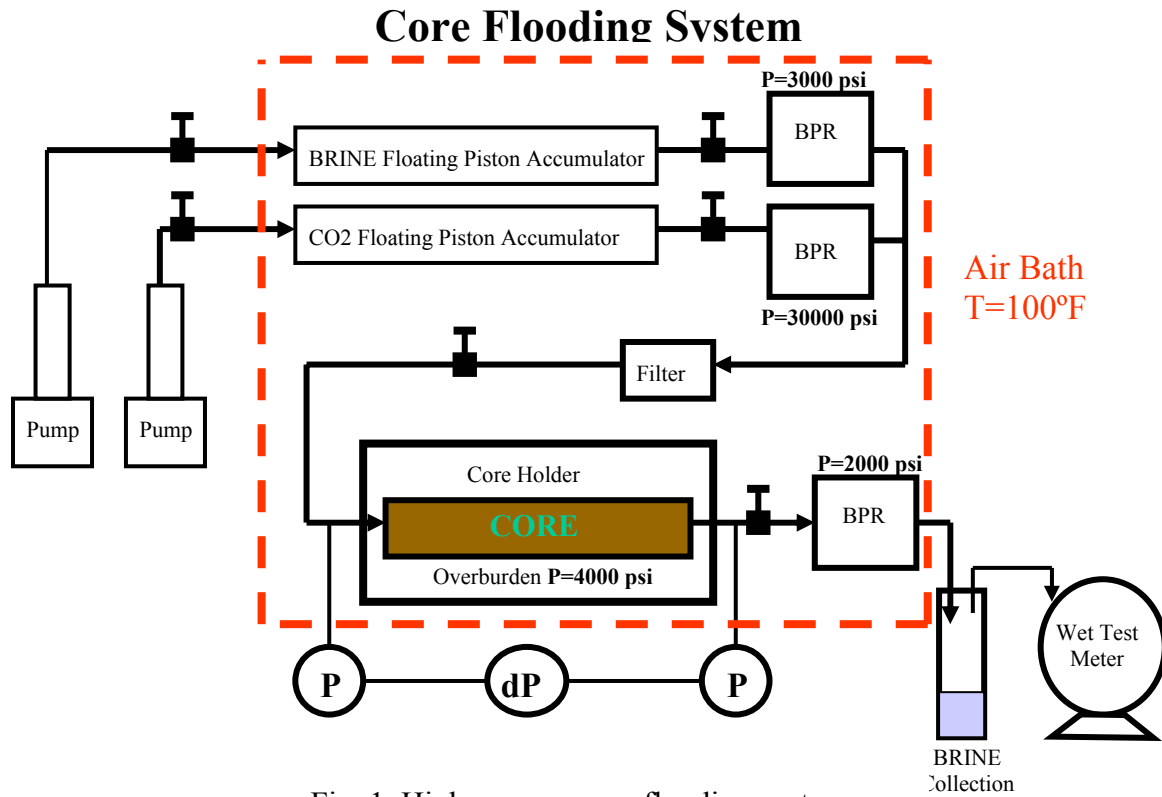


Fig. 1. High pressure coreflooding system.

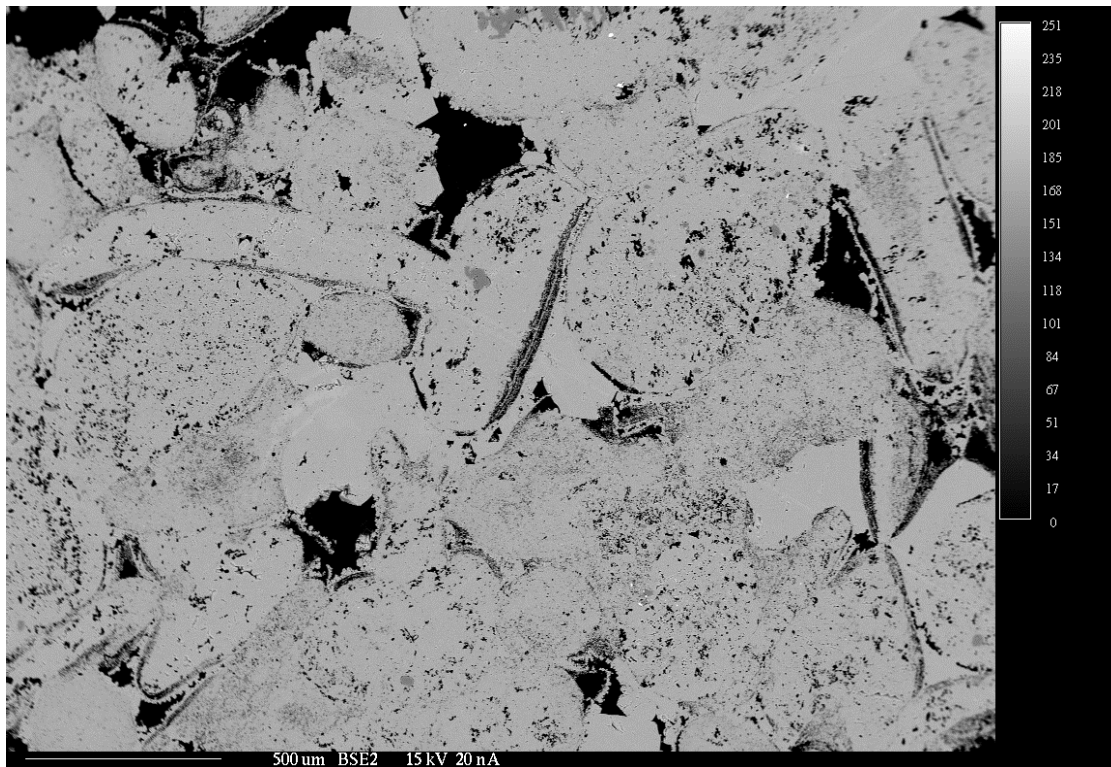


Fig. 2. BSE image of pre-flood Indiana limestone, 500 micron scale.

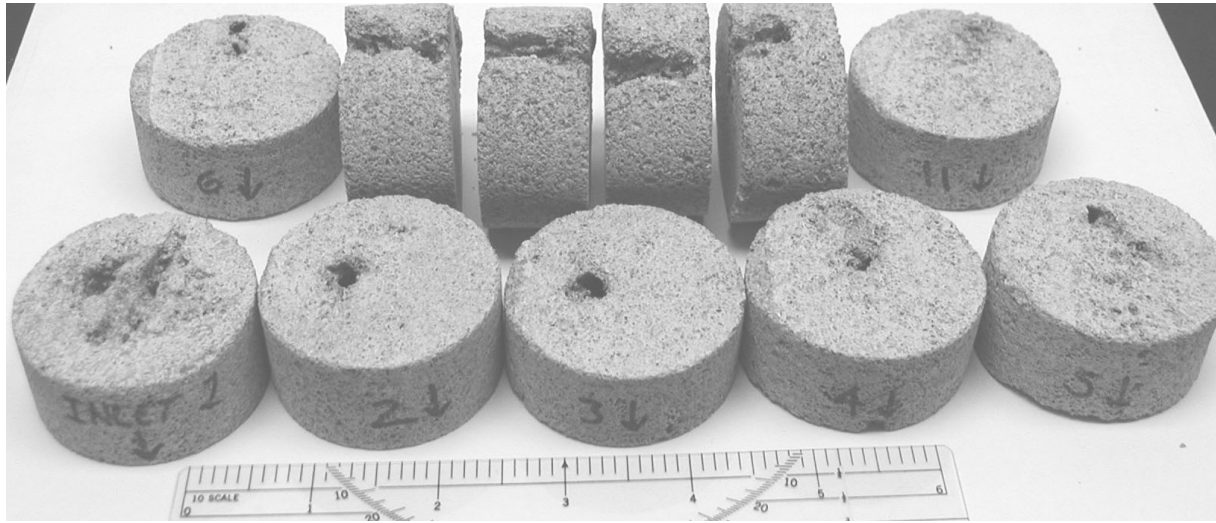


Fig. 3. Photo of post-flood Indiana limestone core, sliced to reveal extent of dissolution channel. Segments are marked sequentially in inches. Note the worm hole that extended half way through the core before it failed.

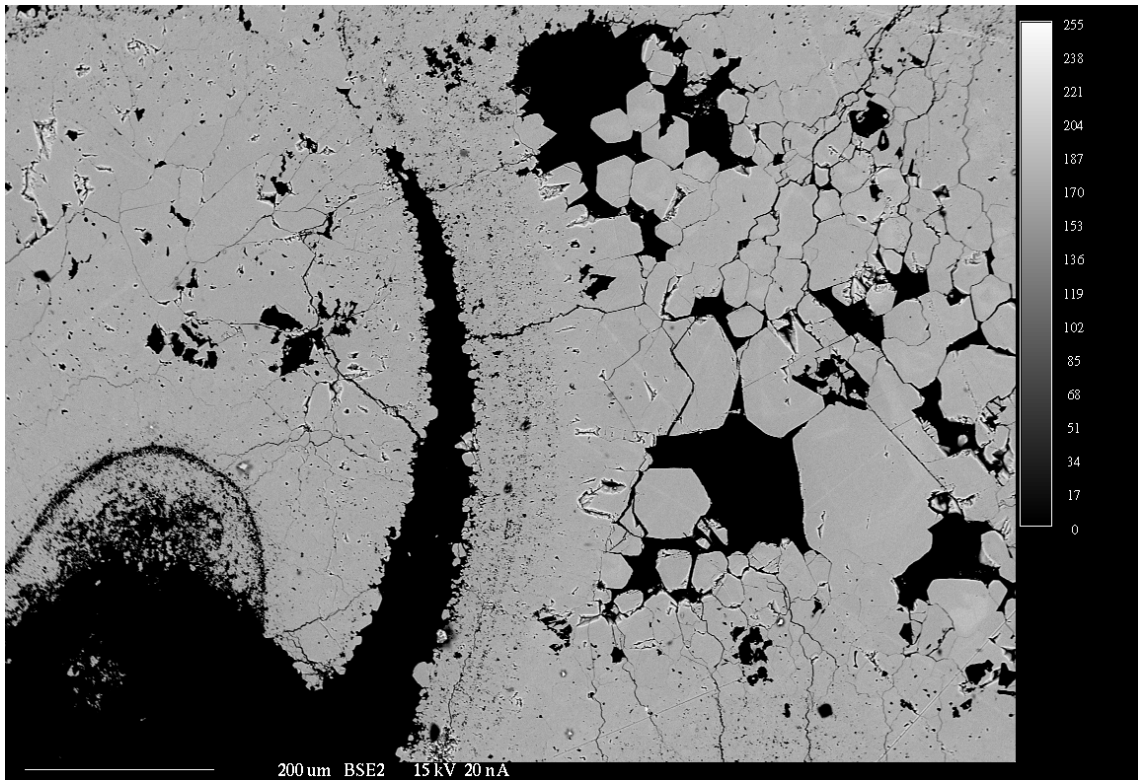


Fig. 4. BSE image of dissolution of grains and cement adjacent to channel, 200 micron scale.

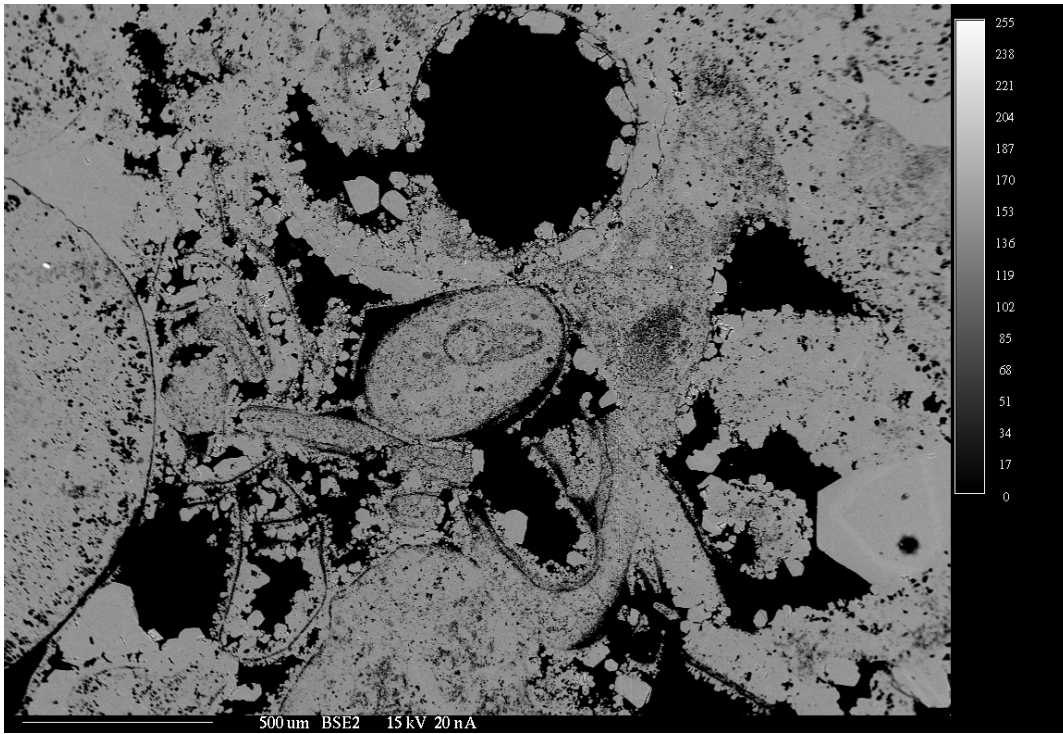


Fig. 5. BSE image of dissolution of grains and cement, 500 micron scale.

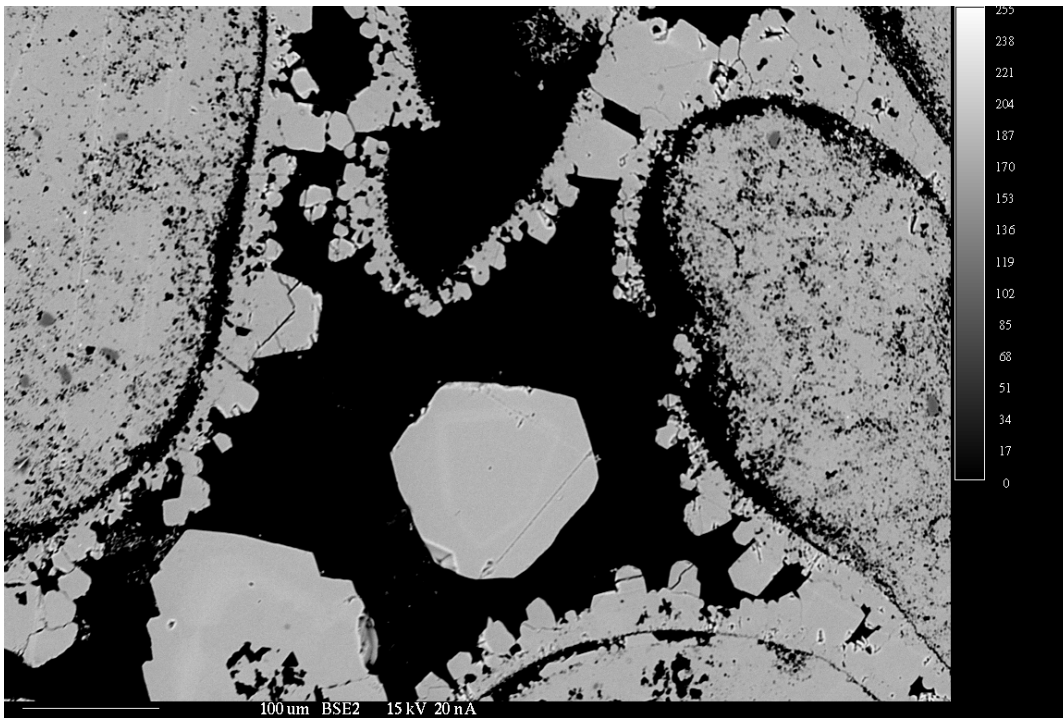


Fig. 6. BSE image of remnant calcite overgrowth and large calcite crystals, 100 micron scale.

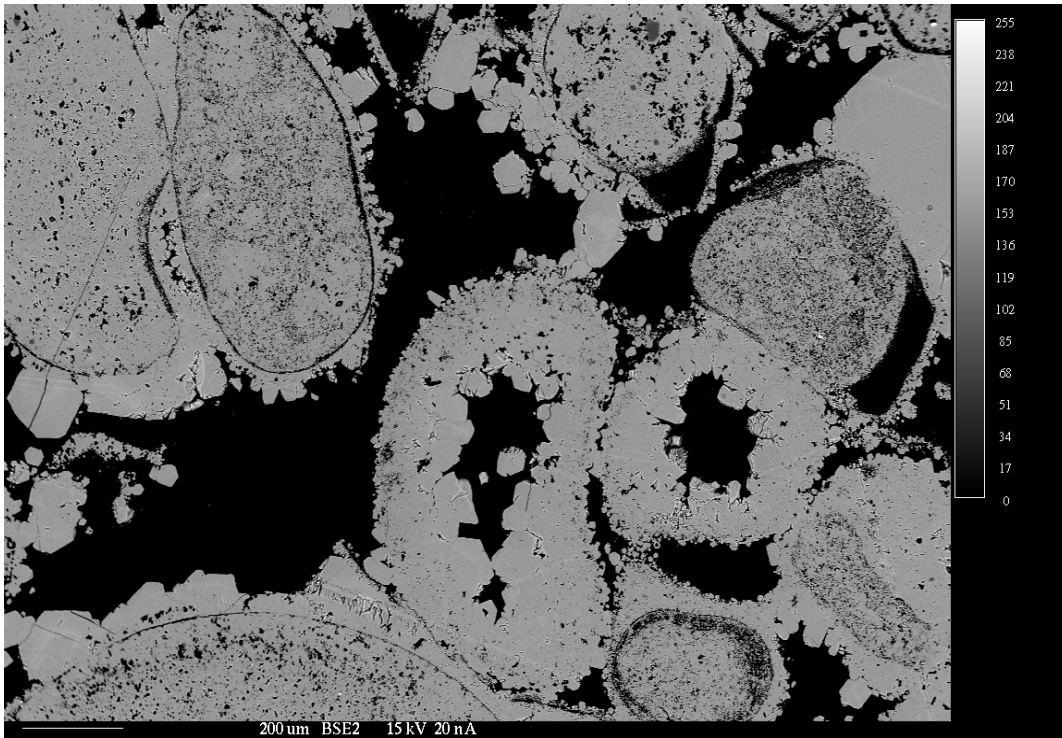


Fig. 7. BSE image of remnant overgrowths, grain replacement and large calcite crystals, 200 micron scale.

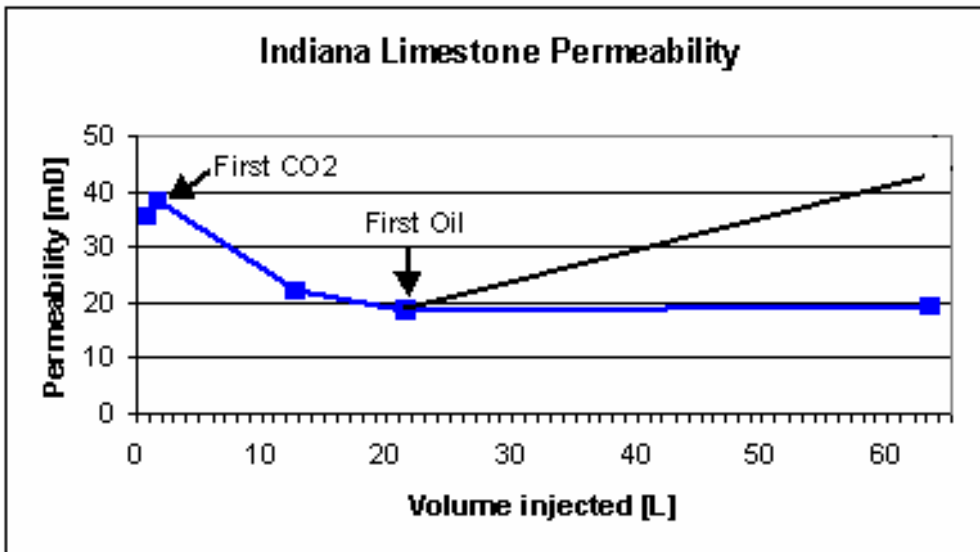


Fig. 8. Indiana limestone core permeability.

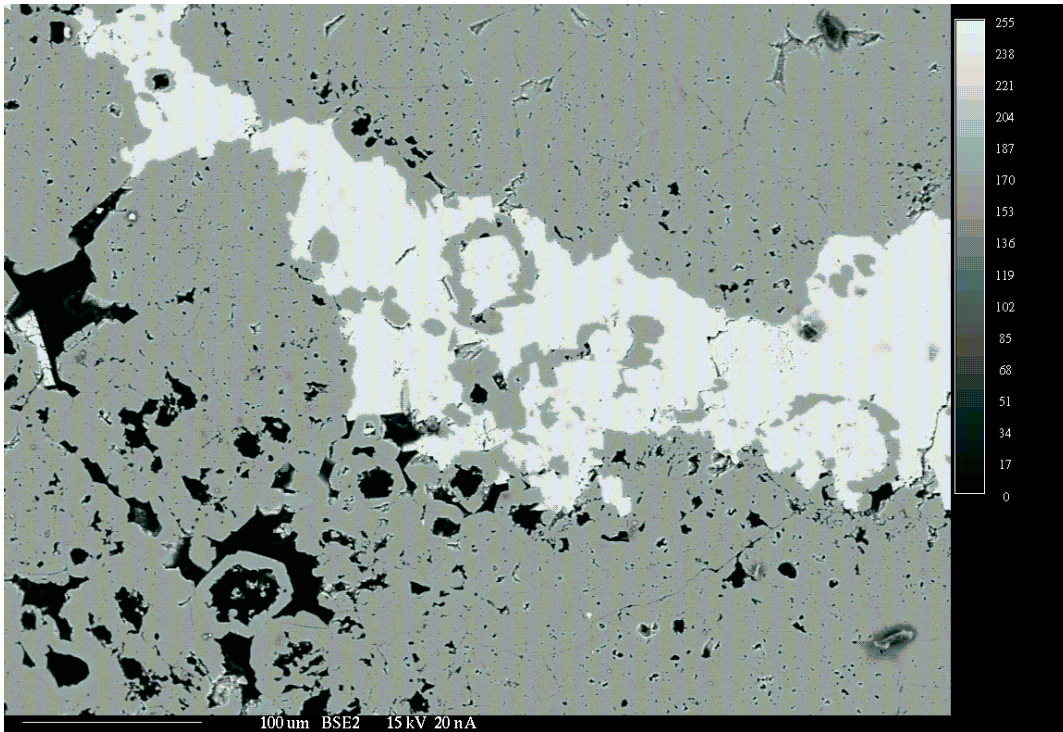


Fig. 9. BSE image of pre-flood Seminole San Andres core, 100 micron scale.

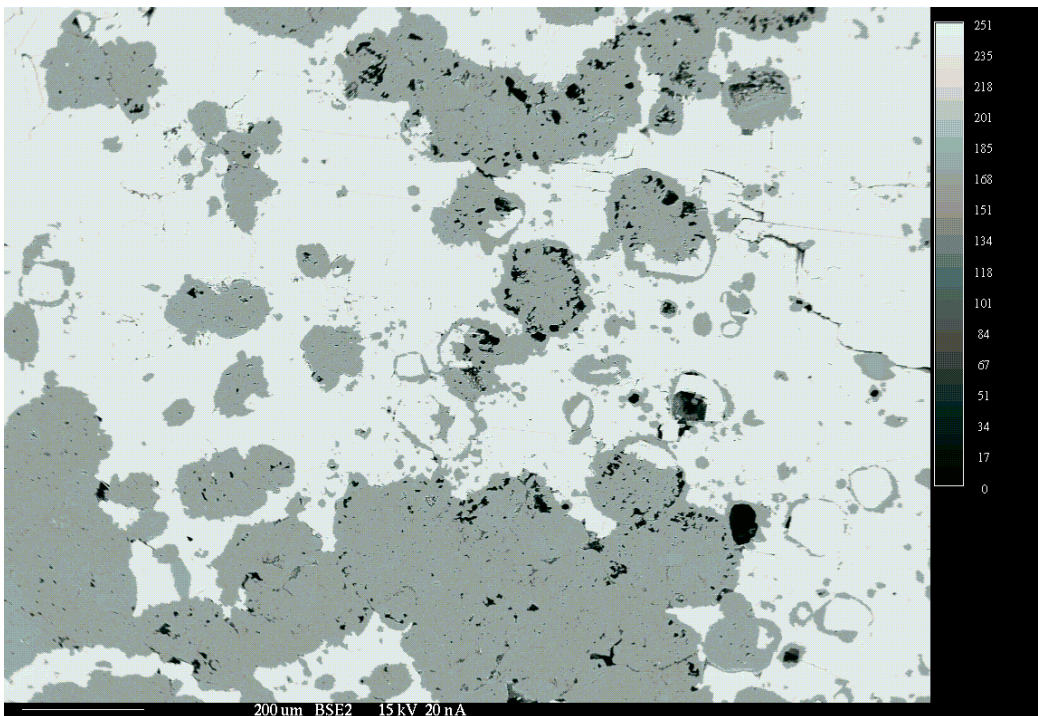


Fig. 10. BSE image of pre-flood Seminole San Andres core, 200 micron scale.

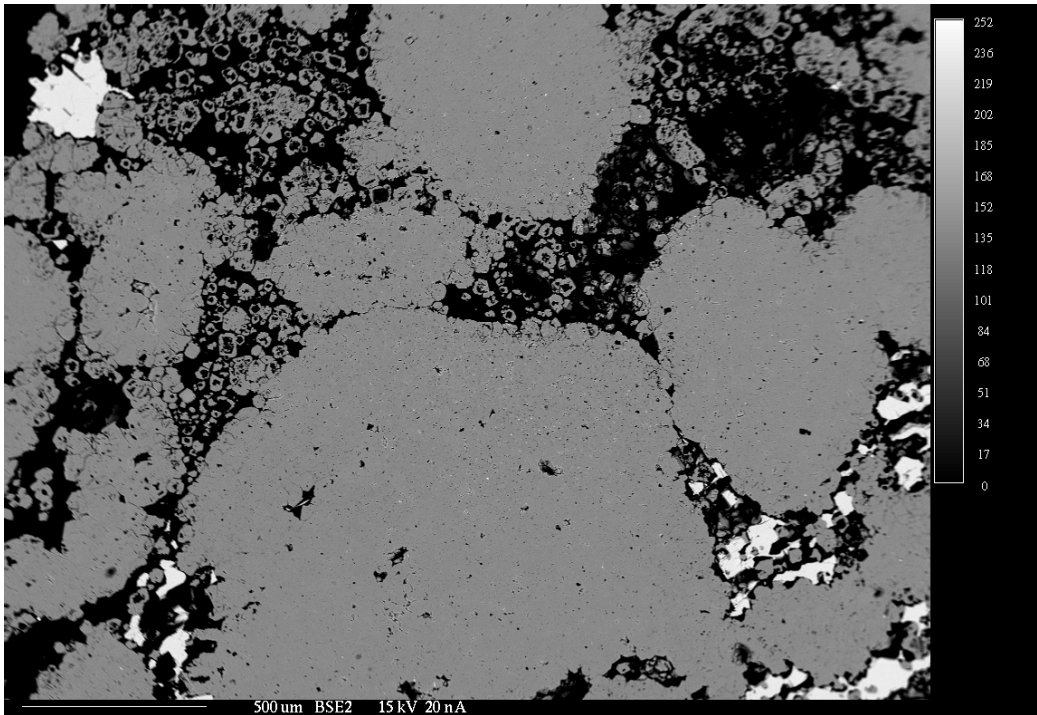


Fig. 11. BSE image of post-flood Seminole San Andres core S139B, 500 micron scale.

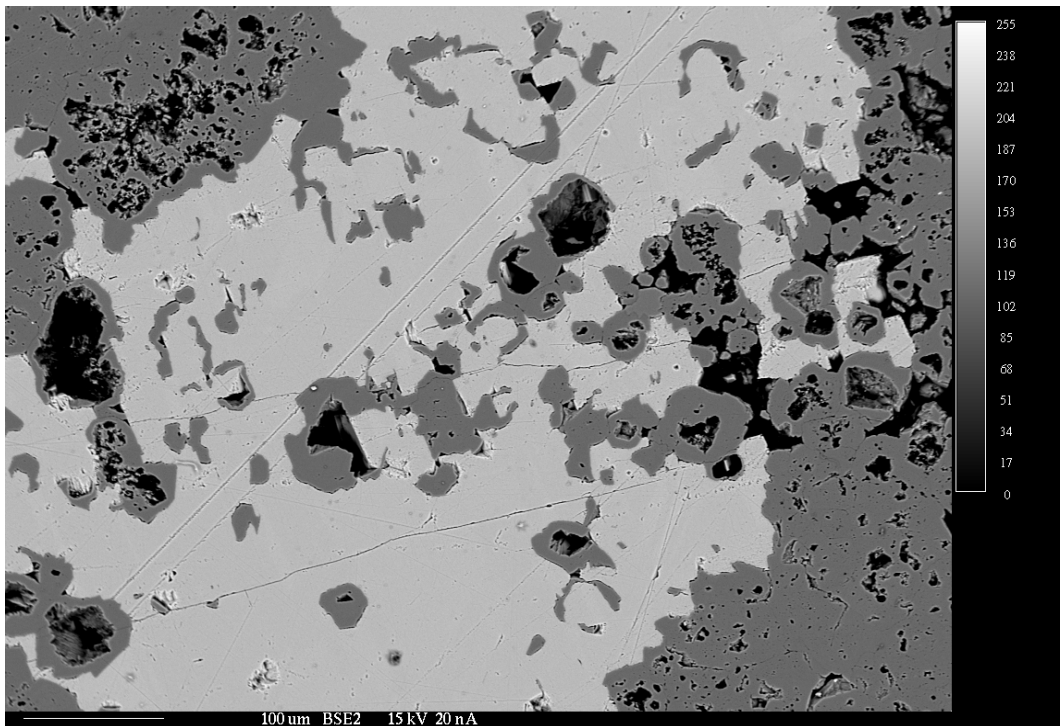


Fig. 12. BSE image of post-flood Seminole San Andres core S139B, 100 micron scale.

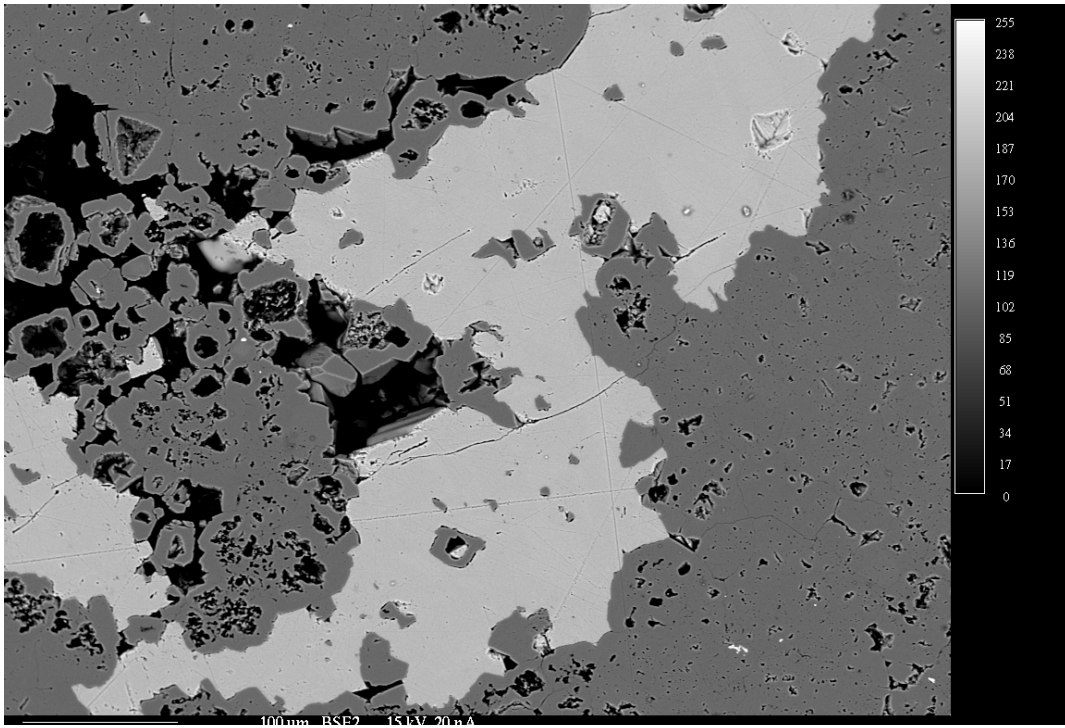


Fig. 13. BSE image of flooded Seminole San Andres core S139B, 100 micron scale.



Fig. 14. Photo of dissolution features in sliced Seminole San Andres core S141B.



Fig. 15. Closeup of anhydrite dissolution channels in Seminole San Andres core S141B.



Fig. 16. Photo of post-flood dissolution features in sliced Seminole San Andres core S139B.

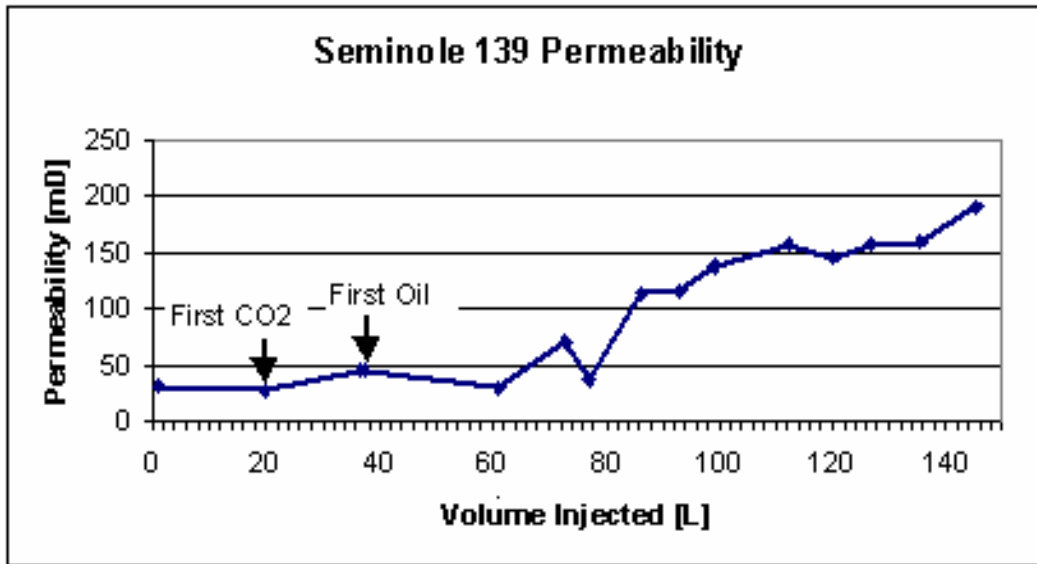


Fig. 17. Seminole San Andres core 139B permeability.

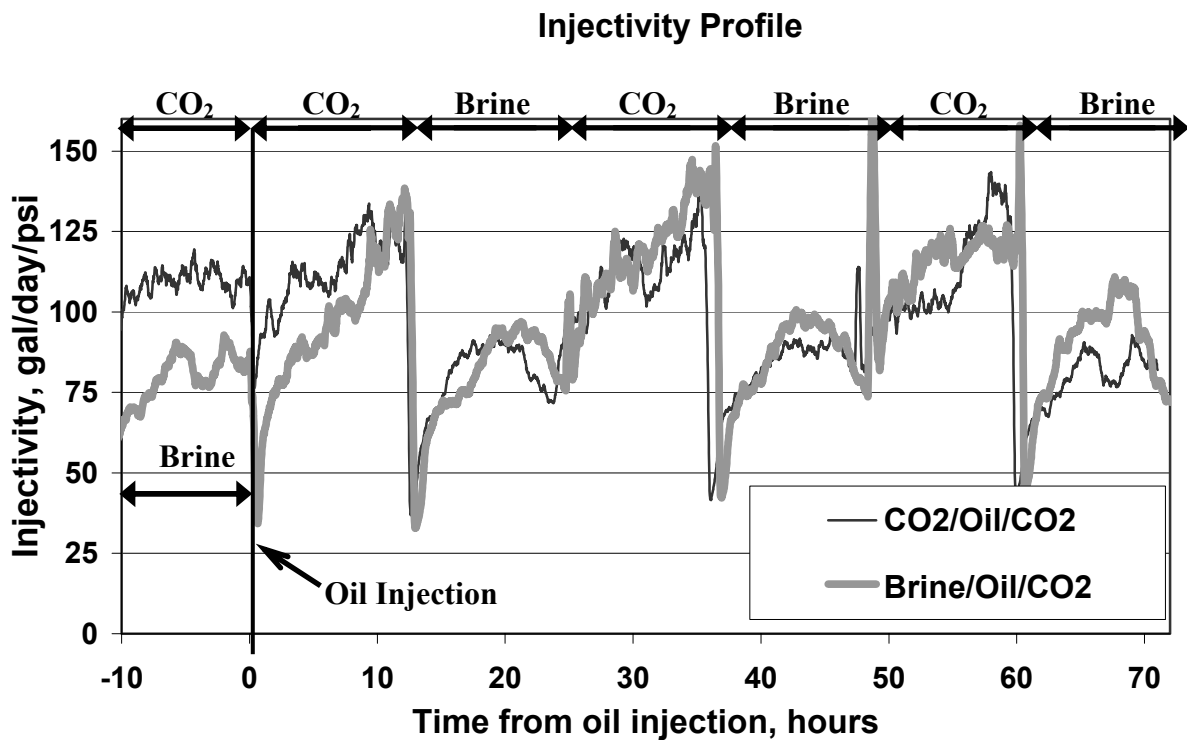


Fig.18. Injectivity profile when the small oil contamination injection was followed by CO₂ half cycle. This figure compares oil injection being preceded by brine to the case where the oil injection was preceded by CO₂.

Injectivity Profile

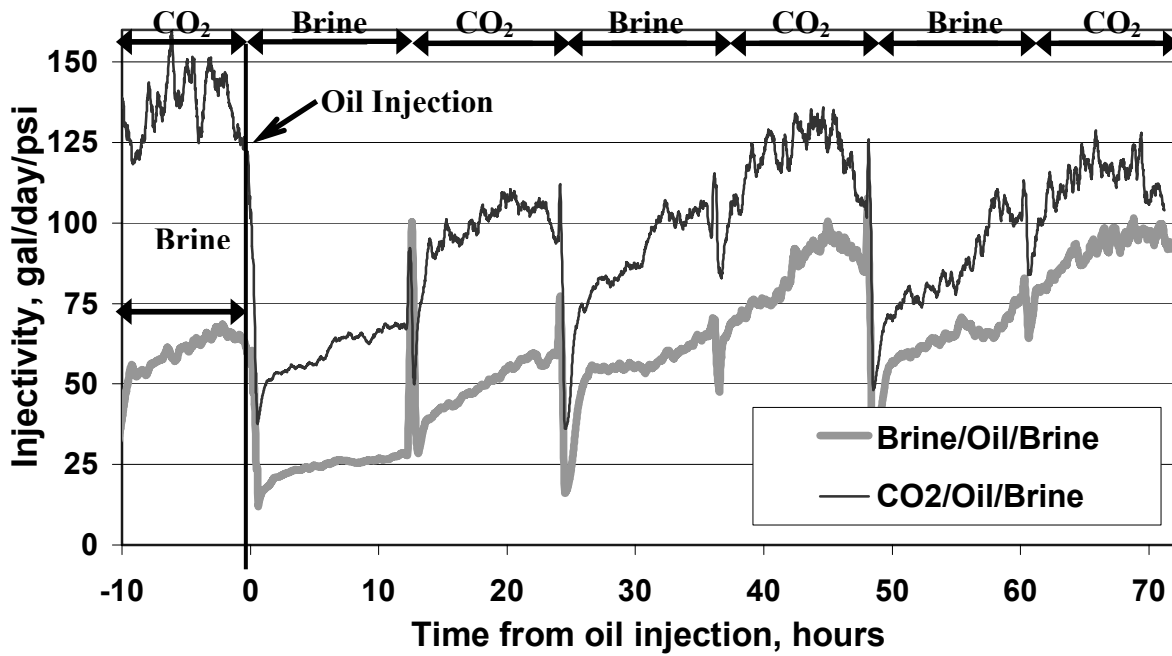


Fig. 19. Injectivity profile when the small oil contamination injection was followed by brine half cycle. This figure compares oil injection being preceded by brine to the case where the oil injection was preceded by CO₂.

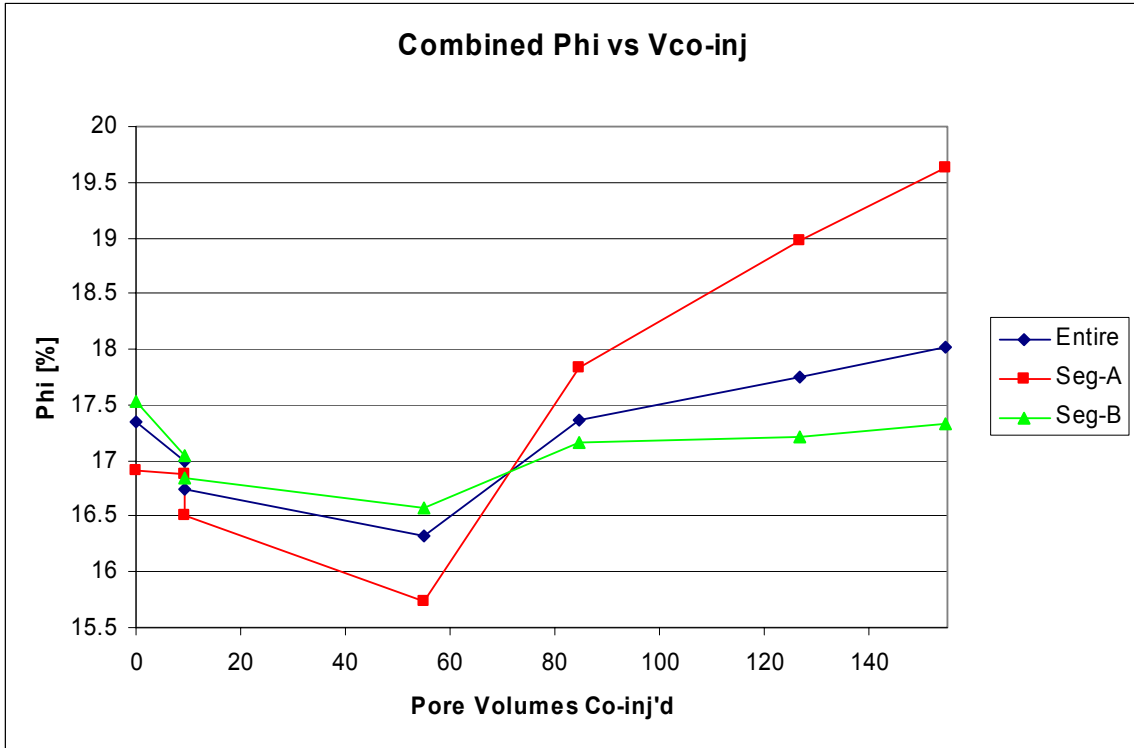


Fig. 20. Porosity trends for the system, Segment A, and Segment B.

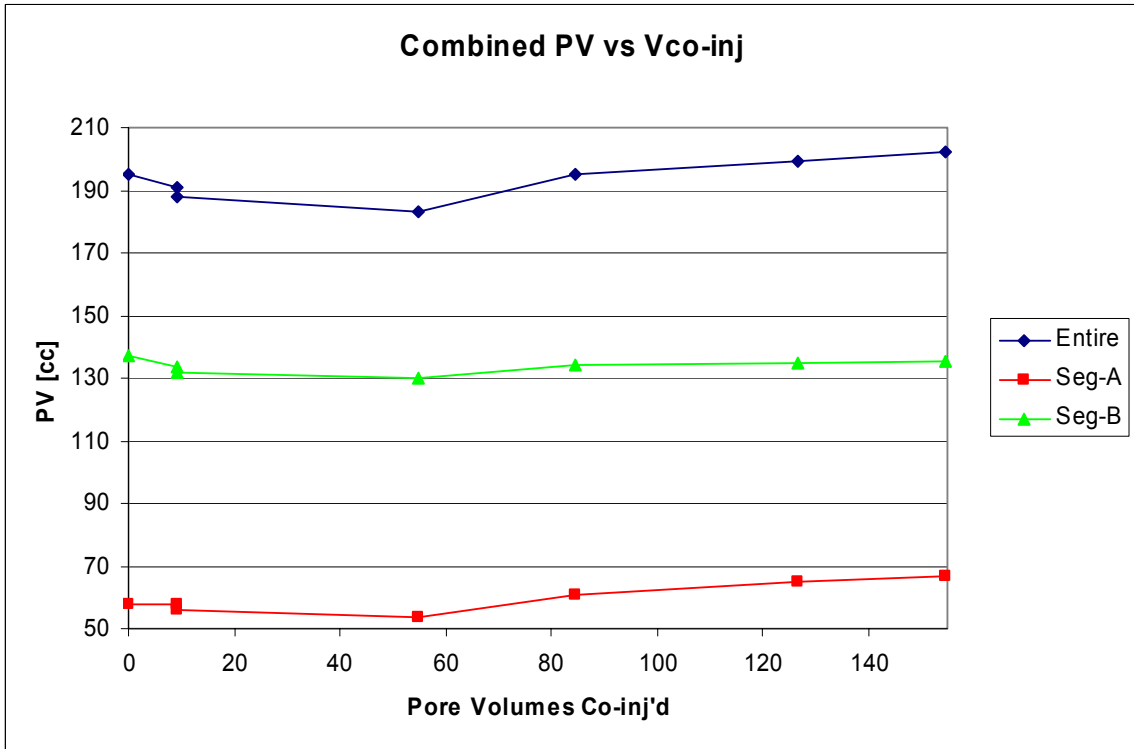


Fig. 21. Pore volume for the system, Segment A, and Segment B.

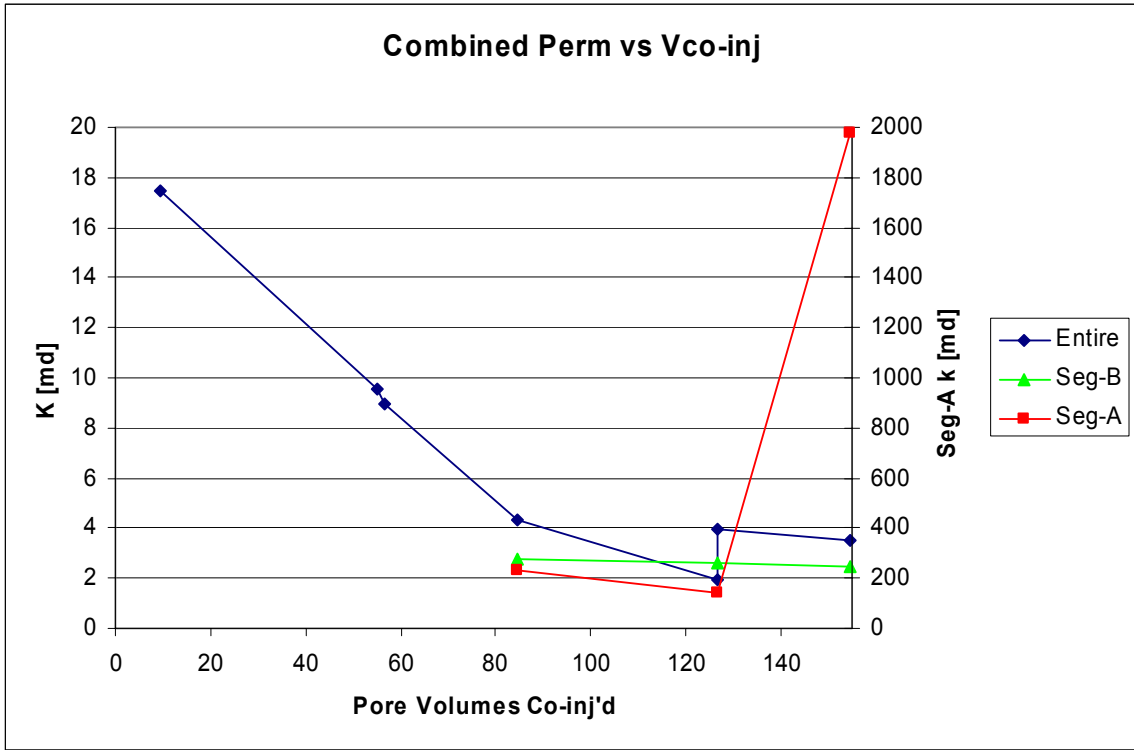


Fig. 22. Permeability trends for the system, Segement A and Segment B.

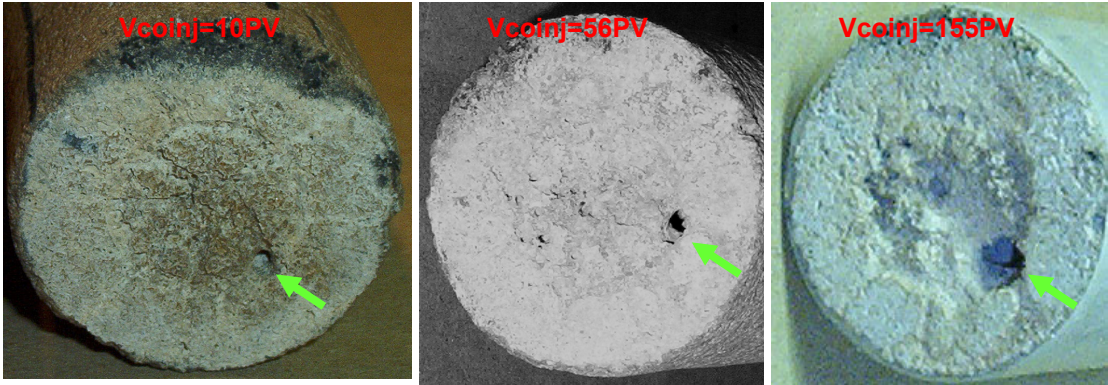


Fig. 23. Development of the solution channel at three points during the flood.

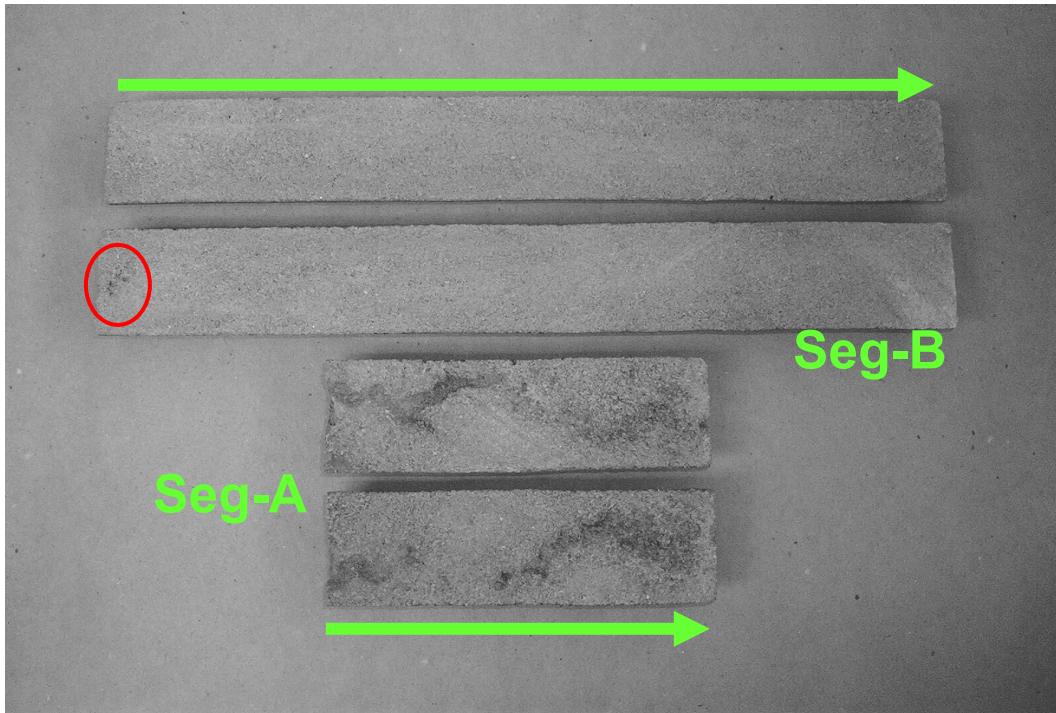


Fig. 24. Sectioned core segments after flooding.

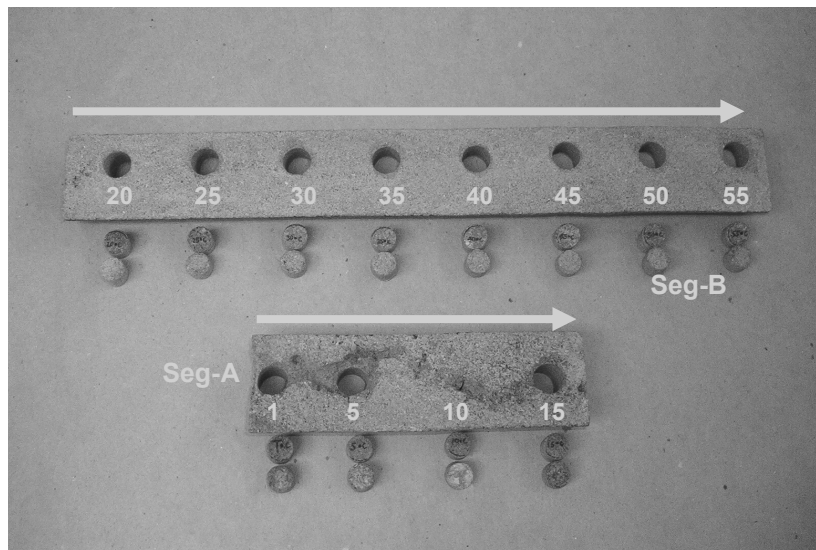


Figure 25. Chemical and BSEI sample locations along the sectioned core.

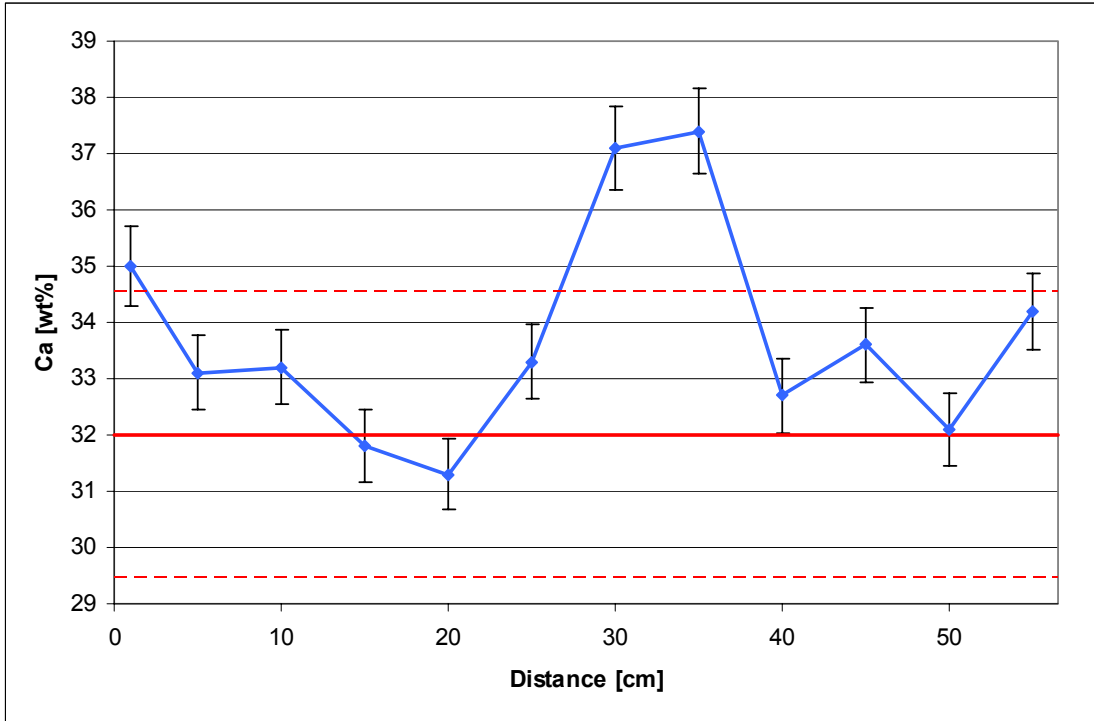


Fig. 26. Ca concentration along the flooded core.

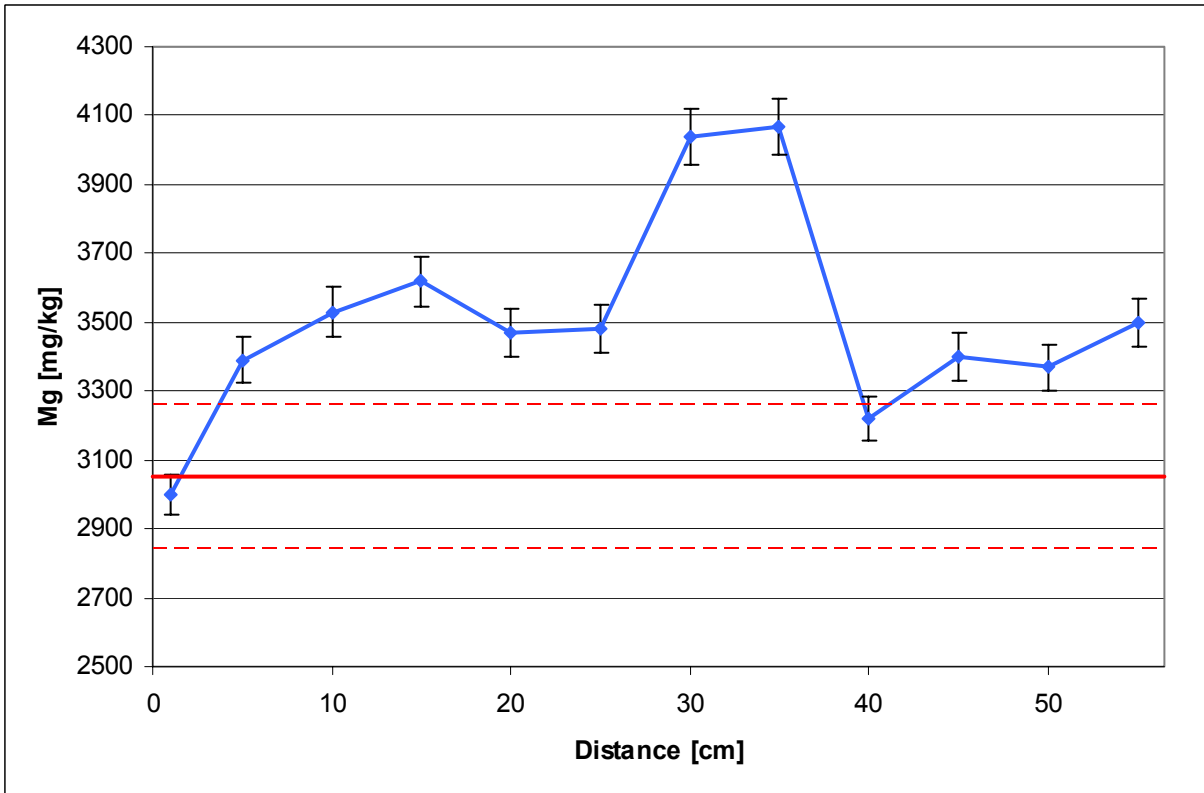


Fig. 27. Mg concentration along the flooded core.

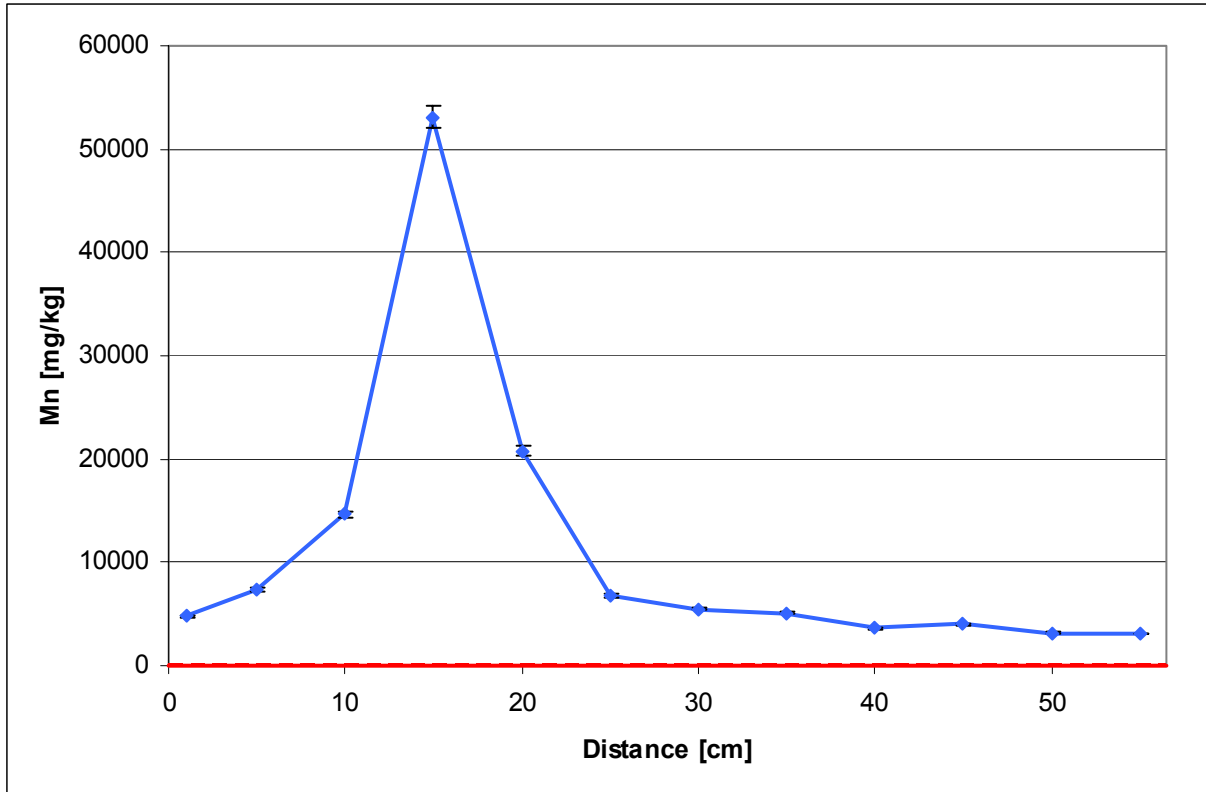


Fig. 28. Mn concentration along the flooded core.

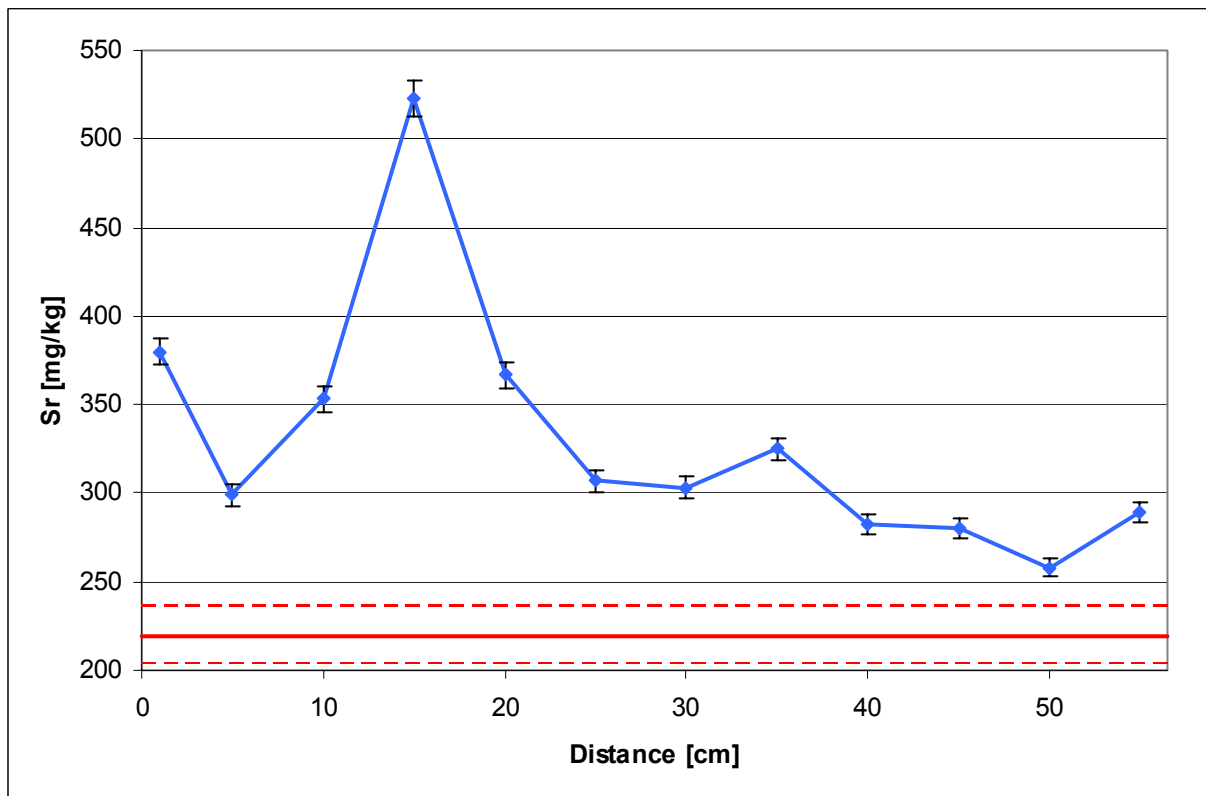


Fig. 29. Sr concentration along the flooded core.

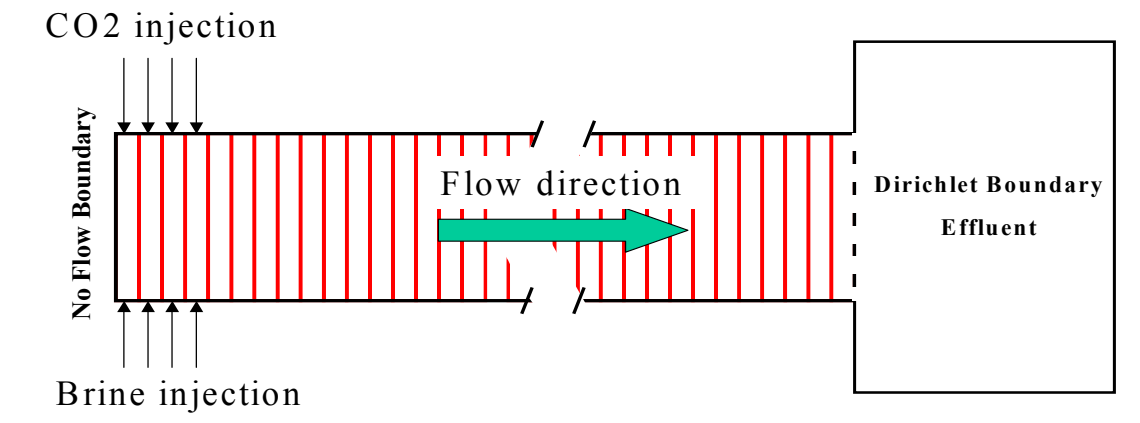


Fig. 30: The model used to represent laboratory core experiments.

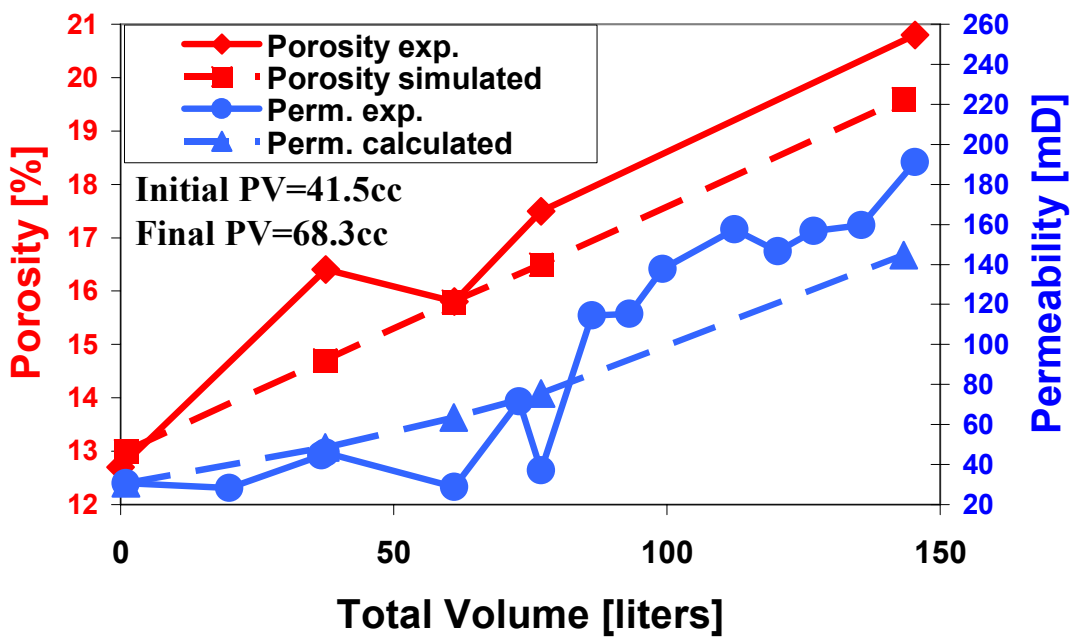


Fig. 31. Experimental vs. simulated total bulk porosity and permeability values as a function of injected fluid volume (see Fig. 17).

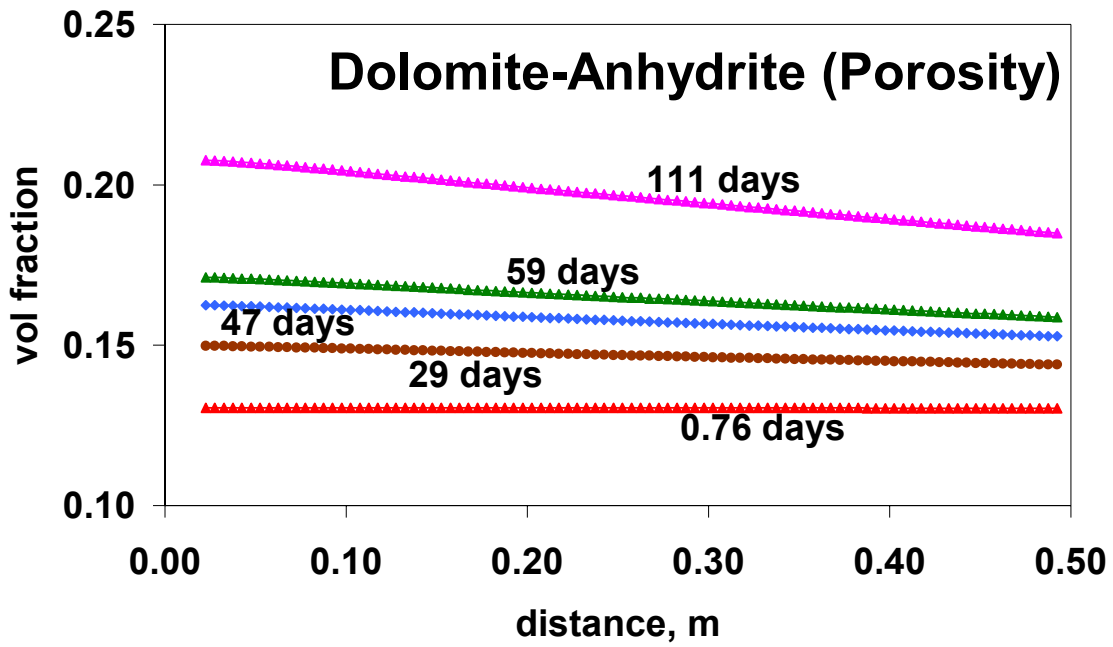


Fig. 32. Porosity volume fraction for the dolomite-anhydrite system at selected times indicated in the figure.

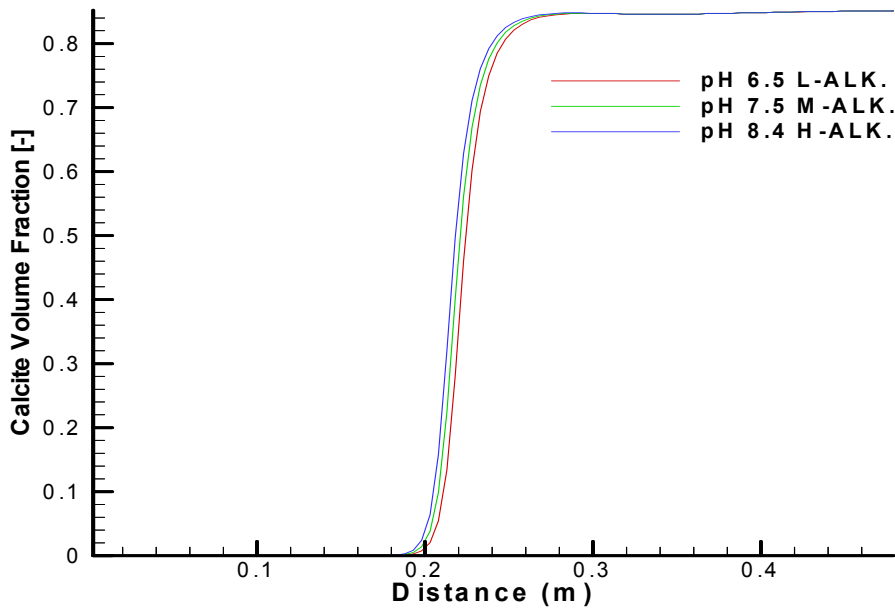


Fig. 33. Calcite volume fraction after 174 days. The results are for three different brine pHs and alkalinities.

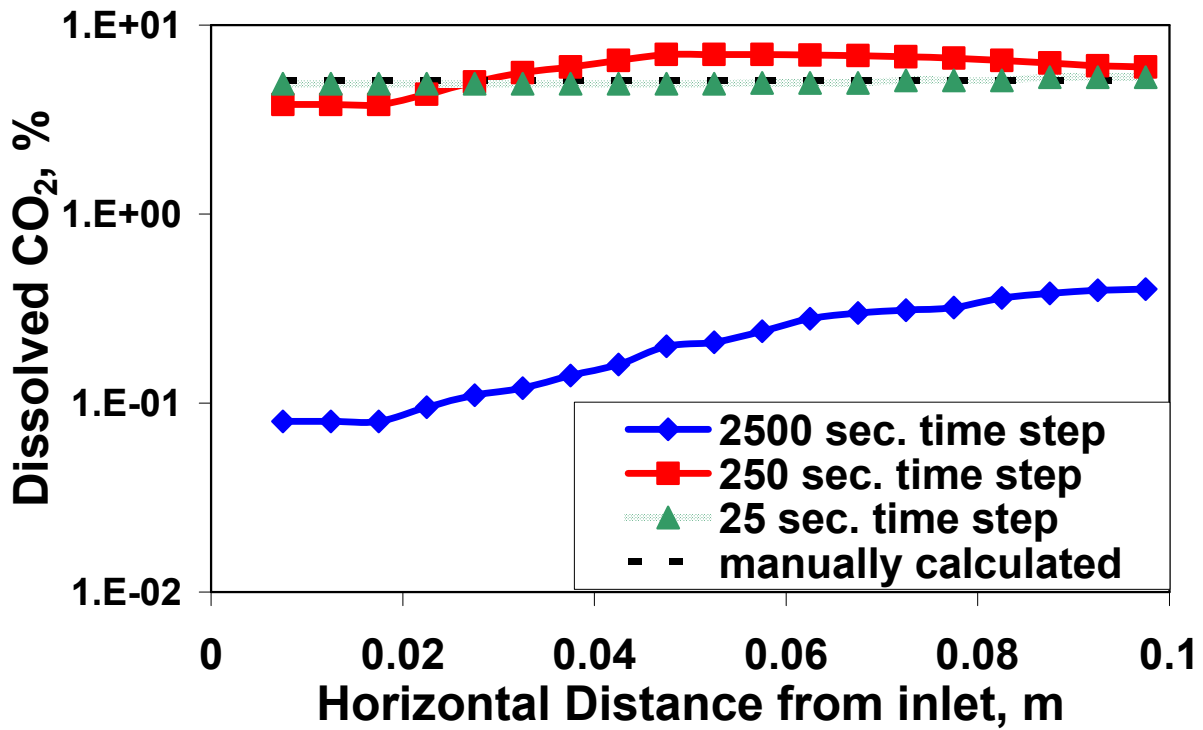


Fig. 34: Effect of increasing time step in TOUGH2 at the first 0.1m of the simulated domain. Manual mass fraction calculation using the Reid et al.⁵⁶ relation in EOSCO2.

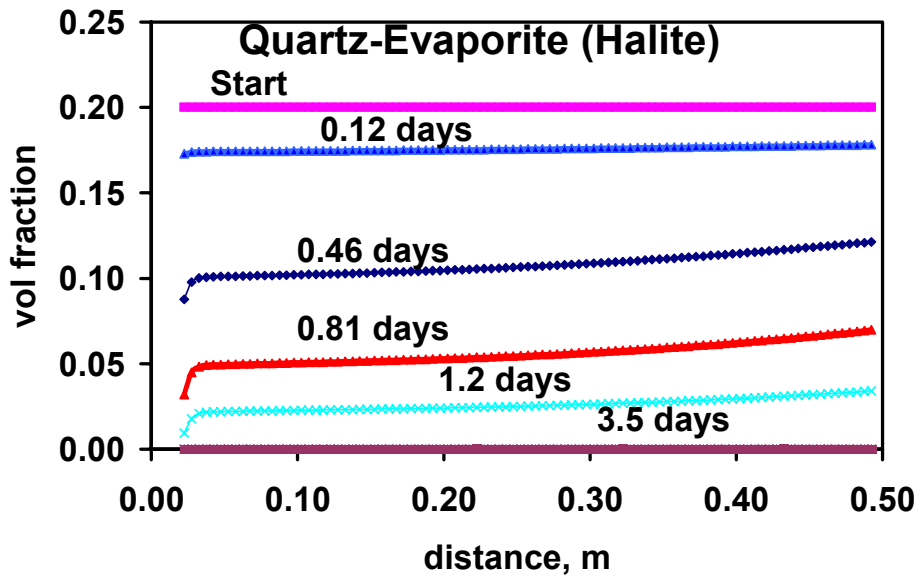


Fig. 35. Volume fraction of halite versus distance into the column at selected times indicated in the figure.

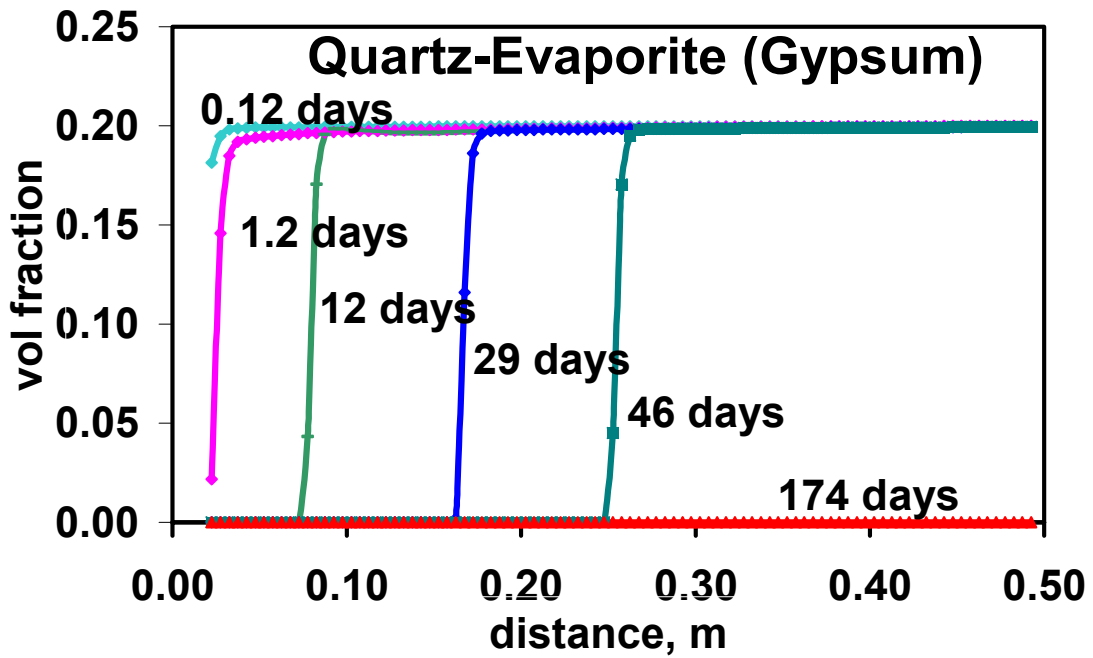


Fig. 36. Volume fraction of gypsum versus distance into the column at selected times indicated in the figure.

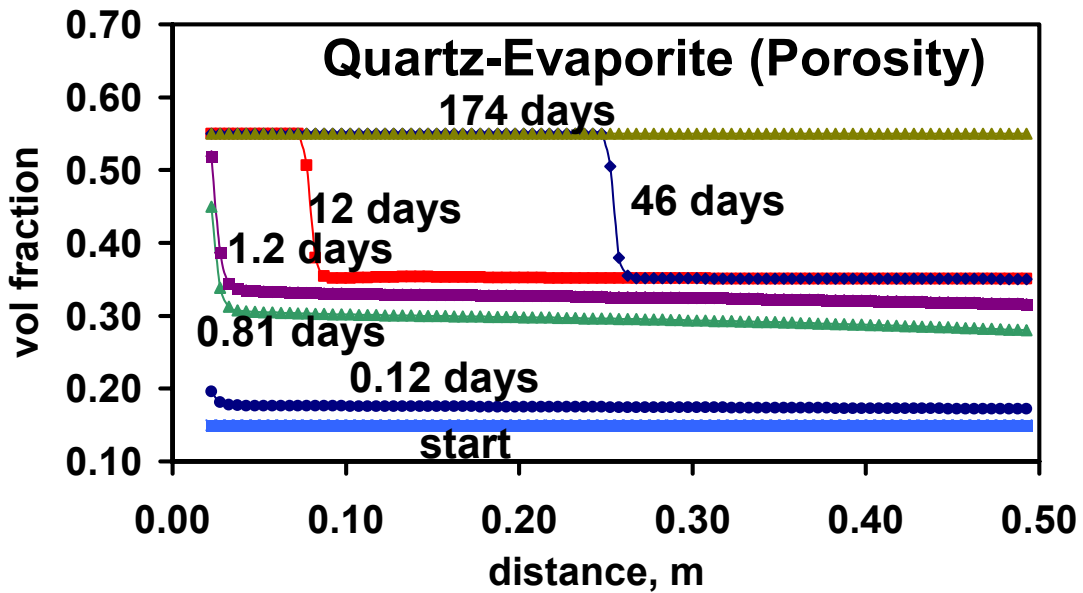


Fig. 37. Porosity volume fraction for the quartz-evaporite system at selected times indicated in the figure.

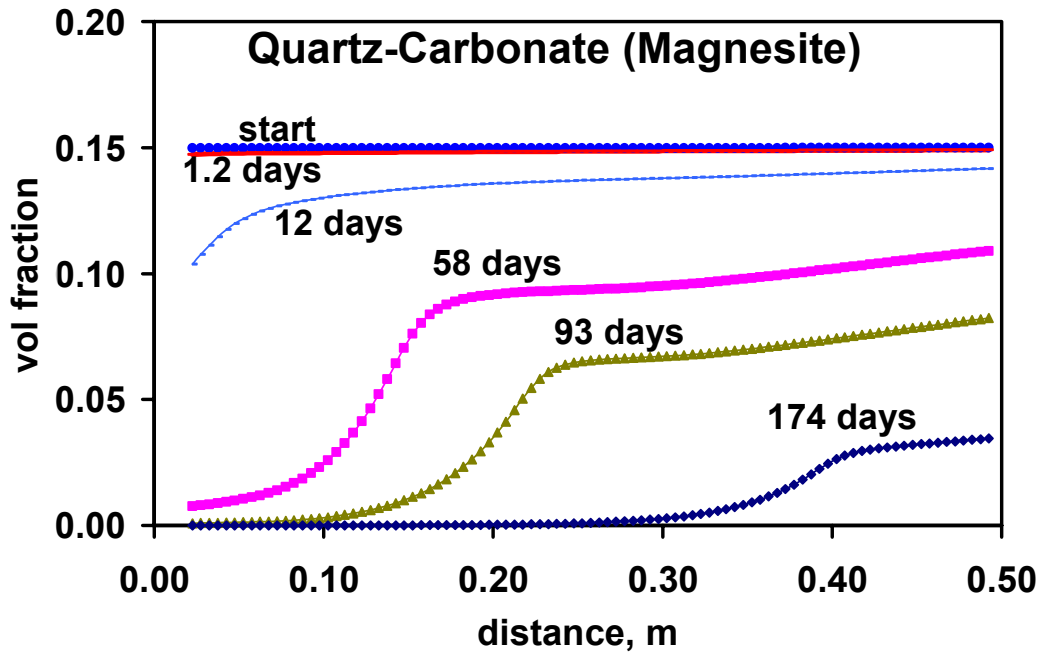


Fig. 38. Volume fraction magnesite versus distance into the column at selected times indicated in the figure.

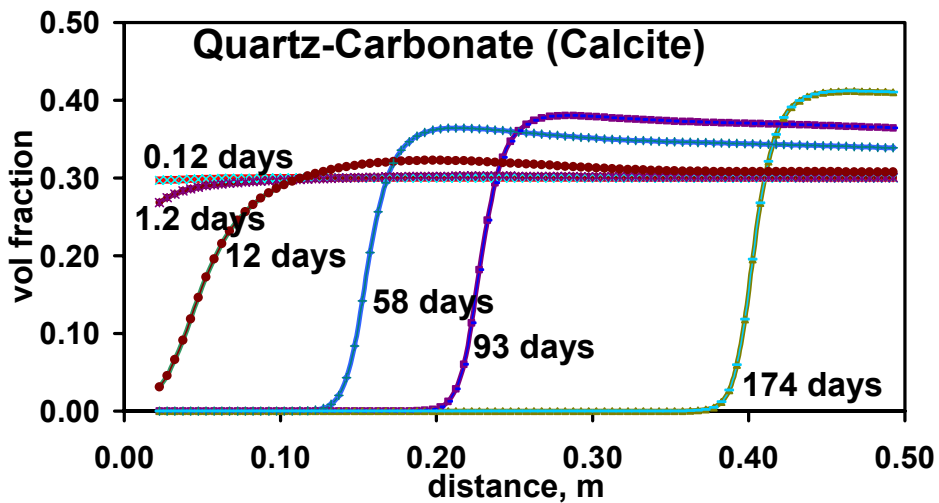


Fig. 39. Volume fraction calcite versus distance into the column at selected times indicated in the figure.

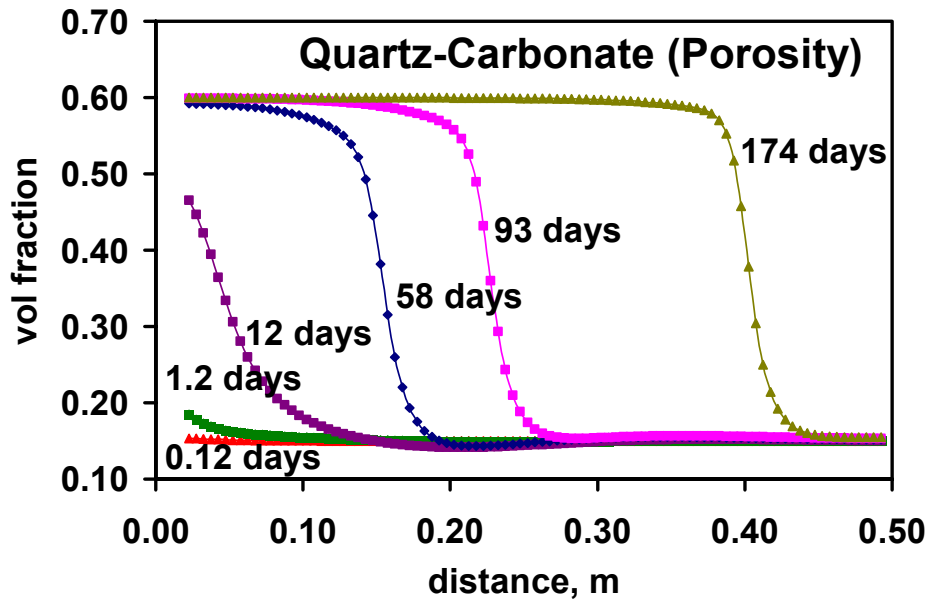


Fig. 40. Porosity volume fraction for the quartz-carbonate system at selected times indicated in the figure.

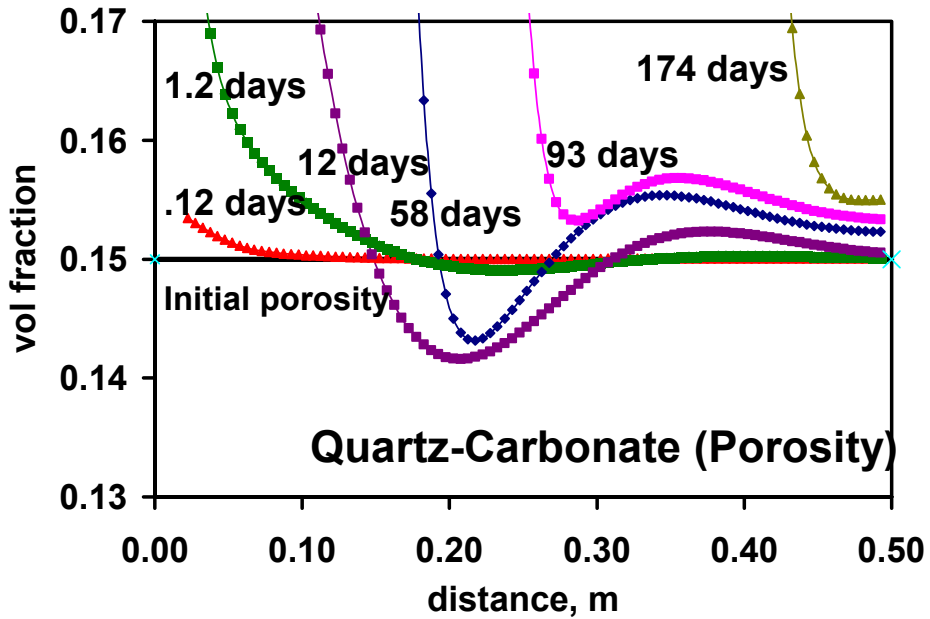


Fig. 41. Plot enlargement of porosity in the quartz-carbonate system near the initial porosity value.

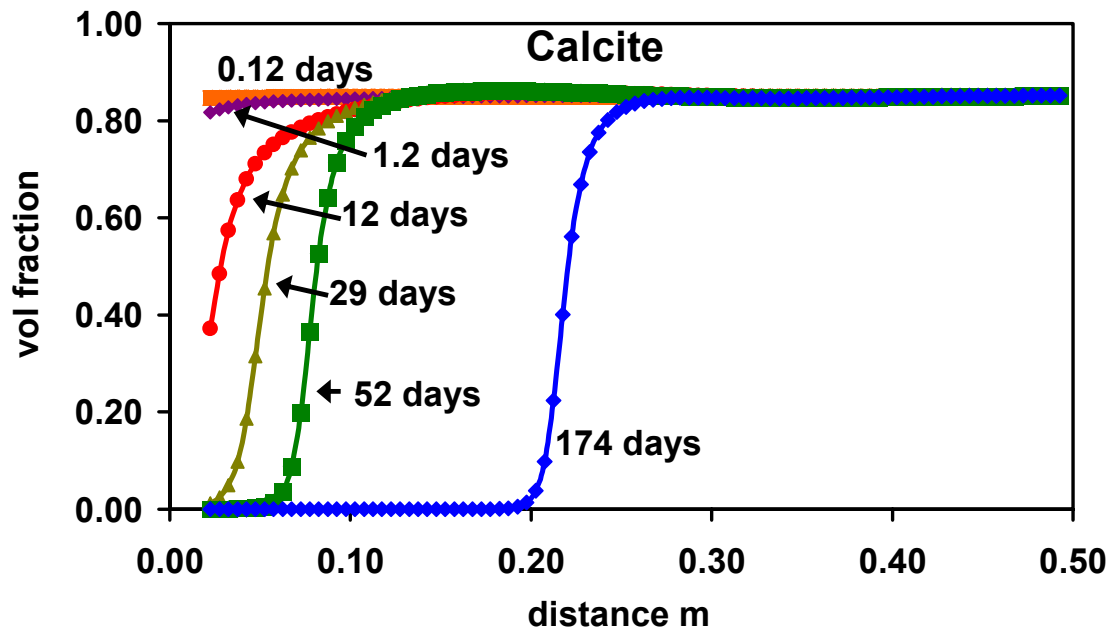


Fig. 42. Volume fraction of calcite versus distance into the column at selected times indicated in the figure.

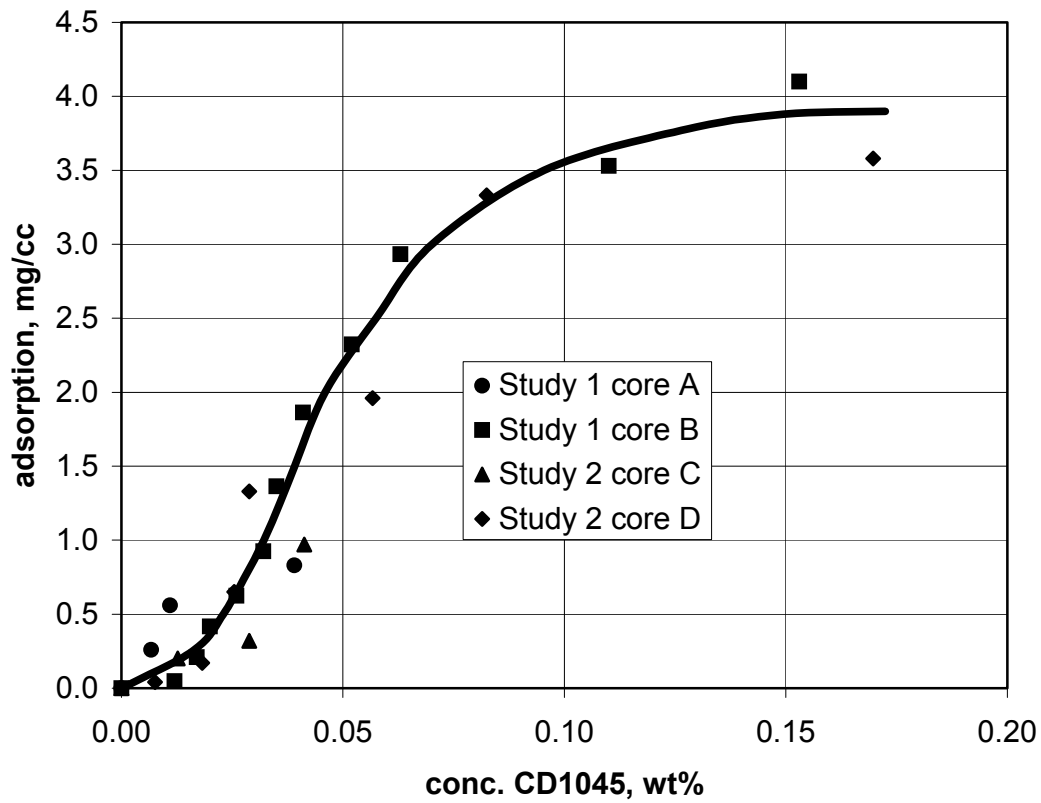


Fig. 43. CD1045 adsorption isotherm data for four Berea core tests using different cores and two different studies.

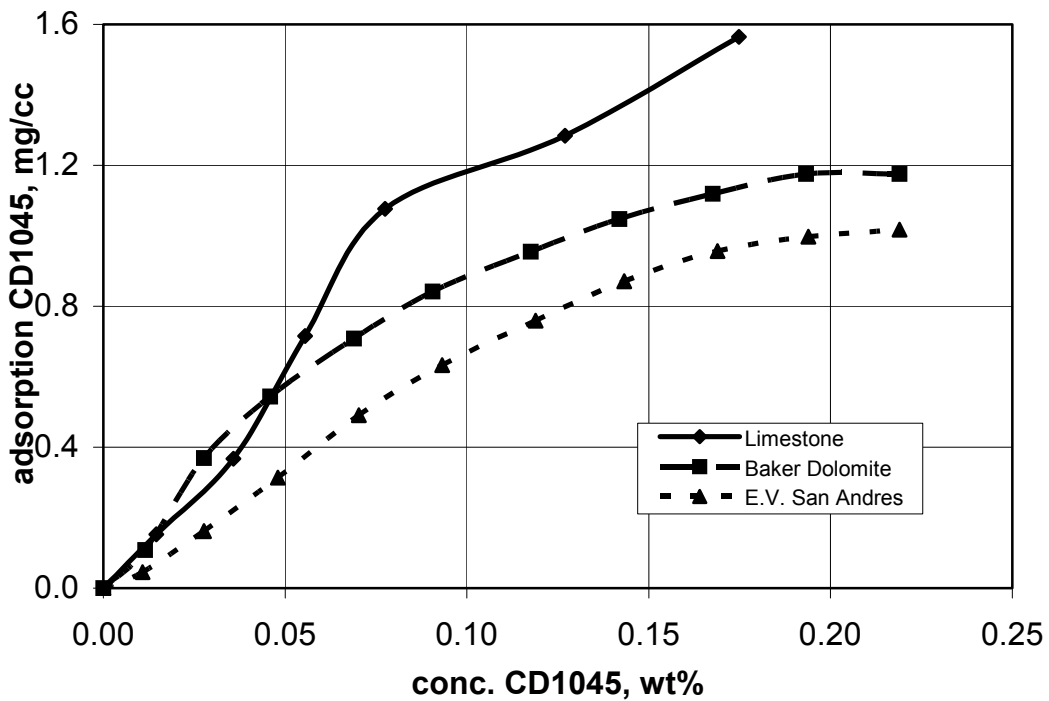


Fig. 44. Comparison of CD1045 adsorption of Indiana limestone, Baker dolomite, and San Andres dolomite.

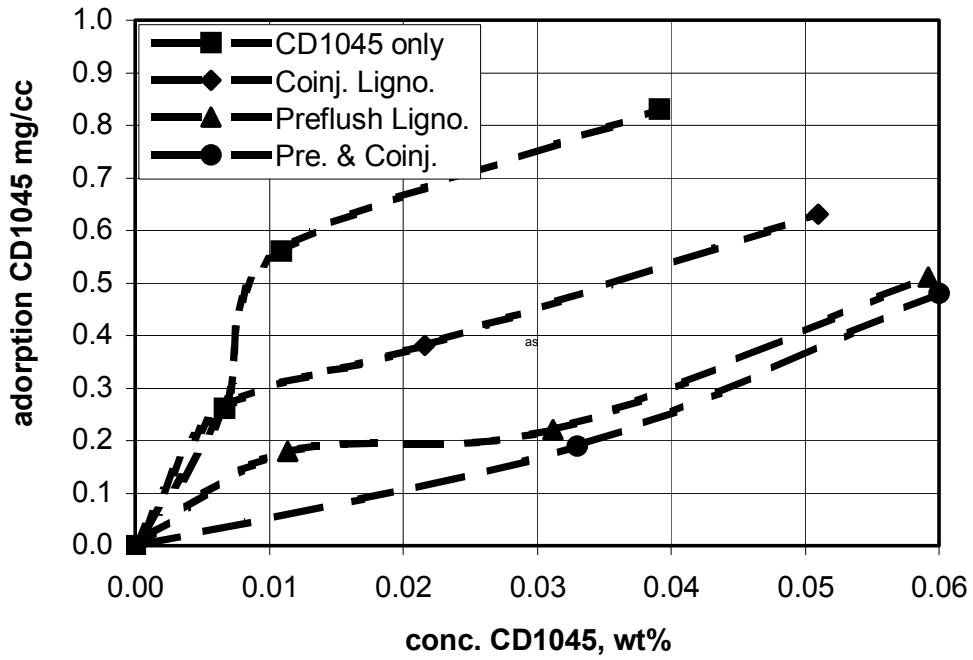


Fig. 45. Lignosulfonate adsorption on Berea sandstone cores. Two different researchers and different cores.

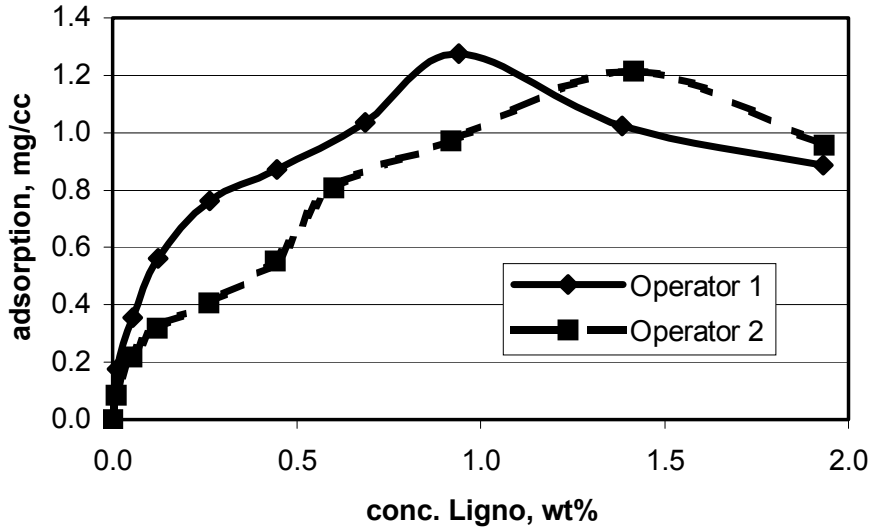


Fig. 46. Adsorption isotherms versus injection methods of CD1045 with and without cosurfactant lignosulfonate in Berea sandstone.

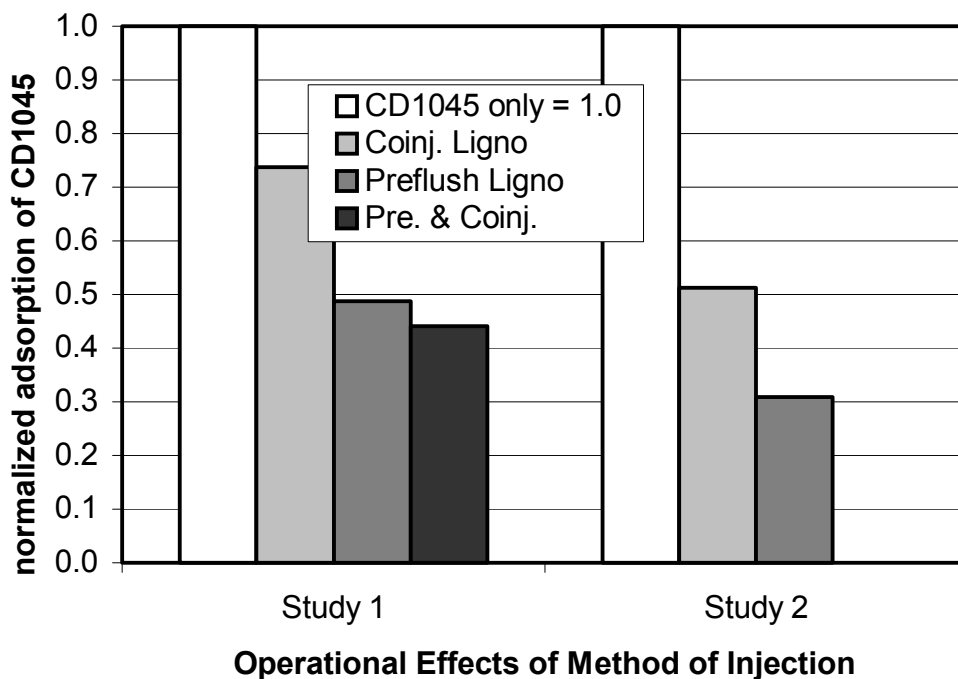


Fig. 47. Comparison of the two series of tests showing adsorption reduction of CD1045 at an equilibrium concentration of 0.05 wt% CD1045 versus injection method of cosurfactant Lignosulfonate in Berea sandstone.

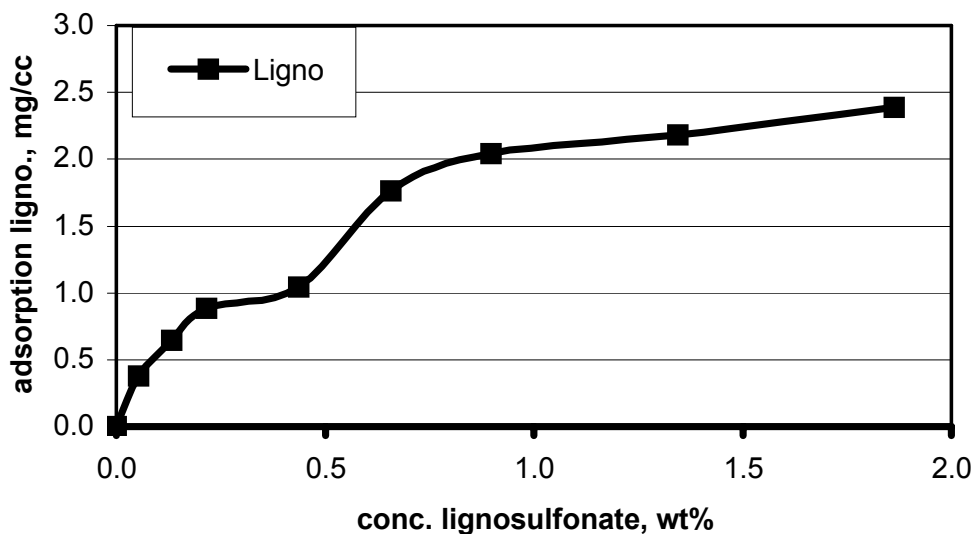


Fig. 48. Lignosulfonate adsorption isotherm in Indiana limestone

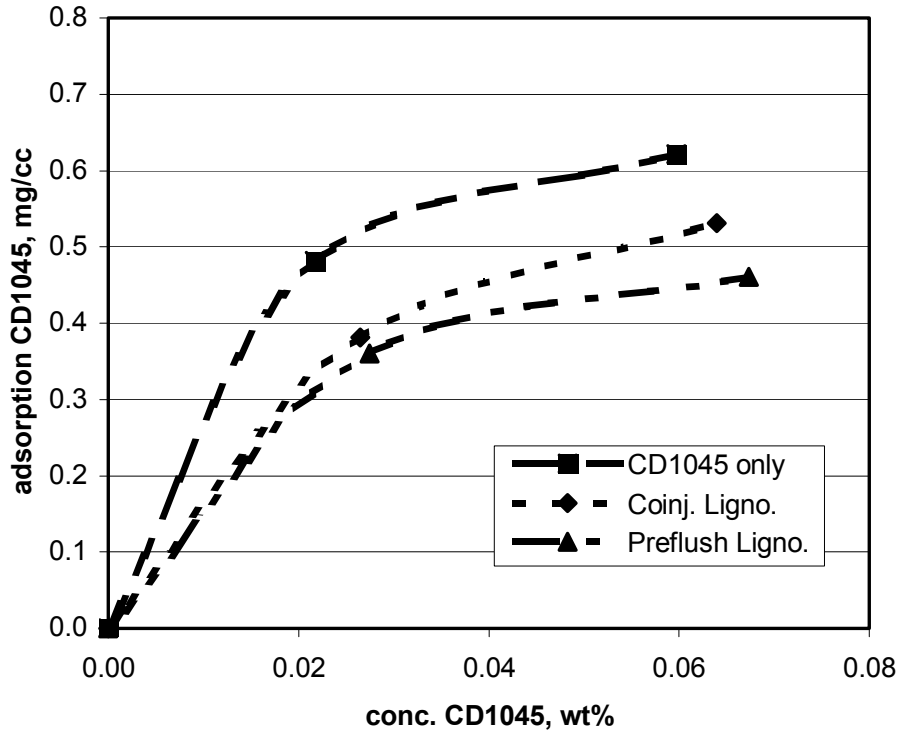


Fig. 49. Adsorption isotherms versus injection methods of CD1045 with and without cosurfactant lignosulfonate in Indiana limestone.

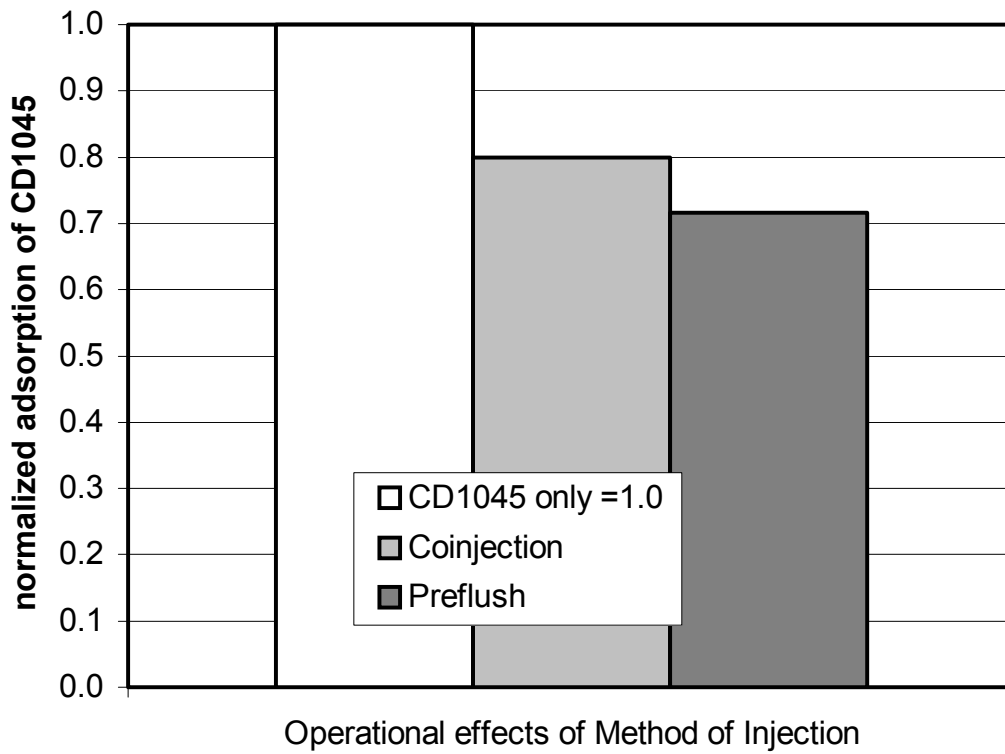


Fig. 50. Comparison of adsorption reduction of CD1045 at an equilibrium concentration of 0.05 wt% versus injection method of cosurfactant lignosulfonate in Indiana limestone.

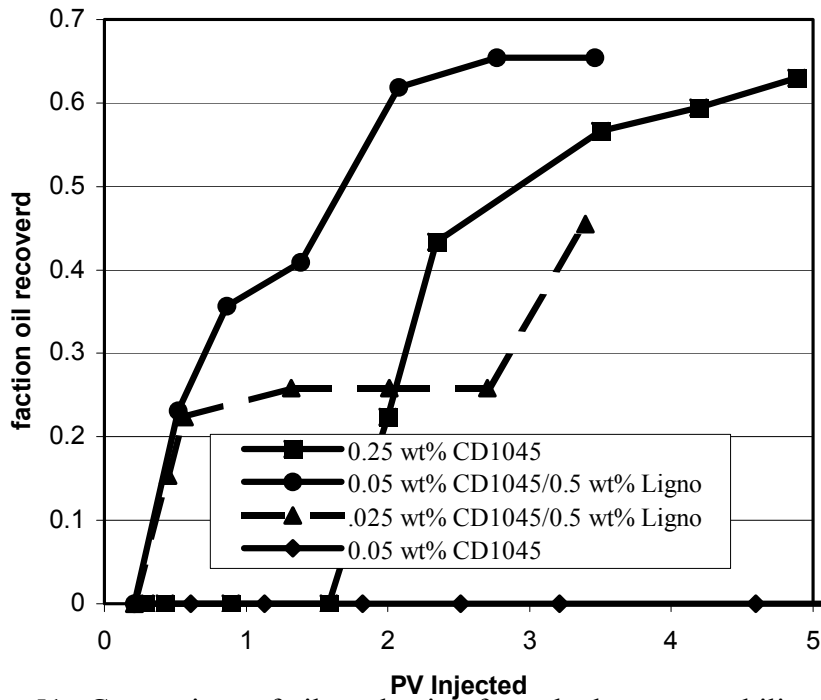


Fig. 51. Comparison of oil production from the low permeability region of a dual permeability core versus injected PV using different surfactant systems.

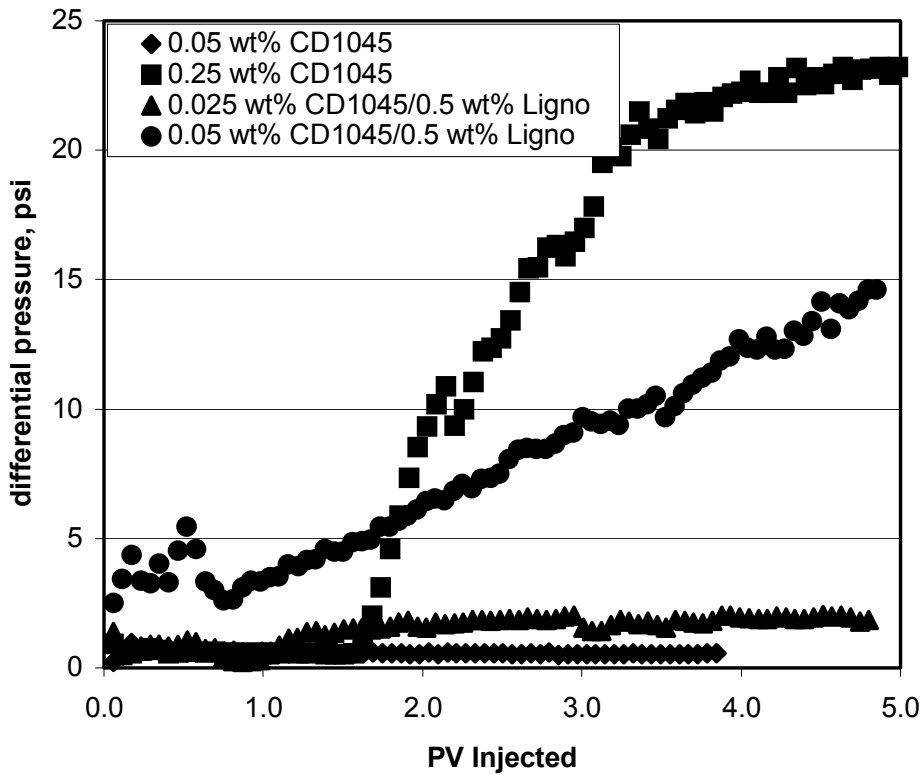


Fig. 52. Comparison of pressure drop across a dual permeability core during fluid injection for different surfactant systems.

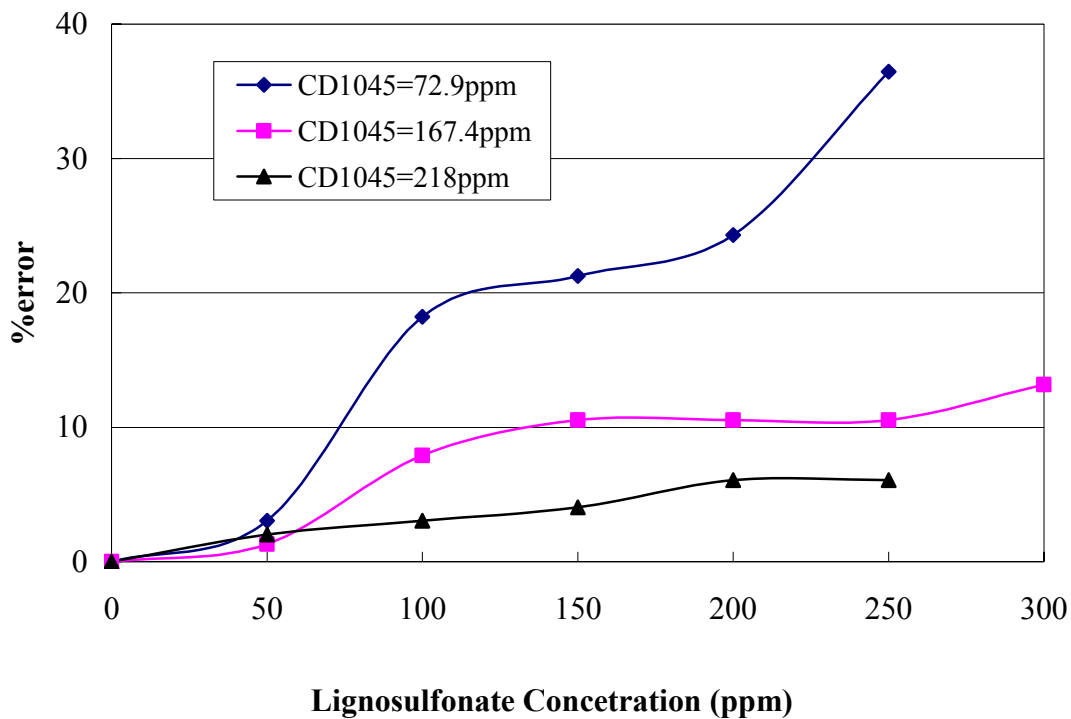


Fig. 53. The influence of lignosulfonate on CD1045 concentration measurement results

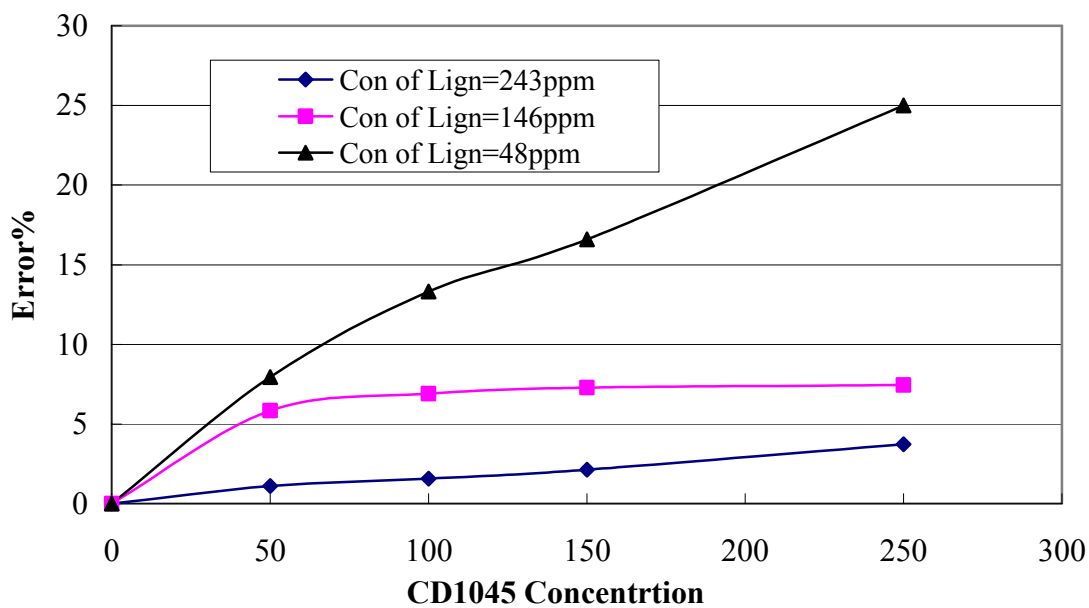


Fig. 54. The influence of CD1045 on lignosulfonate concentration measurement results.

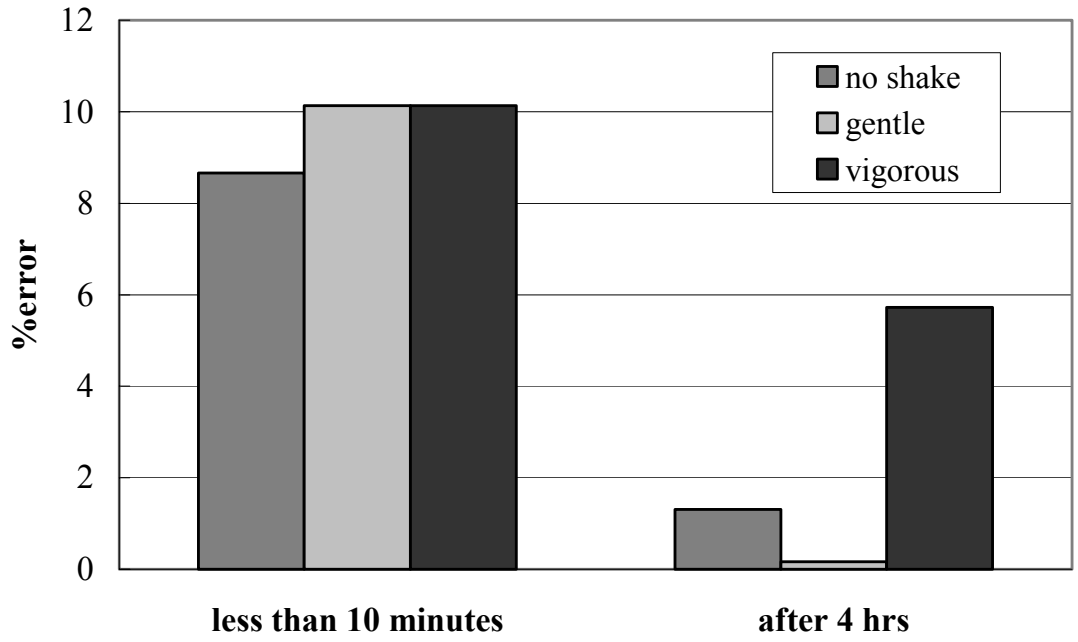


Fig. 55. The influence of shaking methods on measurement error.

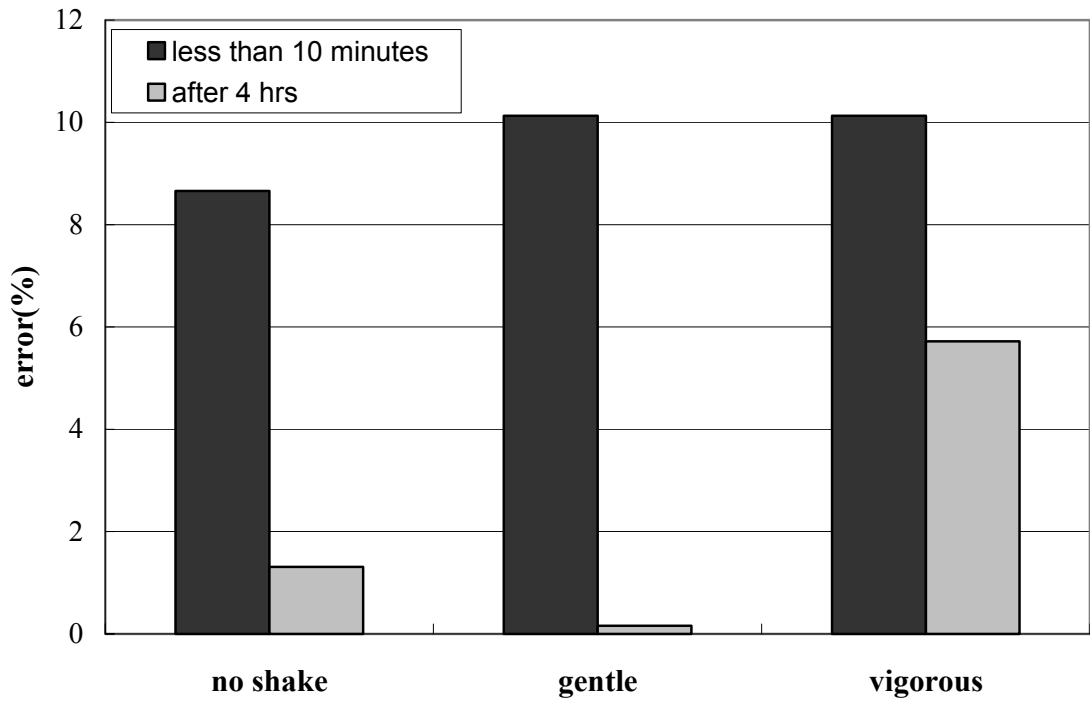


Fig. 56. The influence of delayed measurement time on errors.

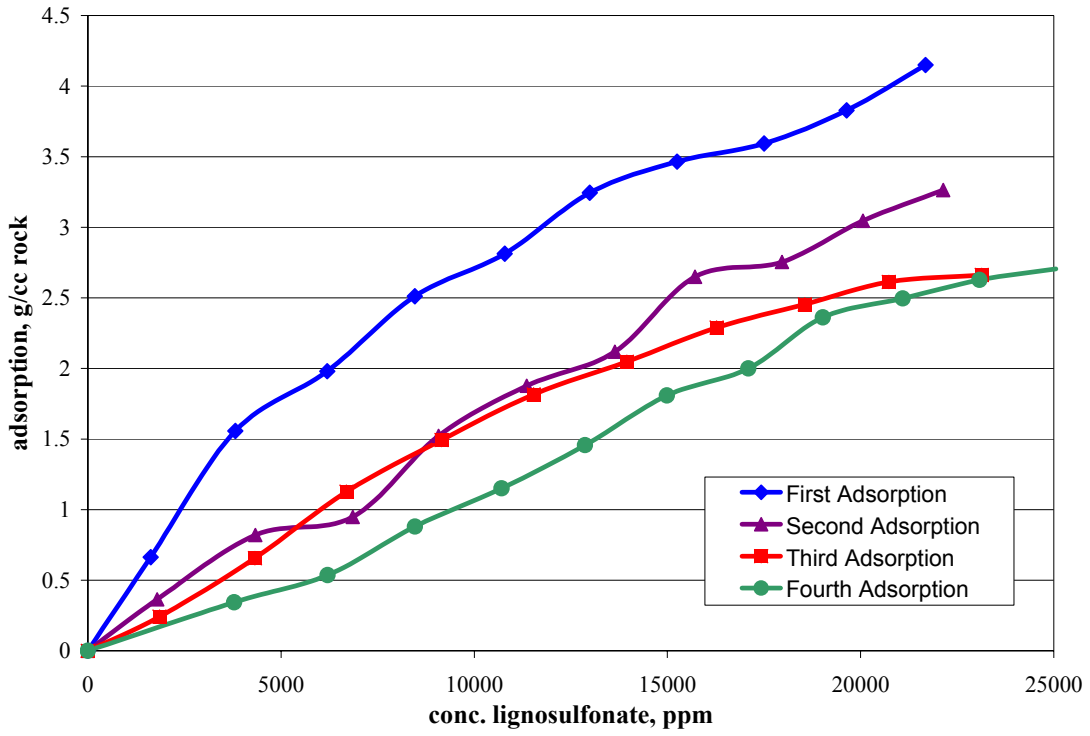


Fig. 57. Four adsorption profiles.

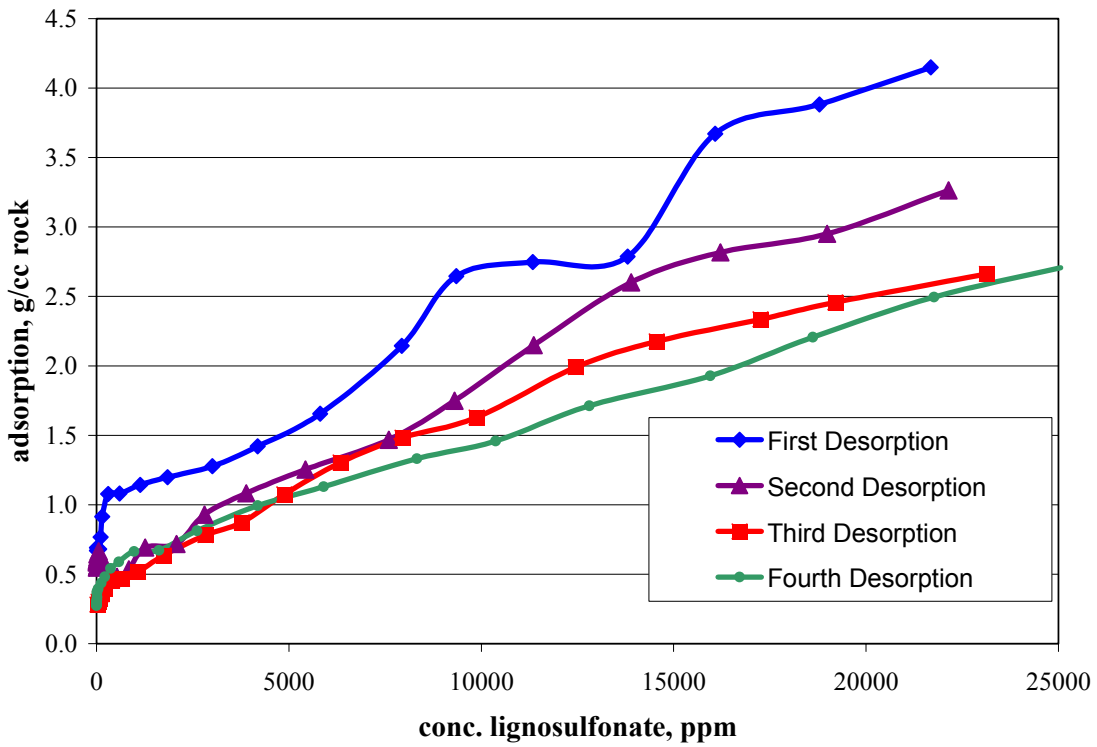


Fig. 58. Four desorption profiles.

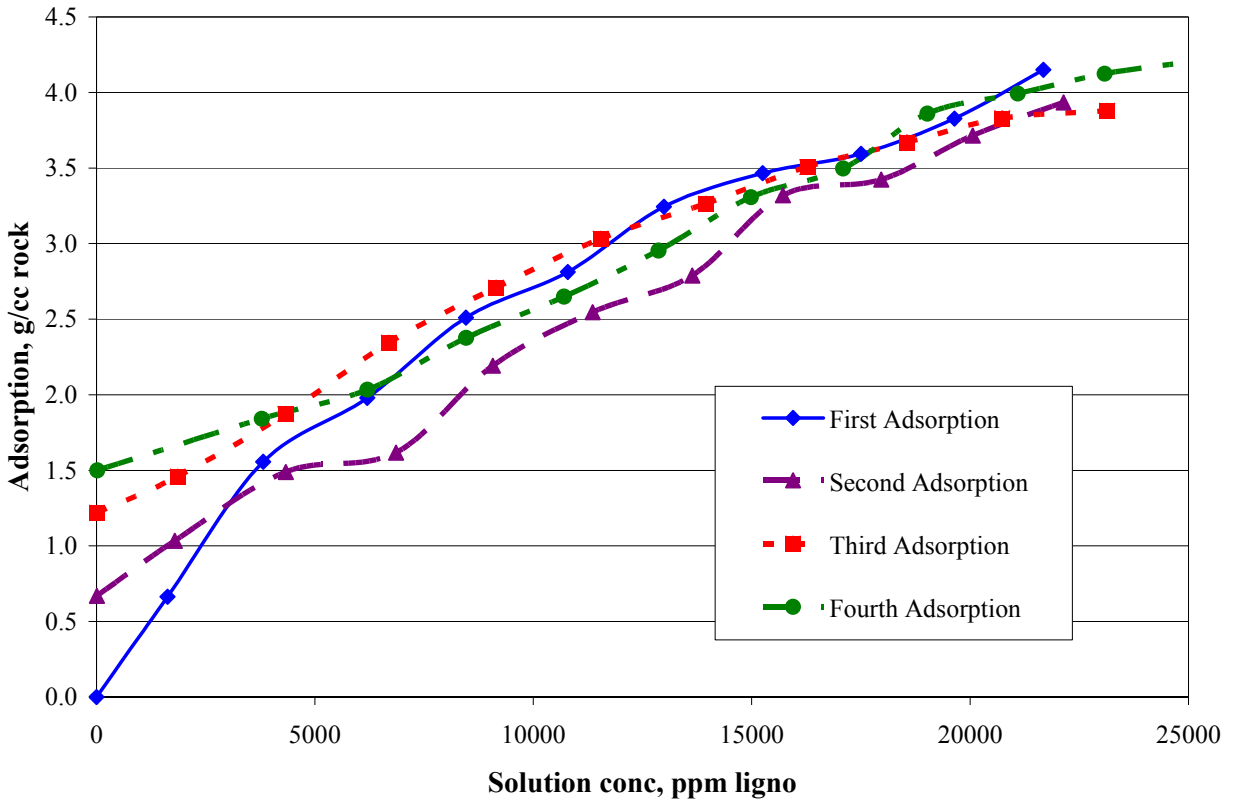


Fig. 59. The four adsorption corrected for the incomplete desorption of the previous run.

APPENDIX A. LIST OF SPE ARTICLES ON EXAMINED RESERVOIRS

Unit	SPE #	Title
New Mexico		
Central Vacuum	63134	Dynamic Reservoir Characterization at Central Vacuum Unit
	60890	Time-Lapse Seismic Monitoring and Dynamic Reservoir Characterization, Central Vacuum Unit, Lea County, New Mexico
	56689	Tracking Miscible Processes in the Subsurface Utilizing Time Lapse Shear Wave Seismic Data
	49292	Time-Lapse Seismic Monitoring and Dynamic Reservoir Characterization, Central Vacuum Unit, Lea County, New Mexico
	38694	Dynamic Reservoir Characterization of a CO2 Huff'n'Puff, Central Vacuum Unit, Lea County, New Mexico
	27656	Potential of the Cyclic CO2 Process in a Waterflooded, Light Oil, Shallow Shelf Carbonate Reservoir
	19666	The Effects of Waterflooding on Reservoir Properties and Producing Operations: Applications for Geochemical Modeling
East Vacuum	66569	Feasibility of Monitoring CO2 Sequestration in a Mature Oil Field Time-Lapse Seismic Analysis
	53714	Management of Water Alternating Gas (WAG) Injection Projects
	39793	History Matching and Modeling the CO-Foam Pilot Test at EVGSAU
	36710	East Vacuum Grayburg San Andres Unit CO2 Flood Ten Year Performance Review: Evolution of a Reservoir Management Strategy and Results of WAG Optimization
	27798	CO2 Foam Field Verification Pilot Test at EVGSAU: Phase IIIC—Reservoir Characterization and Response to Foam Injection
	27786	CO2 Foam Field Verification Pilot Test at EVGSAU: Phase IIIB—Project Operations and Performance Review
	27785	CO2 Foam Field Verification Pilot Test at EVGSAU: Phase IIIA—Surfactant Performance Characterization and Quality Assurance
	27675	Laboratory Flow Tests Used To Determine Reservoir Simulator Foam Parameters for EVGSAU CO2 Foam Pilot
	26478	Reservoir Description by Inverse Modeling: Application to EVGSAU Field
	26391	CO2 EOR Economics for Small-to-Medium-Size Fields
	24928	Update of Industry Experience With CO2 Injection
	24642	CO2 Foam Field Verification Pilot Test at EVGSAU: Phase II -Foam Injection Design and Operating Plan
	24176	CO2-Foam Field Verification Pilot Test at EVGSAU Injection Project Phase I: Project Planning and Initial Results
	19666	The Effects of Waterflooding on Reservoir Properties and Producing Operations: Applications for Geochemical Modeling
	18977	Summary Results of CO2 EOR Field Tests, 1972-1987
	16721	East Vacuum Grayburg-San Andres Unit CO2 Injection Project: Development and Results to Date
State 35 Unit	16722	Development and Results of the Hale/Mable Leases Cooperative Polymer EOR Injection Project, Vacuum (Grayburg-San Andres) Field, Lea County, New Mexico
Loco Hills	339	Successful Pilot Predicts Bright Future for Loco Hills Water Flood, New Mexico
Maljamar (Conoco)	27784	Effect of Pressure on CO2 Foam Displacements: A Micromodel Visualization Study
	26391	CO2 EOR Economics for Small-to-Medium-Size Fields
	24111	Prediction of CO2/Crude Oil Phase Behavior Using Supercritical Fluid Chromatography
	20109	Automated CO2 Injection Control and Well Test Monitoring System

Unit	SPE #	Title
	18977	Summary Results of CO2 EOR Field Tests, 1972-1987
	18976	Innovative Techniques for Converting Old Waterflood Injectors to State-of-the-Art CO2 Injectors
	17371	Tracer Surveys To Identify Channels for Remedial Work Prior to CO2 Injection at MCA Unit, New Mexico
	17323	History Match of the Maljamar CO2 Pilot Performance
	15400	Effect of an Aqueous Phase on CO2/Tetradecane and CO2/Maljamar, Crude-Oil Systems
	15079	Solubility and Extraction in Multiple-Contact Miscible Displacements: Comparison of N2 and CO2 Flow Visualization Experiments
	14940	The Maljamar CO2 Pilot: Review and Results
	14897	Diffusion of CO2 at Reservoir Conditions: Models and Measurements
	14149	Effect of Oil Composition on Minimum Miscibility Pressure-Part 1: Solubility of Hydrocarbons in Dense CO2
	14148	Four-Phase Flash Equilibrium Calculations Using the Peng-Robinson Equation of State and a Mixing Rule for Asymmetric Systems
	14147	Experimental Investigation of the Interaction of Phase Behavior With Microscopic Heterogeneity in a CO2 Flood
	13142	Use of Well Logs To Characterize Fluid Flow in the Maljamar CO Pilot
	12666	First Results From the Maljamar Carbon Dioxide Pilot
	12600	Development and Status of the Maljamar CO2 Pilot
	11337	Formation Damage Potential from Carbon Dioxide-Crude Oil Interaction
Maljamar (Phillips)	26391	CO2 EOR Economics for Small-to-Medium-Size Fields
	18977	Summary Results of CO2 EOR Field Tests, 1972-1987
Adair San Andres	19783	An Evaluation of Waterflood Infill Drilling in West Texas Clearfork and San Andres Carbonate Reservoirs
	16854	Infill Drilling Economic Analysis of Carbonate Oil Reservoirs in West Texas
Anton Irish Bennett	11930	Case History of Large-Volume Fracture Stimulations in a West Texas Waterflood
	35188	Design and Implementation of a Grass-Roots CO2 Project for the Bennett Ranch Unit
	18224	Carbonate Stimulation Optimization Using Hydraulic Fracturing Field Testing
	13095	Improved Formation Evaluation From Pressure and Conventional Cores Taken With Stable Foam-Bennett Ranch Unit (Wasson Field)
	9798	San Andres Reservoir Pressure Coring Project For Enhanced Oil Recovery Evaluation, Bennett Ranch Unit, Wasson Field, West Texas
	16854	Infill Drilling Economic Analysis of Carbonate Oil Reservoirs in West Texas
	15571	Compositional Simulation of the Block 31 Field and Surface Facilities
	13669	Analysis and Correlation of Nitrogen and Lean-Gas Miscibility Pressure
Cordona Lake	26391	CO2 EOR Economics for Small-to-Medium-Size Fields
	24928	Update of Industry Experience With CO2 Injection
Dollarhide	39787	Find Grid CO Injection Process Simulation for Dollarhide Devonian Reservoir
	27642	A Comparative Technical and Economic Analysis of Waterflood Infill Drilling and CO2 Flood in West Texas Carbonate Reservoirs
	26391	CO2 EOR Economics for Small-to-Medium-Size Fields
	20098	Numerical Evaluation of Single-Slug, WAG, and Hybrid CO2 Injection Processes, Dollarhide Devonian Unit, Andrews County, Texas
	18977	Summary Results of CO2 EOR Field Tests, 1972-1987
	17294	State of the Art Installation of CO2 Injection Equipment: A Case Study
	17277	Evaluation and Implementation Of CO2 Injection at the Dollarhide Devonian Unit
		Click also North Dollarhide
Dollarhide (Clearfork AB)	27642	A Comparative Technical and Economic Analysis of Waterflood Infill Drilling and CO2 Flood in West Texas Carbonate Reservoirs
	25853	An Integrated Approach To Characterize Low-Permeability Reservoir Connectivity for Optimal Waterflood Infill Drilling
	19783	An Evaluation of Waterflood Infill Drilling in West Texas Clearfork and San Andres

Unit	SPE #	Title
		Carbonate Reservoirs
	12017	Waterflooding the Grayburg Formation on the J.L. Johnson AB Lease: Experience in the Johnson Field
Ford Geraldine	39794	Compositional Simulations of a CO Flood in Ford Geraldine Unit, Texas
	26391	CO2 EOR Economics for Small-to-Medium-Size Fields
	24928	Update of Industry Experience With CO2 Injection
	20227	A Full-Field Numerical Modeling Study for the Ford Geraldine Unit CO Flood
	20118	The Ford Geraldine Unit CO2 Flood- Update 1990
	18977	Summary Results of CO2 EOR Field Tests, 1972-1987
	17278	The Ford Geraldine Unit CO2 Flood: Operating History
	12197	CO2 Flood: Design and Initial Operations, Ford Geraldine (Delaware Sand) Unit
	6883	Pecos River Water Treatment for Water Injection
	6383	Field Study - Ford Geraldine (Delaware Sand) Unit
GMK South	19046	Utilization of a Black-Oil Simulator as a Monitor of Waterflood Operations in a San Andres Reservoir
Goldsmith	48945	Goldsmith San Andres Unit CO2 Pilot - Design, Implementation, and Early Performance
	39514	Use, Quantification and Learnings From a Vertical Pulse Test Conducted for Barrier
	20137	Evaluation of Alternating Phase Fracture Acidizing Treatment Using Measured Bottomhole Pressure
	16854	Infill Drilling Economic Analysis of Carbonate Oil Reservoirs in West Texas
	9719	Response of North Cowden and Goldsmith Crudes to Carbon Dioxide Slugs Pushed by Nitrogen
	1888	Gas Turbine Driven Centrifugal Pumps for High Pressure Water Injection
Hanford	20229	A Case History of the Hanford San Andres Miscible CO2 Project
Hansford Marmaton	26391	CO2 EOR Economics for Small-to-Medium-Size Fields
	18977	Summary Results of CO2 EOR Field Tests, 1972-1987
	17327	CO2 Injection Increases Hansford Marmaton Production
Huntley (So. & E.)	27762	A Probabilistic Forecasting Method for the Huntley CO2 Projects
Kingdom Abo	9720	Early Implementation of a Full-Scale Waterflood in the Abo Reef, Terry Co. TX. - A Case History
	9475	Early Implementation of a Full-Scale Waterflood in the Abo Reef, Terry Co., TX - A Case History
Levelland	71496	Physical Effects of WAG Fluids on Carbonate Core Plugs
	25413	Application of a Three-Dimensional Hydraulic Fracturing Simulator for Design of Acid Fracturing Treatments
	23974	Analysis of Tertiary Injectivity of Carbon Dioxide
	16854	Infill Drilling Economic Analysis of Carbonate Oil Reservoirs in West Texas
	16716	The Effects Of CO2 Flooding on Wettability of West Texas Dolomitic Formations
	14308	Investigation of Unexpectedly Low Field-Observed Fluid Mobilities During Some CO2 Tertiary Floods
	12148	Pilot Plant Performance of Triethanolamine for Bulk CO2 Separation
	11121	Use of a Novel Liquid Gelling Agent for Acidizing in the Levelland Field
	9786	Utilization of Composition Observation Wells in a West Texas CO2 Pilot Flood
	9785	Carbon Dioxide Displacement of a West Texas Reservoir Oil
	9764	Injection Well Workover Program in the Levelland Field: A Case History
	8831	Design and Implementation of a Levelland Unit CO2 Tertiary Pilot
8410	Design and Operation of the Levelland Unit CO2 Injection Facility	
	5826	Enriched-Gas Miscible Flooding: A Case History of the Levelland Unit Secondary Miscible Project
Mabee	71496	Physical Effects of WAG Fluids on Carbonate Core Plugs
	24163	Interpretation of a CO2 WAG Injectivity Test in the San Andres Formation Using a Compositional Simulator

Unit	SPE #	Title
	22653	A Laboratory and Field Injectivity Study: CO2 WAG in the San Andres Formation of West Texas
Mallet	70068	Conformance Water-Management Team Developments and Solutions on Projects in the Permian Basin
	36711	From Simulator to Field Management: Optimum WAG Application in a West Texas CO2 Flood - A Case History
	20377	Optimization of Waterflood Performance and CO2-Flood Design Using a Modeling Approach, Mallet Unit, Slaughter Field
	16831	Carbonated Waterflood Implementation and Its Impact on Material Performance in a Pilot Project
	16830	CO2 Injection and Production Field Facilities Design Evaluation and Considerations
	12015	Comprehensive Geological and Reservoir Engineering Evaluation of the Lower San Andres Dolomite Reservoir, Mallet Lease, Slaughter Field, Hockley County, Texas
McElroy	59528	Injection-side Application of MARCIT Polymer Gel Improves Waterflood Sweep Efficiency, Decreases Water-Oil Ratio, and Enhances Oil Recovery in the McElroy Field, Upton County, Texas
	38910	Modeling of Waterflood in a Vuggy Carbonate Reservoir
	24873	Waterflood Improvement in the Permian Basin: Impact of In-Situ Stress Evaluations
	24184	Phase Behavior Modeling Techniques for Low-Temperature CO2 Applied to McElroy and North Ward Estes Projects
	20120	Waterflood Pattern Realignment at the McElroy Field: Section 205 Case History
	20105	In-Situ Stress Evaluation in the McElroy Field, West Texas
	853	Pilot Water Flooding in a Dolomite Reservoir, The McElroy Field
Mead Strawn	17134	Evolution of the Carbon Dioxide Flooding Processes
	3103	Carbon Dioxide Test at the Mead-Strawn Field
Means (San Andres)	27642	A Comparative Technical and Economic Analysis of Waterflood Infill Drilling and CO2 Flood in West Texas Carbonate Reservoirs
	26391	CO2 EOR Economics for Small-to-Medium-Size Fields
	24928	Update of Industry Experience With CO2 Injection
	24111	Prediction of CO2/Crude Oil Phase Behavior Using Supercritical Fluid Chromatography
	19783	An Evaluation of Waterflood Infill Drilling in West Texas Clearfork and San Andres Carbonate Reservoirs
	18977	Summary Results of CO2 EOR Field Tests, 1972-1987
	17349	Review of the Means San Andres Unit CO2 Tertiary Project
	16854	Infill Drilling Economic Analysis of Carbonate Oil Reservoirs in West Texas
	15037	An Economic Evaluation of Waterflood Infill Drilling in Nine Texas Waterflood Units
	11987	Design and Operation of a CO2 Tertiary Pilot: Means San Andres Unit
	11023	Infill Drilling To Increase Reserves-Actual Experience in Nine Fields in Texas, Oklahoma, and Illinois
	6739	Improved Techniques for Evaluating Carbonate Waterfloods in West Texas
	3301	Evaluation and Modification of the Means San Andres Unit Waterflood
North Cowden	28385	Integrated Reservoir Characterization: Beyond Tomography
	27671	Hydrocyclone Separation: A Preferred Means of Water Separation and Handling in Oilfield Production
	25655	Geostatistical Application for Exploration and Development: Porosity Estimation From 3-D Seismic Data Calibrated to Well Data
	16716	The Effects Of CO2 Flooding on Wettability of West Texas Dolomitic Formations
	11165	Preliminary Findings From a Study To Perform Automated Metering and Control of Carbon Dioxide Injection With a Liquid Turbine Meter
	9719	Response of North Cowden and Goldsmith Crudes to Carbon Dioxide Slugs Pushed by Nitrogen
	9364	Solar Powered Injection Controller Utilizing Bottom Hole Pressure Sensing Device
North	26391	CO2 EOR Economics for Small-to-Medium-Size Fields

Unit	SPE #	Title
Cross (Crossett)	24210	North Cross (Devonian) Unit CO2 Flood: Status Report
	24115	Role of Three-Hydrocarbon-Phase Flow in a Gas Displacement Process
	23974	Analysis of Tertiary Injectivity of Carbon Dioxide
	18977	Summary Results of CO2 EOR Field Tests, 1972-1987
	17134	Evolution of the Carbon Dioxide Flooding Processes
	6390	North Cross (Devonian) Unit CO2 Flood – Review of Flood Performance and Numerical Simulation Model
	4737	The Use of Numerical Simulation To Design a Carbon Dioxide Miscible Displacement Project
	NA	Click also South Cross, or return to Cross (North and South)
North Dollarhide	27678	North Dollarhide (Devonian) Unit: Reservoir Characterization and CO2 Feasibility Study
North Farnsworth	26391	CO2 EOR Economics for Small-to-Medium-Size Fields
North Ward Estes	71496	Physical Effects of WAG Fluids on Carbonate Core Plugs
	30729	An Overview of the North Ward Estes CO2 Flood
	24643	CO2 Foam Field Trial at North Ward-Estes
	24184	Phase Behavior Modeling Techniques for Low-Temperature CO2 Applied to McElroy and North Ward Estes Projects
	20702	Converting Wells in a Mature West Texas Field for CO2 Injection
	20138	Reservoir Management: A Synergistic Approach
	20099	Converting Wells in a Mature West Texas Field for CO2 Injection
	19654	Design of a Major CO2 Flood, North Ward Estes Field, Ward County, Texas
	17281	Optimization of Fracture Stimulation Within the North Ward Estes Field
	9711	Fireflooding a High-Gravity Crude in a Watered-Out West Texas Sandstone
	5831	Alkaline Waterflooding: Design and Implementation of a Field Pilot
	1147	Reinjection of Large Volumes of Produced Water in Secondary Operations
	Reinecke	59717
56882		Use of Full-Field Simulation to Design a Miscible CO2 Flood
56524		Spatial Distribution of Oil and Water in Horizontal Pipe Flow
Robertson	70034	Improved Permeability Estimates in Carbonate Reservoirs Using Electrofacies Characterization: A Case Study of the North Robertson Unit, West Texas
	68801	Neural-Network Approach To Predict Well Performance Using Available Field Data
	62557	Swept Volume Calculations and Ranking of Geostatistical Reservoir Models Using Streamline Simulation
	59715	Tiltmeter Hydraulic Fracture Mapping in the North Robertson Field, West Texas
	35433	Flow Unit Characterization of a Shallow Shelf Carbonate Reservoir: North Robertson Unit, West Texas
	27668	Improved Reservoir Management With Water Quality Enhancement at the North Robertson Unit
	19783	An Evaluation of Waterflood Infill Drilling in West Texas Clearfork and San Andres Carbonate Reservoirs
	16854	Infill Drilling Economic Analysis of Carbonate Oil Reservoirs in West Texas
	15568	Quantitative Analysis of Infill Performance: Robertson Clearfork Unit
	15037	An Economic Evaluation of Waterflood Infill Drilling in Nine Texas Waterflood Units
	11023	Infill Drilling To Increase Reserves- Actual Experience in Nine Fields in Texas, Oklahoma, and Illinois
	6739	Improved Techniques for Evaluating Carbonate Waterfloods in West Texas
	4064	Efficient Removal of Oxygen in a Waterflood By Vacuum Deaeration
SACROC (Kelly Snyder)	56882	Use of Full-Field Simulation to Design a Miscible CO2 Flood (also in Reinecke)
	35359	SACROC Unit Carbon Dioxide Flood -- Multidisciplinary Team Improves Reservoir Management and Decreases Operating Costs

Unit	SPE #	Title
	27762	A Probabilistic Forecasting Method for the Huntley CO2 Projects
	27642	A Comparative Technical and Economic Analysis of Waterflood Infill Drilling and CO2 Flood in West Texas Carbonate Reservoirs
	26391	CO2 EOR Economics for Small-to-Medium-Size Fields
	24928	Update of Industry Experience With CO2 Injection
	19023	A New Approach to SACROC Injection Well Testing
	18977	Summary Results of CO2 EOR Field Tests, 1972-1987
	17321	Definitive CO2 Flooding Response in the SACROC Unit
	15916	Surface Processing of Carbon Dioxide in EOR Projects
	14923	Phase Equilibria in the SACROC Oil/CO2, System
	12645	A Laboratory Study of CO2 Foam Properties and Displacement Mechanism
	11162	Ten Years of Handling CO2 for SACROC Unit
	7091	Performance Review of a Large-Scale CO2-WAG Enhanced Recovery Project, SACROC Unit Kelly-Snyder Field
	7090	SACROC Tertiary CO2 Pilot Project
	6391	Corrosion and Operational Problems, CO2 Project, Sacroc Unit
	5536	Reservoir Description by Simulation at SACROC - A Case History
	5052	Compressibility Factors for CO2-Methane Mixtures
	4804	Design and Operation of a Supercritical CO2 Pipeline-Compression System SACROC Unit, Scurry County, Texas
	4667	Effect of Supercritical Carbon Dioxide (CO2) on Construction Materials
	4083	Evaluation and Design of a CO2 Miscible Flood Project-SACROC Unit, Kelly-Snyder Field
	1147	Reinjection of Large Volumes of Produced Water in Secondary Operations
	933	Desorption of Oxygen From Water Using Natural Gas for Countercurrent Stripping
Salt Creek	56882	Use of Full-Field Simulation to Design a Miscible CO2 Flood
	39667	Permeability Predictions in Carbonate Reservoirs Using Optimal Non-parametric
	23958	Case Histories of Step Rate Tests in Injection Wells
Seminole (main pay and ROZ)	71496	Physical Effects of WAG Fluids on Carbonate Core Plugs
	59691	San Andres and Grayburg Imbibition Reservoirs
	36515	Integrated Reservoir Characterization Study of a Carbonate Ramp Reservoir: Seminole San Andres Unit, Gaines County, Texas
	27715	Critical Scales, Upscaling, and Modeling of Shallow-Water Carbonate Reservoirs
	27642	A Comparative Technical and Economic Analysis of Waterflood Infill Drilling and CO2 Flood in West Texas Carbonate Reservoirs
	26391	CO2 EOR Economics for Small-to-Medium-Size Fields
	24928	Update of Industry Experience With CO2 Injection
	24702	Defining Flow Units in Dolomitized Carbonate-Ramp Reservoirs
	19783	An Evaluation of Waterflood Infill Drilling in West Texas Clearfork and San Andres Carbonate Reservoirs
	17290	New Fiberglass Liner Completion Technique Salvages Old Injection Wells for Use as WAG Injection Wells
	16854	Infill Drilling Economic Analysis of Carbonate Oil Reservoirs in West Texas
	10022	The Role of Numerical Simulation in Reservoir Management of a West Texas Carbonate Reservoir
	8274	Improved Reservoir Characterization: A Key to Future Reservoir Management for the West Seminole San Andres Unit
	7796	Sheep Mountain CO2 Production Facilities - A Conceptual Design
	6738	Reservoir Data Pays CO2 West Seminole San Andres Unit, Gaines County, Texas
	4064	Efficient Removal of Oxygen in a Waterflood By Vacuum Deaeration
Sharon Ridge	65029	Mineral Scale Control in a CO2 Flooded Oilfield
	56882	Use of Full-Field Simulation to Design a Miscible CO2 Flood (SPERE, June 1999)
	39629	Use of Full-Field Simulation to Design a Miscible CO2 Flood
	3443	Performance of Sharon Ridge Canyon Unit with Water Injection

Unit	SPE #	Title
	37	Pressure Maintenance Operations in the Sharon Ridge Canyon Unit, Scurry County, Tex.
Slaughter Estate	27642	A Comparative Technical and Economic Analysis of Waterflood Infill Drilling and CO ₂ Flood in West Texas Carbonate Reservoirs
	26624	Reservoir Management in Tertiary CO ₂ Floods
	26391	CO ₂ EOR Economics for Small-to-Medium-Size Fields
	23974	Analysis of Tertiary Injectivity of Carbon Dioxide
	19375	Slaughter Estate Unit CO ₂ Flood: Comparison Between Pilot and Field-Scale Performance
	18977	Summary Results of CO ₂ EOR Field Tests, 1972-1987
	16830	CO ₂ Injection and Production Field Facilities Design Evaluation and Considerations
	16716	The Effects Of CO ₂ Flooding on Wettability of West Texas Dolomitic Formations
	10727	Slaughter Estate Unit Tertiary Miscible Gas Pilot Reservoir Description
	9796	Slaughter Estate Unit Tertiary Pilot Performance
	8830	Slaughter Estate Unit CO ₂ Pilot - Surface and Downhole Equipment Construction and Operation in the Presence of H ₂ S
Slaughter Field	71496	Physical Effects of WAG Fluids on Carbonate Core Plugs
	70068	Conformance Water-Management Team Developments and Solutions on Projects in the Permian Basin
	27648	Normalization of Cased-Hole Neutron Logs, Slaughter Field, Cochran and Hockley Counties, Texas
	27642	A Comparative Technical and Economic Analysis of Waterflood Infill Drilling and CO ₂ Flood in West Texas Carbonate Reservoirs
	26335	Coiled-Tubing Sidetrack: Slaughter Field Case History
	24928	Update of Industry Experience With CO ₂ Injection
	20377	Optimization of Waterflood Performance and CO ₂ -Flood Design Using a Modeling Approach, Mallet Unit, Slaughter Field
	20115	Reactivity of San Andres Dolomite
	19375	Slaughter Estate Unit CO ₂ Flood: Comparison Between Pilot and Field-Scale Performance
	16831	Carbonated Waterflood Implementation and Its Impact on Material Performance in a Pilot Project
	14308	Investigation of Unexpectedly Low Field-Observed Fluid Mobilities During Some CO ₂ Tertiary Floods
	14288	A CO ₂ Injection Measurement and Control System
	12015	Comprehensive Geological and Reservoir Engineering Evaluation of the Lower San Andres Dolomite Reservoir, Mallet Lease, Slaughter Field, Hockley County, Texas
	7570	Use of Fine Salt as a Fluid Loss Material in Acid Fracturing Stimulation Treatments
	4070	A Modeling Approach for Optimizing Waterflood Performance, Slaughter Field Chickenwire Pattern
	1576	Computer Processing of Log Data Improves Production In Chaveroo Field
	341	Small Propane Slug Proving Success in Slaughter Field Lease
Slaughter Frazier	16830	CO ₂ Injection and Production Field Facilities Design Evaluation and Considerations
Slaughter Sundown	49168	Simulation of a CO ₂ Flood in the Slaughter Field with Geostatistical Reservoir Characterization
	35410	Improved CO ₂ Flood Predictions Using 3D Geologic Description and Simulation on the Sundown Slaughter Unit
	30742	Horizontal Well Applications in a Miscible CO ₂ Flood, Sundown Slaughter Unit, Hockley County, Texas
South Cowden	59691	San Andres and Grayburg Imbibition Reservoirs
	56609	Use of Sacrificial Agents in CO ₂ Foam Flooding Application
	39666	Incorporating Seismic Attribute Porosity into a Flow Model of the Grayburg Reservoir
	37470	The Evaluation of Two Different Methods of Obtaining Injection Profiles in CO ₂ WAG Horizontal Injection Wells
	37218	Laboratory Evaluation of Surfactants for CO ₂ -Foam Applications at the South Cowden Unit

Unit	SPE #	Title
	36650	Characterization of Diagenetically Altered Carbonate Reservoirs, South Cowden Grayburg Reservoir, West Texas
	35429	Determination of Relative Permeability and Trapped Gas Saturation for Predictions of WAG Performance in the South Cowden CO ₂ Flood
	35222	An Integrated Study of the Grayburg/San Andres Reservoir, Foster and South Cowden Fields, Ector County, Texas
	28334	Innovative Approach to CO ₂ Project Development Holds Promise for Improving CO ₂ Flood Economics in Smaller Fields Nearing Abandonment
	27658	Proposal for an Integrated Study of the Grayburg/San Andres Reservoir, Foster and South Cowden Fields, Ector County, Texas
	27655	Design and Implementation of a CO ₂ Flood Utilizing Advanced Reservoir Characterization and Horizontal Injection Wells in a Shallow Shelf Carbonate
		Click also North Cowden, or return to Cowden (North and South)
South Welch	27676	CO ₂ Operating Plan, South Welch Unit, Dawson County, Texas
	26391	CO ₂ EOR Economics for Small-to-Medium-Size Fields
	18977	Summary Results of CO ₂ EOR Field Tests, 1972-1987
	12664	CO ₂ Miscible Flooding Evaluation of the South Welch Unit, Welch San Andres Field
Sprayberry Trend	10759	The Effect of Lateral Anisotropy on Flood Pattern Dimensions and Orientation
	405	Large Scale Waterflood Performances Sprayberry Field, West Texas
Twofreds	26614	Update Case History: Performance of the Twofreds Tertiary CO ₂ Project
	26391	CO ₂ EOR Economics for Small-to-Medium-Size Fields
	18977	Summary Results of CO ₂ EOR Field Tests, 1972-1987
	14439	Performance of the Twofreds CO ₂ Injection Project
	8382	Twofreds Field a Tertiary Oil Recovery Project
	1792	Pressure Maintenance by Water Injection In the Twofreds (Delaware) Field Unit
Waddell	1146	Pressure Maintenance by Bottom-Water Injection in a Massive San Andres Dolomite Reservoir
Wasson	71496	Physical Effects of WAG Fluids on Carbonate Core Plugs
	24185	CO ₂ Miscible Flood Simulation Study, Roberts Unit, Wasson Field, Yoakum County, Texas
	24111	Prediction of CO ₂ /Crude Oil Phase Behavior Using Supercritical Fluid Chromatography
	23974	Analysis of Tertiary Injectivity of Carbon Dioxide
	19783	An Evaluation of Waterflood Infill Drilling in West Texas Clearfork and San Andres Carbonate Reservoirs
	19666	The Effects of Waterflooding on Reservoir Properties and Producing Operations: Applications for Geochemical Modeling
	19596	Outcrop/Subsurface Comparisons of Heterogeneity in the San Andres Formation
	16716	The Effects Of CO ₂ Flooding on Wettability of West Texas Dolomitic Formations
	15037	An Economic Evaluation of Waterflood Infill Drilling in Nine Texas Waterflood Units
	14288	A CO ₂ Injection Measurement and Control System
	13116	Effect of Phase Behavior on CO ₂ Displacement Efficiency at Low Temperatures: Model Studies With an Equation of State
	11592	CO ₂ Flooding: Its Time Has Come
	11125	Interpretation of Pressure-Composition Phase Diagrams for CO ₂ /Crude-Oil Systems
	10686	An Investigation of Phase Behavior-Macroscopic Bypassing Interaction in CO ₂ Flooding
	8367	The Effect of Phase Behavior on CO ₂ -Flood Displacement Efficiency
	3570	Use of the SP Log in Waterflood Surveillance
	2472	Three Porosity Movable Oil Plot Vs Single Porosity Movable Oil Plot to Improve Completion Results in the Wasson Field
Wasson Cornell	16854	Infill Drilling Economic Analysis of Carbonate Oil Reservoirs in West Texas
	15037	An Economic Evaluation of Waterflood Infill Drilling in Nine Texas Waterflood Units
	10292	CO ₂ Flood Performance Evaluation for the Cornell Unit, Wasson San Andres Field
	9762	Success of a High-Friction Diverting Gel in Acid Stimulation of a Carbonate Reservoir - Cornell Unit, San Andres Field

Unit	SPE #	Title
Wasson Denver	59548	Denver Unit Infill Drilling and Pattern Reconfiguration Program
	56549	Reservoir Characterization and Development Plan of the Wasson San Andres Denver Unit Gas Cap
	29116	Field-Scale CO ₂ Flood Simulations and Their Impact on the Performance of the Wasson Denver Unit
	27674	The Denver Unit CO ₂ Flood Transforms Former Waterflood Injectors Into Oil Producers
	27642	A Comparative Technical and Economic Analysis of Waterflood Infill Drilling and CO ₂ Flood in West Texas Carbonate Reservoirs
	26391	CO ₂ EOR Economics for Small-to-Medium-Size Fields
	24928	Update of Industry Experience With CO ₂ Injection
	24644	Quantitative CO ₂ Flood Monitoring, Denver Unit, Wasson (San Andres) Field
	24157	Overview of Production Engineering Aspects of Operating the Denver Unit CO ₂ Flood
	24156	Production Performance of the Wasson Denver Unit CO ₂ Flood
	19783	An Evaluation of Waterflood Infill Drilling in West Texas Clearfork and San Andres Carbonate Reservoirs
	19725	Analyzing the Flowing Performance of Oil Wells: Denver Unit CO ₂ Flood
	19596	Outcrop/Subsurface Comparisons of Heterogeneity in the San Andres Formation
	18883	Equilibrium Acid Fracturing: A New Fracture Acidizing Technique for Carbonate Formations
	17335	Comparison of Laboratory- and Field-Observed CO ₂ Tertiary Injectivity
	16854	Infill Drilling Economic Analysis of Carbonate Oil Reservoirs in West Texas
	14308	Investigation of Unexpectedly Low Field-Observed Fluid Mobilities During Some CO ₂ Tertiary Floods
	13132	Effect of CO ₂ Flooding on Dolomite Reservoir Rock, Denver Unit, Wasson (San Andres) Field, TX
	8406	Production Technology Experience in a Large Carbonate Waterflood, Denver Unit, Wasson San Andres Field
	6385	Denver Unit 10-Acre Infill Pilot Test and Residual Oil Testing
Wasson ODC	35402	Field Test of Foam to Reduce CO ₂ Cycling
	27642	A Comparative Technical and Economic Analysis of Waterflood Infill Drilling and CO ₂ Flood in West Texas Carbonate Reservoirs
	17754	A Brief History of the Wasson EOR Project
	16830	CO ₂ Injection and Production Field Facilities Design Evaluation and Considerations
Wasson South	70063	South Wasson Clear Fork Reservoir Model: Outcrop to Subsurface via Rock-Fabric Method
	24160	Early CO ₂ Flood Experience at the South Wasson Clearfork Unit
	19783	An Evaluation of Waterflood Infill Drilling in West Texas Clearfork and San Andres Carbonate Reservoirs
Wasson Willard	27642	A Comparative Technical and Economic Analysis of Waterflood Infill Drilling and CO ₂ Flood in West Texas Carbonate Reservoirs
	24928	Update of Industry Experience With CO ₂ Injection
	19783	An Evaluation of Waterflood Infill Drilling in West Texas Clearfork and San Andres Carbonate Reservoirs
	16854	Infill Drilling Economic Analysis of Carbonate Oil Reservoirs in West Texas
	15037	An Economic Evaluation of Waterflood Infill Drilling in Nine Texas Waterflood Units
	7051	A Method for Projecting Full-Scale Performance of CO ₂ Flooding in the Willard Unit
	7050	Coring for In-Situ Saturations in the Willard Unit CO ₂ Flood Mini-Test
	7049	Use of Time-Lapse Logging Techniques in Evaluating the Willard Unit CO ₂ Flood Mini-Test
	6389	Case History: A Pressure Core Hole
	6388	A Review of the Willard (San Andres) Unit CO ₂ Injection Project
Welch	62588	Interwell Seismic for Reservoir Characterization and Monitoring
	39808	West Welch CO ₂ Flood Simulation with an Equation of State and Mixed Wettability
	35160	Characterization of Rock Types With Mixed Wettability Using Log and Core Data - DOE

Unit	SPE #	Title
		Project Welch Field, Dawson County, Texas
	27676	CO ₂ Operating Plan, South Welch Unit, Dawson County, Texas
	12664	CO ₂ Miscible Flooding Evaluation of the South Welch Unit, Welch San Andres Field
	39	History of the Welch Field San Andres Pilot Water Flood
Wellman	48948	Wellman Unit CO ₂ Flood: Reservoir Pressure Reduction and Flooding the Water/Oil
	22898	Reservoir Performance of a Gravity-Stable Vertical CO ₂ Miscible Flood: Wolfcamp Reef Reservoir, Wellman Unit
	11129	Numerical Simulation of a Gravity Stable, Miscible CO ₂ Injection Project in a West Texas Carbonate Reef
	10065	A Technique for Obtaining In-Situ Saturations of Underpressured Reservoirs
West Welch	39809	Improving Flow Simulation Performance with a Seismic-Enhanced Geologic Model
	39808	West Welch CO ₂ Flood Simulation with an Equation of State and Mixed Wettability
	35160	Characterization of Rock Types With Mixed Wettability Using Log and Core Data - DOE Project Welch Field, Dawson County, Texas